UNIVERSITY OF CALGARY

Determination of Solubility Parameter of Methane in Heavy Oil

by

Daniela Paniagua Fernández

A THESIS

SUBMITTED TO THE FACULTY OF GRADUATE STUDIES

IN PARTIAL FULFILMENT OF THE REQUIREMENTS FOR THE

DEGREE OF MASTER OF SCIENCE

GRADUATE PROGRAM IN CHEMICAL ENGINEERING

CALGARY, ALBERTA

JUNE, 2021

Abstract

Asphaltenes are the least soluble fraction of crude oil and can phase separate from the oil due changes in pressure, temperature, or oil composition. Some examples where asphaltene precipitation occur in oilfield operations are: dilution of a heavy oil with an incompatible solvent (*e.g.* an *n*-alkane), depressurization of a light conventional oil during production, and gas injection into a light conventional oil reservoir. Methane is often a major component of the dissolved gases in a crude oil and has a significant negative impact in the oil's ability to solubilize asphaltenes.

The Modified Regular Solution (MRS) model has been previously used to model asphaltene precipitation from heavy oils and bitumen diluted with *n*-alkanes at different temperatures and pressures. The input parameters of the MRS model are the mole fractions, molar volumes, and solubility parameters of the bitumen (characterized into SARA fractions), and the *n*-alkane solvent. However, the MRS model is not yet able to predict asphaltene solubility in the presence of dissolved gases, such as methane, because the solubility parameter of the dissolved methane is unknown. To determine these parameters, asphaltene onsets and yields from mixtures of bitumen, *n*-pentane, and methane were measured at temperatures of 21 and 130°C and pressures of 10 and 60 MPa. The onsets (solvent content at which precipitation first occurred) were measured by titrating the bitumen with a mixture of methane and *n*-pentane in a High-Pressure Microscope. Asphaltene yields (mass of asphaltenes divided by mass of bitumen in feed) were measured in a blind cell apparatus for mixtures with the same methane content as the onset measurements.

The methane solubility parameter was determined by fitting the MRS model to the measured asphaltene precipitation data. The fitted values ranged from 6.1 to 9.5 $MPa^{0.5}$ depending on the temperature. A correlation for the methane solubility parameter was developed for use in the MRS model. The MRS model using the correlation matched the onsets and yields with average deviations of 1.1 wt% solvent and 8.1 wt%, respectively. The updated model now applies to *in situ* heavy oils that contain dissolved methane.

Acknowledgments

I would like to acknowledge my supervisor Dr. Harvey Yarranton for his excellent work as a professor, I can say without shadow of a doubt that you have been one of the best professors I have ever had. Your guidance, continuous support, and patience were vital to overcome the challenges that arouse while completing my thesis. I cannot thank you enough for the opportunity to be part of your excellent research group.

I would also like to acknowledge the amazing work of the two lab managers from our research group. Florian, thank you so much for the challenging questions and for sharing your knowledge with me. You have shaped me into a better engineer and a better person. Elaine, thank you for your administrative support and for the candy.

I want to give a special mention to my dear friends, John and Tatiana. I am very glad to have shared this journey with you guys, thank you for always being there for me. I would also like to thank the friends I met here, especially Franklin, Javier, Andres, Andrea, Diego, Maria E., Laura, and Nicson. We have had good times together; I will always hold them close to my heart.

Thanks to the sponsors of the NSERC Industrial Research Chair in Heavy Oil Properties and Processing, including NSERC, Canadian Natural Resources Limited (CNRL), CNOOC Nexen, Ecopetrol, Petrobras, Schlumberger, Suncor Energy, Virtual Materials Group, Alberta Innovates, and ConocoPhillips for their financial support.

Finally, I would like to thank my family for their love and support. I could not have done it without you.

Dedication

To my grandma:

Thank you for your guidance and love
I miss you everyday and I will always love you

Table of Contents

List of Tables

List of Figures and Illustrations

List of Symbols, Abbreviations and Nomenclature

Upper Case Symbols

A^{assoc}	Associating molecules contribution to Helmholtz energy
A^{chain}	Covalent bonds contribution to Helmholtz energy
A_0^{disp}	Dispersion contribution to Helmholtz energy
A_0^{hs}	Hard-sphere contribution to Helmholtz energy
A^{res}	Residual Helmholtz energy
A^{seg}	Dispersion forces contribution to Helmholtz energy
B_A	Fitting and fluid specific parameter, Eq. 5.3
D_{ij}	Function of solubility parameter in Eq. 4.6
H_m	Fitting parameter akin to Henry's constant of methane in bitumen, Eq, 5.4
H/F	Mass ratio of the heavy phase to feed components
K	Equilibrium ratio
MW	Molecular weight
P	Absolute Pressure
$P_{v,p}$	*n*-Pentane vapor pressure, Eq. 5.5
R	Universal gas constant
T	Absolute Temperature
V_{avail}	Available volume in the blind cell
W_A	Cumulative mass fraction of the C_5-asphaltene pseudo-components
$X(T_r)$	*n*-Pentane vapor pressure function, Eq, 5.10
X_A	Fraction of unbonded sites in CPA-EoS, Eq. 2.9
Y	Yield

Lower Case Symbols

a	Intermolecular attractive parameter in EoS
a_1, a_2, b_1, b_2	Fluid specific parameters for effective density, Eq. 4.13
a_o, b_o, c_o, a_1, b_1	Fluid specific parameters for aromatics and resins, Eq. 4.15
b	Volume occupied by one mole of molecules parameter in EoS

c	Volume-translation parameter in EoS
f	Fugacity
g	Radial distribution function in CPA-EoS, Eq 2.9
k	Binary interaction parameter, Eq. 2.6
	Temperature dependence of the solubility parameter
l	Interaction parameter
m	Mass
	Function of the acentric factor in PR-EoS, Eq. 2.2
	Average number of segments per molecule in PC-SAFT EoS, Eq. 2.18
	Component specific constant to calculate density, Eq 4.16 and 4.18
n	Total component number
w	Mass fraction
x	Mole fraction

Greek Letters

$\alpha(T_r, \omega)$	Dimensionless function of the reduced temperature in PR-EoS
β	Shape factor in Gamma distribution function for asphaltene fraction
$\beta^{A_iB_i}$	Association volume in CPA-EoS
γ	Activity coefficient
Γ	Gamma distribution function
δ	Solubility Parameter
$\Delta^{A_iB_i}$	Association strength in CPA-EoS
ΔU^{vap}	Internal energy of vaporization
$\varepsilon^{A_iB_i}$	Association energy in CPA-EoS
ε/κ	Segment-segment interaction energy in PC-SAFT EoS
ρ	Mass density
σ	Diameter of each molecular segment in PC-SAFT EoS
ϕ	Volumetric fraction
ω	Acentric factor

Superscripts

$21℃$	Property evaluated at 21°C
$25℃$	Property evaluated at 25°C
α	Phase
F	Feed
H	Heavy-liquid phase (C_5-asphaltene rich)
L	Liquid phase
	Light-Liquid Phase (solvent-rich phase)
o	Standard condition
V	Vapor phase

Subscripts

A	Type of site on a given molecule in CPA-EoS, Eq. 2.9
	C_5-asphaltene pseudo-component
b	Bitumen
c	Critical property
i	Component i
j	Component j
k	Component k
m	Mixture
max	Maximum
min	Minimum
P	*n*-Pentane
$P*$	Pitch* yield
r	Reduced property
S	Solvent
ToP	Property at standard temperature and system pressure
$ToPo$	Property at standard temperature and standard pressure
TP	Property at system temperature and system pressure

Abbreviations

AAD	Average Absolute Deviation
API	American Petroleum Institute
APR	Advanced Peng Robinson
BPR	Back Pressure Regulator
CEoS	Cubic Equation of State
CPA	Cubic Plus Association
EOR	Enhanced Oil Recovery
EoS	Equation of State
FH	Flory-Huggins
GC	Gas Chromatography
HPM	High-Pressure Microscope
LLE	Liquid-Liquid Equilibrium
MAD	Maximum Average Deviation
MRS	Modified Regular Solution
NRTL	Non-Random Two Liquid
OF	Objective Function
PC-SAFT	Perturbed Chain Statistical Association Fluid Theory
PR	Peng-Robinson
PVT	Pressure-Volume-Temperature
L	Liquid
RS	Regular Solution
SAFT	Statistical Association Fluid Theory
SARA	Saturates, Aromatics, Resins and Asphaltenes
SKR	Soave-Redlich-Kwong
TBP	True Boiling Point
TI	Toluene Insolubles
UNITAR	United Nations Institute for Training and Research
V	Vapor
VL	Vapor-Liquid
VLE	Vapor-Liquid Equilibrium

VLL	Vapor-Liquid-Liquid
VLLL	Vapor-Liquid-Liquid-Liquid
VPO	Vapor Pressure Osmometry
W	Water
WVLL	Water-Vapor-Liquid-Liquid

Chapter 1. Introduction

The estimated worldwide reserves of crude oil is 1.7 trillion barrels of which 167 billion barrels (10%) are located in Canada (BP, 2019; *Energy Fact Book of Natural Resources of Canada*, 2018). Approximately 96% of Canada's proven reserves are heavy oil and bitumen, defined as unconventional crude oils with API gravity in the range of 10-19° for heavy oil and below 10° for bitumen. The defining characteristics of a major portion of these fluids are their high asphaltene contents and their viscosities, which can be as high as 1,000,000 mPa·s at standard conditions giving a virtually immobile oil at reservoir temperature and pressure (Gray, 2015). As conventional oil reserves have depleted over the past few decades, oil and gas companies have been adapting their current processes to maximize production in conventional reservoirs, and have been developing strategies to treat heavy oils, bitumen, and heavy feedstock residues. Heavy oils (and bitumens) contain a significant fraction of asphaltenes. The precipitation of asphaltenes can be an advantage for some processes involving heavy oil and solvents and a challenge for others.

Asphaltenes are the heaviest, most polar, and most aromatic fraction of crude oil and can form a separate phase from the crude oil due changes in pressure, temperature, or oil composition. The phase separation is termed precipitation because the separated heavy phase often appears in the form of glassy solid particles. However, the separated heavy phase may be a liquid at some conditions. Three well-known situations where asphaltene precipitation can occur during the production and processing of crude oils are: 1) dilution of a heavy oil with an incompatible solvent (*e.g.* an *n*-alkane); 2) depressurization of a light conventional oil; 3) gas injection into the reservoir. Each application is discussed in more detail below.

- Heavy oils are diluted with solvents to reduce viscosity and facilitate transportation through pipelines to processing refineries. The solvents typically include *n*-alkanes, gas condensates, light crude oils or refinery distillation products. These solvents may reduce asphaltene solubility in the heavy oil leading to its precipitation and resulting in the obstruction of pipelines, fouling of production facilities, and poisoning of catalysts in hydrotreating processes (Usui *et al.*, 2004). In some cases, heavy oils are diluted with a solvent to deliberately precipitate asphaltenes; for example, in deasphalting and oil sands froth treatment processes.

- Asphaltene precipitation can occur when light highly undersaturated oils are depressurized during production. The asphaltenes in these oils are barely stable and the small change in the oil's ability to solubilize them when the density decreases with depressurization is enough to trigger precipitation. (Kord and Ayatollahi, 2012). This type of asphaltene precipitation is a particularly high risk in ultra-deep sea oil production due to the high content of dissolved gases, especially methane. A variety of experimental results have shown that methane tends to favour asphaltene precipitation (Dehghani *et al.*, 2007; Zanganeh *et al.*, 2018).
- Enhanced Oil Recovery (EOR) by gas injection can also cause asphaltene precipitation, even for crude oils with asphaltene contents as low as 0.1 wt% (Punnapala and Vargas, 2013). Asphaltene precipitation followed by an EOR gas injection process can alter the reservoir wettability, reduce permeability, and reduce the sweep efficiency (Jafari and Naderi, 2014). Therefore, the amount of gas that can be dissolved into the oil before having asphaltene precipitation is an important parameter to consider in the design of an optimal gas injection scheme.

In these applications, oilfield operators must anticipate potential asphaltene precipitation scenarios in order to avoid or mitigate production problems or to appropriately design and operate processes involving asphaltene precipitation. Hence, it is necessary to identify the conditions at which asphaltenes begin to precipitate and in some cases the amount of precipitation.

There are several thermodynamic models that can be used to model asphaltene precipitation, including equations of state such as Cubic Plus Association (CPA) (Li and Firoozabadi, 2010a) or Perturbed Chain SAFT (PC-SAFT) (Tavakkoli *et al*., 2016); and also including activity coefficient models such as Regular Solution Theory (Akbarzadeh *et al.,* 2005). This thesis focuses on regular solution theory. Regular solution theory was first adapted to model asphaltene precipitation by Hirschberg *et al*. (1984). They developed a modified regular solution model that included both the enthalpic contribution from regular solution theory and an entropic contribution from mixing different sized molecules. They also described asphaltenes as monodisperse polymeric particles with defined physical properties (density, molecular weight, and solubility parameter). Kawanaka *et al*. (1991) and later Yarranton and Masliyah (1996) modified this approach to account for the continuous distribution of asphaltene properties. Alboudwarej *et al*. (2003) and Akbarzadeh *et al*. (2004) extended the model asphaltene precipitation from mixtures of heavy oil and solvents over

a wide range of temperatures and pressures. Ramos-Pallares and Yarranton (2020) extended the model to include the partitioning of all components to both liquid phases, not just the asphaltenes and resins.

The current version of the Modified Regular Solution (MRS) model is not yet able to predict asphaltene solubility data in the presence of dissolved gases, such as methane, because it lacks accurate solubility parameters for the dissolved gas components. The onset (condition at which precipitation starts), and the yield (amount of precipitation) are very sensitive to the input solubility parameters, therefore, more accurate solubility parameters of the dissolved gases are required to have confidence when using the MRS model to predict asphaltene precipitation from crude oils at reservoir conditions. Methane, in particular, has a significant negative impact on a crude oil's ability to solubilize asphaltenes (Dehghani *et al.*, 2007; Zanganeh *et al.*, 2018) and is the focus of this thesis. Including more accurate solubility parameters for methane will improve the model's ability to predict asphaltene precipitation from *in situ* conventional and heavy oils which contain dissolved methane.

1.1.Objectives

The goal of this thesis is to determine the solubility parameter of methane in heavy oil as a function of temperature and pressure. To do so, asphaltene precipitation data from bitumen, *n*-pentane, and methane mixtures will be fitted using a MRS model. The input properties (density, molecular weight, and solubility parameters) for the bitumen and *n*-pentane required for the MRS model have already been established. The density of the dissolved methane is determined using an established effective density correlation. Therefore, the only unknown input for the model is the solubility parameter of methane. The specific objectives of the project are as follows:

1. Determine the solubility parameter distribution of the asphaltene fraction by fitting the MRS model to the asphaltene precipitation data from bitumen and *n*-pentane mixtures.
2. Extend the pressure dependencies in the correlations for the asphaltene solubility parameters up to 60 MPa. To do so, adjust the asphaltene solubility parameters in the MRS model to fit previously measured asphaltene onsets and yields from mixtures of bitumen and *n*-pentane at temperatures of 21 and 130°C and pressures of 10 and 60 MPa. Then correlate the fitted parameters to temperature and pressure.

3. Measure the saturation pressures of bitumen, *n*-pentane, and methane mixtures at temperatures of 50 and 130°C. These measurements were performed in a blind cell PVT apparatus.
4. Measure asphaltene precipitation data, including onsets and yields, from bitumen, *n*-pentane, and methane mixtures at temperatures of 21 and 130°C and pressures of 10 and 60 MPa. These measurements were performed in a blind cell PVT apparatus for yields and in a high-pressure microscope apparatus for onsets.
5. Determine the solubility parameter of methane by fitting the MRS model to the collected asphaltene precipitation data.
6. Develop a temperature and pressure dependent correlation for the solubility parameter of methane.

1.2.Thesis Structure

This thesis is organized into six chapters, and the remaining chapters are outlined below.

Chapter Two provides some background on crude oil chemistry and asphaltene precipitation of live and dead oils. Previous phase behavior measurements for diluted heavy oils and conventional depressurized oils are briefly discussed. Finally, some of the thermodynamic models used to predict the phase behavior of these systems are presented.

Chapter Three lists the materials and selected properties of the bitumen samples used in this thesis. The apparatus and experimental procedures used to measure saturation pressures, onsets of asphaltene precipitation, and asphaltene yields are described in this chapter.

Chapter Four provides the modeling approach followed in this thesis to predict asphaltene precipitation data using the MRS model. The main assumptions of the model, the fluid characterization, and the correlations to determine the properties of the different pseudo-components are presented.

Chapter Five presents the experimental data and modeling results from mixtures of bitumen and *n*-pentane, and mixtures of bitumen, *n*-pentane, and methane. Updated pressure and temperature

dependent correlation for the solubility parameters of the asphaltene fraction, along with a new developed temperature dependent correlation for the solubility parameter of methane are presented. The performance of the MRS in predicting the asphaltene precipitation data from bitumen, *n*-pentane, and methane mixtures is discussed.

Chapter Six summarizes the major contributions of this thesis and provides recommendations for future studies.

Chapter 2. Literature Review

This chapter presents an overview of the background material currently available to understand the asphaltene precipitation of live and dead oils. The first section presents a brief description of to the chemistry of crude oil, followed by a more detailed discussion on asphaltenes. The second section summarizes asphaltene related phase behavior and the thermodynamic models used to predict this phase behavior.

2.1. Chemistry of Crude Oil and Asphaltenes

2.1.1. Crude Oil

Petroleum is a naturally occurring mixture of hydrocarbons formed from organic matter decomposition at high pressures and temperatures. It can be a solid (coal), a liquid (crude oil), or a gas. The focus of this thesis is heavy oils and bitumens. Heavy oils and bitumen are subsets of crude oils defined based on their density as shown in Table 2.1. For convenience, in this thesis, the term "heavy oil" will be used to describe both heavy oils and bitumen unless referring to a specific oil.

Table 2.1. UNITAR classification of crude oils at 15.6°C.

Classification	Viscosity, MPa·s	Density, kg/m^3	API Gravity
Conventional oil	$<10^2$	<900	>20°
Heavy oil	10^2-10^5	900-1000	10°-19°
Bitumen	$>10^5$	>1000	<10°

Crude oils contain variable amounts of sulfur, nitrogen, oxygen, and trace metals such as nickel and vanadium (Speight, 2014). The exact composition of crude oil varies with the location, type of geological formation, and depth of the reservoir from which is produced. Consequently, crude oils exhibit a wide variety in composition and physical properties (Speight, 2014). Nonetheless, the elemental composition of a crude oil tends to fall within the relatively narrow ranges, as shown in Table 2.2.

Table 2.2. Elemental composition of a crude oil (Fahim *et al.*, 2010).

Element	Composition (wt%)
Carbon	83.0-87.0
Hydrogen	10.0-14.0
Sulfur	0.05-6.0
Nitrogen	0.1-0.2
Oxygen	0.05-2
Metals (Ni, V)	< 1000 ppm

The main chemical components of crude oils are hydrocarbons which are generally classified as follows (Fahim *et al.*, 2010):

- *Paraffins* are saturated hydrocarbons that have the general formula C_nH_{2n+2}. Normal paraffins are unbranched linear chain molecules. Isoparaffins are branched non-linear hydrocarbon chains. The simplest molecule of this broad series is methane, the main component of natural gas and the solvent of interest for this thesis.
- *Olefins* are unsaturated hydrocarbons containing carbon-carbon double or triple bonds. Olefins are not naturally present in crude oil but can be formed during conversion processes.
- *Naphthenes or cycloparaffins* are saturated ring-shaped hydrocarbons that have the general formula C_nH_{2n}. Naphthenes commonly have rings with five or six carbon atoms usually with paraffinic side chains. Multi-ring naphthenes are present in the heavier fractions of crude oil. The multi-rings can be fused or non-fused if they share more than one carbon atom. Naphthenes are the most abundant class of hydrocarbons in most crude oils.
- *Aromatics* are unsaturated cyclic compounds composed by one or more benzene rings. Aromatics can be classified as mono- or polyaromatic depending on the number of rings of the molecule. The hydrogen atoms in the benzene rings are usually substituted by another atom or alkyl group, increasing the complexity of aromatic compounds as the number of benzene rings increases. Light petroleum fractions contain a higher number of mono-aromatics compounds, while polyaromatics are normally found in the heavier petroleum cuts.

Crude oils can include volatile compounds such as light alkanes (methane, ethane, propane, butane) or non-hydrocarbon gases like carbon dioxide (CO_2), nitrogen (N_2), and hydrogen sulfide

(H_2S). Crude oils with dissolved gases are known as live oils. The dissolved gases can be released by reducing crude oil pressure below the saturation value. Crude oils with no dissolved gases are known as dead oils.

The chemical composition of crude oils is required to predict their properties and thermodynamic behavior. However, it is not possible or practical to determine the molecular structure and content of each of the millions of chemical species in crude oils. Instead, crude oils are characterized as a set of pseudo-components that represent the properties distribution within the oil. For conventional crude oils, the characterization is usually based on volatility; that is, the oil is divided into pseudo-components representing boiling point intervals using a true boiling point (TBP) or a gas chromatography (GC) assay. This characterization method is less useful for heavy oils because they have a very low content of distillable components, usually less than 30 wt% (Castellanos-Díaz *et al*., 2014).

Heavy oils are more commonly characterized based on SARA fractionation. This method divides the oil in pseudo-components based on the chemical families as saturates, aromatics, resins and asphaltenes. Saturates, aromatics, and resins are adsorption classes and the asphaltene fraction is a solubility class. Saturates are a mixture of paraffinic and naphthenic compounds. Aromatics, resins, and asphaltenes are a continuum of poly-nuclear aromatic species of increasing molecular weight, density, aromaticity, heteratom content, and polarity. The asphaltenes are the components most prone to precipitate from an oil and are discussed in more detail below.

2.1.2. Asphaltenes

Asphaltenes are the heaviest, most polar, and most aromatic fraction of crude oil. They are defined in terms of their solubility as the fraction of crude oil soluble in aromatic solvents such as toluene, but insoluble in an excess of *n*-alkane solvents such as *n*-pentane or *n*-heptane (Speight, 2014). Asphaltenes can precipitate upon a change in pressure, temperature or crude oil composition. Asphaltene precipitation is usually undesirable because it can damage the reservoir and cause fouling in production and processing facilities. The properties of precipitated asphaltenes and the extent of precipitation depend on the type of solvent, dilution ratio, contact time, temperature, and the precipitation method (Alshareef, 2020).

Asphaltenes are not a pure component, but rather consist of hundreds of thousands of molecular species. However, there are common attributes to all asphaltenes (Chacón-Patiño *et al.*, 2017):

- They consist of poly-condensed aromatic rings with aliphatic side chains of various lengths, combined with heteroatoms of nitrogen, oxygen, sulfur, as well as traces of heavy metals such as nickel and vanadium.
- They have similar functional groups such as thiols, sulfides, disulfides, thiophenes, acids, phenols, ketones, pyridines, pyrroles and porphyrins (Speight, 2014).
- Their atomic H/C ratio varies within a narrow range of 1.15 ±0.5.

Asphaltene chemical complexity poses a major challenge: there is not a distinctive molecular structure able to describe the whole range of field and laboratory observations on asphaltene behavior. Two main structural models have been proposed to represent asphaltene molecules, the continental structure and the archipelago structure. The continental structure consists of a highly condensed aromatic core surrounded by peripheral alkyl chains (Figure 2.1a). This was the dominant model for several decades and is supported by a variety of experimental techniques, including X-ray diffraction and mass spectrometry. However, this structure fails to explain key aspects in asphaltene behavior, such as the chemistry of the upgrading products, solvent entrainment within the molecular structure, and the occlusion of saturates and alkyl aromatic crude oil components within the asphaltene network (Chacón-Patiño *et al.*, 2017; Gray *et al.*, 2011).

The archipelago structure consists of smaller and more dispersed aromatic cores connected by alkyl bridges (Figure 2.1b). This structure better describes the afore mentioned asphaltene behavior. Recently it has been shown that many experimental methods are biased towards continental structures and fail to detect archipelago structures (McKenna *et al.*, 2013). It now appears that both continental and archipelago structures coexist in petroleum asphaltenes. The proportion of each structure is sample dependent (Mullins *et al.*, 2012).

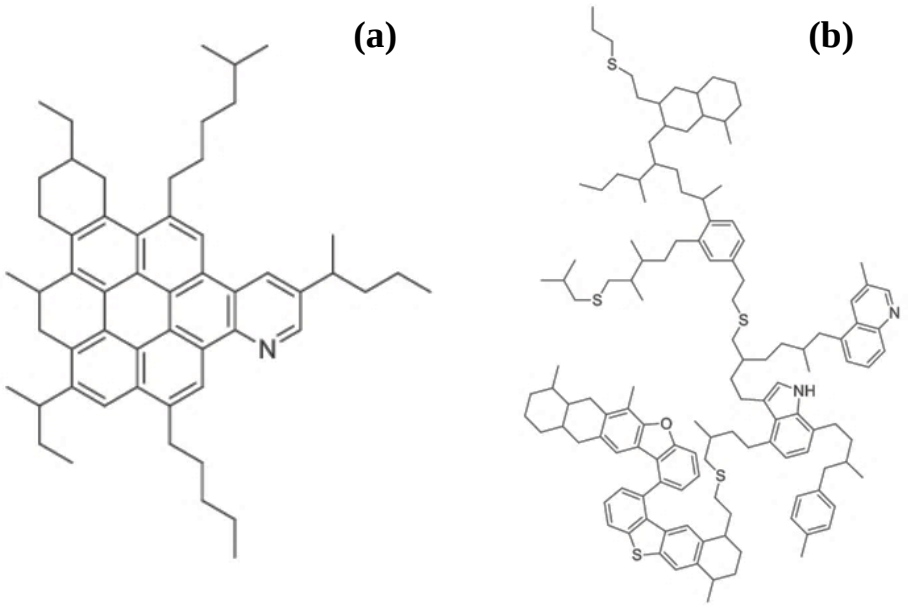

Figure 2.1. Representative molecular structures of asphaltenes: a) continental structure $C_{55}H_{69}N$ with a molecular weight of 744.14 g/mol; b) archipelago structure $C_{131}H_{178}N_2OS_5$ with a molecular weight of 1957.15 g/mol (Alshareef, 2020).

2.1.3. Asphaltene Self-Association

Asphaltenes tend to self-associate into molecular aggregates of colloidal dimension. Asphaltene self-association has been observed in different experimental techniques including vapor pressure osmometry (VPO) (Yarranton *et al.*, 2000), interfacial tension measurements (Rogel *et al.*, 2000; Yarranton *et al.*, 2000), isothermal titration calorimetry (Merino-Garcia and Andersen, 2003) and small-angle X-ray scattering (Dickie and Yen, 1967; Tanaka *et al.*, 2004). Due to their tendency to self-associate, the average molecular weight of asphaltenes increases with increasing asphaltene concentration and therefore different measurement techniques have produced a wide range of molecular weight values, ranging from 500 to 200,000 g/mol (McKenna *et al.*, 2013). VPO measurements show that molecular weight of an asphaltene monomer is approximately 1000 g/mol (Yarranton, 2005) but there are reported values ranging from 500 to 2100 g/mol (Acevedo *et al.*, 2005; Groenzin and Mullins, 1999; Wargadalam *et al.*, 2002) . VPO measurements also indicate that asphaltenes form nano-aggregates of 2-6 monomers with an average molecular weight ranging from 3000 to 10,000 g/mol (Yarranton *et al.*, 2000; Powers et *al.*, 2016).

The self-association mechanism is not yet fully understood and has been attributed to a variety of molecular interactions which are mostly governed by the molecular structure of the asphaltenes. The driving molecular interaction of the continental structure is considered to be π-π stacking. With the archipelago structure, aggregates can be held together either by π-π stacking, acid-base and/or hydrogen bonds (Yarranton, 2005).

There are two schools of thought regarding asphaltene self-association, colloidal theory and supramolecular theory. The colloidal theory states that asphaltene nano-aggregates are solid particles dispersed as a colloidal suspension. The asphaltene nano-aggregates are stabilized by resins that are either adsorbed onto or surround the nano-aggregates. This theory is supported by small angle X-ray scattering and X-ray diffraction, which validate asphaltene aggregation as the result of colloidal stacks held together via π-π bonds (Yen *et al.*, 1961).

In the colloidal perspective, asphaltene precipitation is considered to be a colloidal instability. If a disturbance such as the addition of a solvent causes sufficient resins desorb or leave the immediate surroundings of the nano-aggregates, then the attraction forces between the nano-aggregates cause them to aggregate creating larger structures that eventually can physically separate from the oil. Most colloidal models present asphaltene precipitation as an irreversible process, but it has been proven that asphaltene aggregates can dissociate upon changes in temperature or composition (Tanaka *et al.*, 2004). This theory also assumes that dilution of crude oil will drive away the resins surrounding asphaltenes allowing precipitation, however the opposite effect is observed when crude oil is diluted with toluene and other aromatic solvents. Finally, the colloidal theory is not consistent with the formation of liquid asphaltene-rich phases observed at elevated temperatures.

The supramolecular theory assumes that asphaltenes nano-aggregates are formed by asphaltenes, resins, and aromatic compounds in a manner analogous to polymerization (Agrawala and Yarranton, 2001). The nano-aggregates are not held together by chemical bonds but rather by a variety of mechanisms including dispersion forces, $\pi-\pi$ bonding, hydrogen bonding, and polar interactions. Some asphaltenes can contain multiple active sites capable of linking with more than one other asphaltene; hence, contributing to nano-aggregate growth. Other molecules may have only a single active site terminating the nano-aggregate growth. Molecules with multiple active

sites are mainly asphaltenes and are known as propagators. Molecules with single active sites are mainly resins and are known as terminators. The nano-aggregates are considered to be in solution with the oil medium.

In the supramolecular view, asphaltene precipitation is a conventional phase transition. This mechanism predicts reversible precipitation and is consistent with the formation of a liquid asphaltene-rich phase that includes components from other oil fractions and solvent. The models used for asphaltene precipitation (discussed later) all explicitly or implicitly assume that asphaltene nano-aggregates are dissolved rather than dispersed in the oil.

There is no conclusive evidence to determine which self-association mechanism is correct and possibly both mechanisms occur simultaneously. However, due to its relative simplicity and ability to predict asphaltene phase behavior, the supramolecular model and conventional phase equilibrium calculations will be used in this thesis.

2.2. Asphaltene Precipitation from Crude Oils

As mentioned before, asphaltene precipitation is a phase separation between asphaltene molecules/nano-aggregates and the crude oil that occurs upon changes in pressure, temperature and/or composition of the crude oil. There are several situations that can trigger asphaltene precipitation during the production and processing of crude oils including:

1. diluting a heavy oil (or bitumen) with a poor solvent (precipitant). The precipitant could be a light solvent (*e.g.*, carbon dioxide, nitrogen, methane) or a paraffinic solvent (*e.g.*, butane, pentane, heptane).
2. blending a crude oil with another crude oil or with a refinery product.
3. reacting a crude oil for example in visbreaking, cracking, and hydrotreating processes.
4. depressurizing a conventional oil.

In each case, it is necessary to predict the conditions at which asphaltene precipitation occurs to design and optimize operational processes. This thesis is concerned with non-reactive applications involving methane (Items 1 and 4) and these are discussed in more detail below.

2.2.1. Bitumen/n-Alkane Phase Behavior

Mixtures of bitumen and *n*-alkanes exhibit complex multiphase behavior, including vapor-liquid (VL), liquid-liquid (LL), vapor-liquid-liquid (VLL) and vapor-liquid-liquid-liquid (VLLL). The phase behavior depends on pressure, temperature, solvent content, *n*-alkane carbon number, and composition of the bitumen.

The phase behavior of methane and bitumen mixtures has been studied by Mehrotra and Svrcek (1988) for temperatures ranging from 15°C to 100°C and pressures up to 10 MPa and by Nourozieh *et al.*, (2016) for temperatures ranging from 50°C to 150°C and pressures up to 8 MPa. Both studies reported a well defined VL region, where the vapor phase at equilibrium was virtually pure methane. The solubility of methane in bitumen was less than 2 wt% (Figure 2.2a), which was not enough to trigger the formation of a second liquid phase.

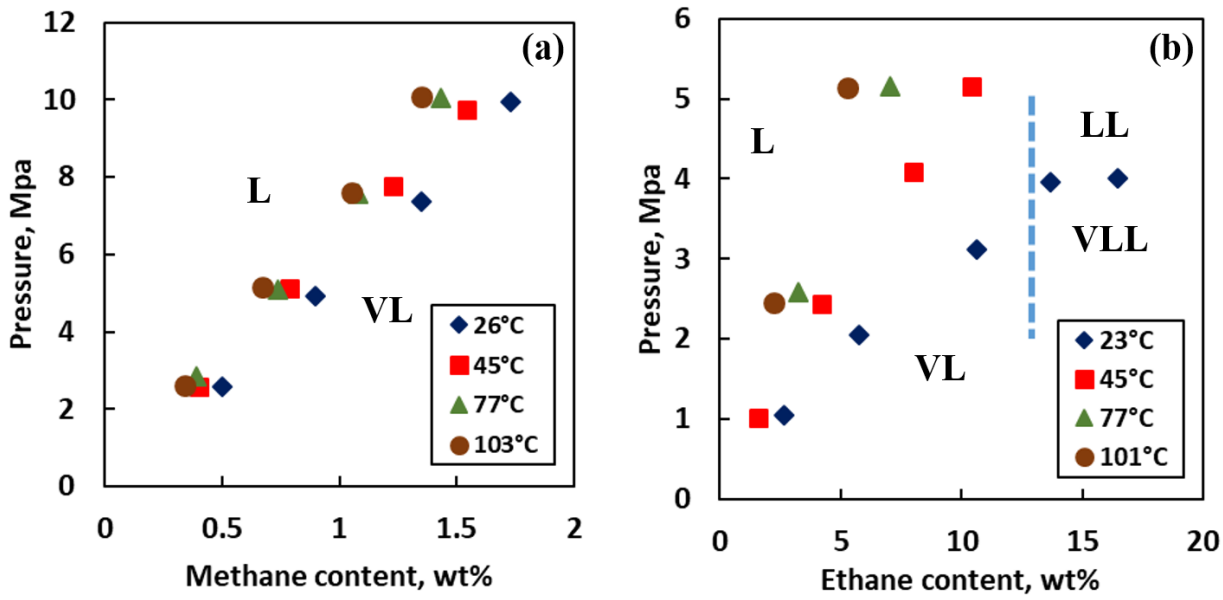

Figure 2.2. Pressure composition diagram for mixtures of Cold Lake bitumen and: a) methane; b) ethane. Data from Mehrotra and Svrcek (1988).

Ethane and bitumen mixtures can exhibit both VL and VLL regions, as shown in Figure 2.2b, at temperatures from 15°C and 100°C and pressures up to 10 MPa (Mehrotra and Svrcek,1988). Only VLE was observed for temperatures higher than 23°C because the ethane solubility decreases with

temperature (Fu *et al.*, 1988; Haddadnia *et al.*, 2018). Two liquid phases were observed at 23°C at ethane contents higher than 10 wt%; the two liquid phases were an ethane-rich phase (L_2) and a bitumen-rich phase (L_1). Nourozieh *et al.* (2016) measured the two liquid phase properties and compositions at 21°C for pressures up to 8 MPa and showed that increasing the pressure and/or the ethane content increased the separation of light components from the bitumen-rich phase.

The phase behavior of propane and Athabasca bitumen mixtures has been reported by Badamchi-Zadeh *et al.,* (2009) for temperatures from 10 to 50°C and pressures up to 1.5 MPa and by Nourozieh *et al.*, (2016) for temperatures from 50 to 200°C and pressures up to 10 MPa. Both studies reported the existence of VL and LL regions. Badamchi-Zadeh *et al.,* (2009) reported that the formation of the second liquid phase was observed at propane contents higher than 20 wt%. Dini *et al.*, (2016) outlined the phase diagram for a mixture of propane and Peace River bitumen at temperatures from 30 to 120°C and pressures from 1 to 6 MPa reporting VL, LL and VLL regions and defining the liquid phases as low density and high density. Mancilla-Polanco *et al.* (2018) studied the phase behavior of propane/bitumen mixtures at temperatures from 20 to 180°C and pressures up to 10 MPa reporting the existence of VL, LL and VLL regions (Figure 2.3). They observed that the second liquid phase formed at propane contents between 20 to 35 wt% depending on the pressure. The liquid phases were defined as a propane-rich phase (L_1) and an asphaltene-rich phase (L_2). Approximately 60 wt% of the bitumen partitioned to the asphaltene-rich liquid phase. They also found that the asphaltene-rich liquid phase morphology was a function of temperature and propane content. At temperatures below 90°C and propane contents less than 40 wt%, the asphaltene-rich phase appeared as solid particles (Figures 2.3a and 2.3b). At higher temperatures and propane contents, the asphaltene-rich phase was a liquid.

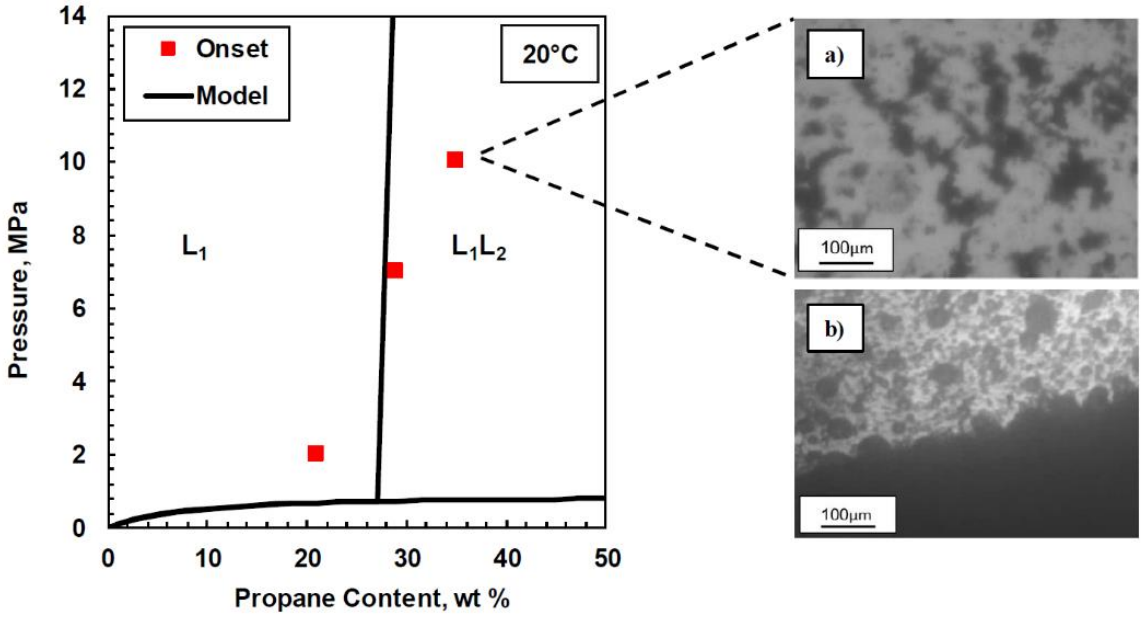

Figure 2.3. Pressure composition diagram for a mixture of propane and a Western Canadian bitumen at 20°C. Micrograph image of asphaltenes phase morphology at: a) 20°C and 10 MPa; b) 50 and 2 MPa. Data and images from Mancilla-Polanco *et. al*, (2018).

Most investigations on the phase behavior of butane and bitumen mixtures have focused on the solubility of *n*-butane in bitumen and reporting only VL regions (Yazdani and Maini, 2007; Nourozieh *et. al.*, 2017; Azinfar *et. al*., 2018). However, two studies have observed VLL regions as well. Gao and Li (2017) studied the phase behavior of water/*n*-butane/bitumen mixtures at temperatures up to 160°C and pressures up to 10 MPa reporting a WVLL region consisting of a water phase (W), a solvent-rich liquid phase, and an asphaltene rich liquid phase. Perez-Claro *et al.* (2019) studied the phase behavior of *n*-butane/bitumen mixtures at temperatures from 100 to 150°C and pressures from 2 to 10 MPa and they observed L, VL, LL and VLL regions. The second liquid phase appeared at *n*-butane contents higher than 39 wt% and was an asphaltene-rich liquid phase. Approximately 40 to 50 wt% of the bitumen partitioned to the asphaltene-rich liquid phase. The morphology of this phase depended on the temperature and *n*-butane content. At *n*-butane contents near 40 wt% and temperatures below 130°C, the phase consisted of small particles. At higher *n*-butane contents and temperatures above 130°C, it was a liquid.

Johnston *et al.* (2017a) examined the phase behavior of *n*-pentane/bitumen mixtures at temperatures from 23 to 180°C and pressures up to 10 MPa and reported L, VL, VLL and LL regions. The second liquid phase was an asphaltene-rich phase with approximately 25 wt% of the bitumen partitioning to this phase. It appeared at a solvent content of approximately 50 wt% at most temperatures and pressures.

Overall, the following general trends were observed for *n*-alkane diluted bitumen as the *n*-alkane carbon number increased: 1) the formation of the second liquid phase occurred at higher *n*-alkane contents; 2) the second liquid phase transitioned from a solvent-rich liquid phase to an asphaltene-rich liquid phase; 3) the saturation pressure of the mixture decreased due to the lower volatility of the solvent.

For flow assurance, it is important to determine the onset of asphaltene precipitation, where the onset is defined as the condition of temperature, pressure, or precipitant content at which the asphaltene-rich liquid phase first appears. For deasphalting process, it is necessary to determine not only the onset but also the amount and composition of the heavy phase. The amount of precipitation is often defined as a yield; that is, the mass of asphaltenes (or bitumen) that partitions into the heavy phase divided by the mass of bitumen in the feed. The yield data is commonly plotted versus the solvent content and presented as a solubility curve, as shown in Figure 2.4.

For *n*-alkane and bitumen mixtures, the asphaltene solubility increases (heavy phase amount decreases) with the carbon number of the *n*-alkane solvent. More solvent is required to initiate asphaltene precipitation when asphaltene solubility increases; that is, the onset increases. Asphaltene solubility increases with pressure, indicating that bitumen becomes a better solvent for asphaltenes due to the increase in the fluid density. Several studies have reported an increase in asphaltene solubility in *n*-pentane diluted bitumen as temperature increases up to 100°C (Akbarzadeh *et al.*, 2005; Hu and Guo, 2001; Johnston *et al.*, 2017a). Above 100°C the asphaltene solubility seems to slightly decrease. However, asphaltene solubility is not sensitive to temperature in propane and *n*-butane diluted bitumen (Mancilla-Polanco *et al.*, 2019; Perez-Claro *et al.*, 2019).

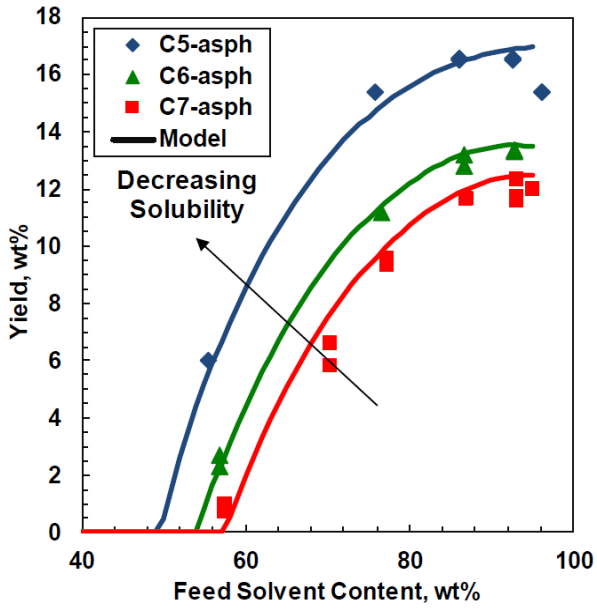

Figure 2.4. Asphaltene yield curve at room temperature for an Athabasca bitumen diluted with different *n*-alkanes. Data from Akbarzadeh *et al.*(2005).

2.2.2. Phase Behavior of Depressurized Live Oils

Asphaltene precipitation caused by depletion is common for highly under-saturated light to medium oils with low asphaltene contents (de Boer *et al.*, 1995; Joshi *et al.*, 2001). The reservoir pressure of a highly under-saturated oil is well above the bubble point such that the oil can experience large pressure drops without evolving any gas. When the oil is depressurized, its molar volume increases significantly with respect to asphaltene molar volume. This difference in molar volumes reduces the asphaltene solubility (see Section 2.3) and triggers asphaltene precipitation. As the pressure decreases, the amount of precipitated asphaltene increases reaching a maximum at the bubble point where the difference in the molar volumes of the oil and the asphaltenes is largest (minimum asphaltene solubility). Below the bubble point, the light components partition to the vapor phase and the density of the oil (liquid phase) increases, re-establishing some of the lost asphaltene solubility. At this point precipitated asphaltenes may redissolve into the oil, although the redissolution kinetics may be slow (days to months).

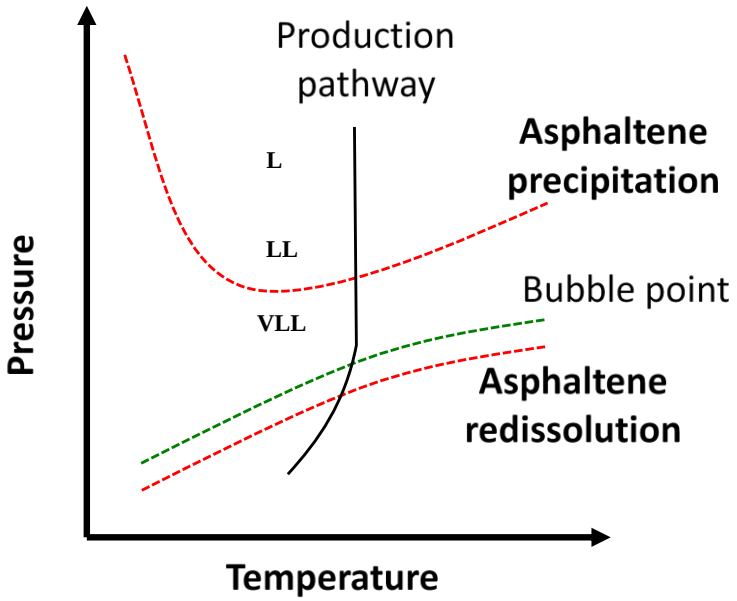

Figure 2.5. Typical Pressure-Temperature diagram for a live oil.

The stability of an oil with respect to asphaltene precipitation depends significantly on the methane content of the oil because methane is a very poor solvent for asphaltenes. Dehghani *et al*. (2007) studied the effect of pressure on asphaltene stability using two recombined oils with methane contents of 19 and 30 mol% respectively. More asphaltene precipitation was observed for the oil with the higher methane content, even though it was the oil with the lower content of heavy components.

Zanganeh *et al*. (2018) studied the effect of nitrogen, carbon dioxide and natural gas (CH_4) on pressure-induced asphaltene precipitation from a synthetic oil prepared using toluene and *n*-heptane. They observed that increasing methane composition from 5 to 20 mol% resulted in an increase of more than 60% in the mass of precipitated asphaltenes. They also investigated the morphology of precipitated asphaltenes using an image analysis software and reported that increasing temperature from 35 to 90°C increased the asphaltene particles diameter. They observed a similar behavior for carbon dioxide. Nitrogen did not affect the amount of asphaltene precipitation.

Romero-Yanes *et al.* (2020) observed the formation of an asphaltene rich-liquid phase in several mixtures of reservoir fluids (intermediate API) recombined with methane at a 75 mol% concentration. The liquid phase formed above the bubble point and disappeared below the bubble point for fluid samples with asphaltene contents lower than 1.0 wt%. The liquid phase remained for fluid samples with higher asphaltene contents demonstrating the limitations of asphaltene redissolution. This study showed that even at minimal asphaltene contents, crude oils will experience phase transitions when mixed with methane at high dilutions. They also investigated the morphology of the asphaltene rich-liquid phase, showing that precipitated asphaltenes appeared as solid particles that grew in size when the pressure was reduced.

2.3. Asphaltene Precipitation Models

The most common modeling approaches used to describe phase behavior of bitumen and solvent mixtures are equations of state (EoS) and activity coefficient models such as the regular solution theory. Equations of state can be used to determine the entire phase diagram but can be inaccurate in the LL region; that is, for asphaltene precipitation. Activity coefficient models only describe the LL region and, in petroleum applications, are used only to model asphaltene precipitation. Both modeling approaches are discussed in the following section.

2.3.1. Equations of State

Cubic Equations of State:

Cubic equations of state (CEoS) have been extensively applied in the oil and gas industry to predict phase equilibrium due to their good accuracy and relatively low mathematical complexity. There are several forms of CEoS and one of the most popular for hydrocarbon applications is the Peng-Robinson (PR) equation of state (Peng and Robinson, 1976), given by:

$$P = \frac{RT}{v-b} - \frac{a\alpha(T_r,\omega)}{v(v+b)+b(v-b)} \qquad \textbf{(2.1)}$$

where P is pressure, R is the ideal gas constant, T is the system temperature, v is the molar volume, a is an intermolecular attraction parameter, b is the volume occupied by one mole of molecules and the term $\alpha(T_r,\omega)$ is given by:

$$\alpha(T_r,\omega) = \left(1 + m\left(1-\sqrt{T_r}\right)\right)^2 \qquad \textbf{(2.2)}$$

where T_r is the reduced temperature and m is a function of the acentric factor (ω), given by:

$$m = 0.37464 + 1.5422\omega - 0.26992\omega^2 \quad \textbf{(2.3)}$$

For pure components, a and b can be written in terms of the critical properties, as follows:

$$a = 0.45724\frac{R^2T_c^2}{P_c} \quad \textbf{(2.4)}$$

$$b = 0.07780\frac{RT_c}{P_c} \quad \textbf{(2.5)}$$

where T_c and P_c are the critical temperature and pressure, respectively. For mixtures, a and b can be calculated from the pure component parameters using mixing rules. The classic van der Waals mixing rules are given by:

$$a_m = \sum_i \sum_j x_i x_j \sqrt{a_i a_j}\left(1 - k_{ij}\right) \quad \textbf{(2.6)}$$

$$b_m = \sum_i x_i b_i \quad \textbf{(2.7)}$$

where $a_m$and b_m are the corresponding PR-EoS parameters for the mixture, x_i and x_j are the mole fractions of component i and j, respectively, k_{ij} is a binary interaction parameter. The binary interaction parameter is usually determined minimizing the difference between the experimental data and the model predictions, therefore is considered as a fitting parameter. The van der Waals mixing rules are defined as symmetric because there is only one interaction parameter per binary pair ($k_{ij} = k_{ji}$). Symmetric mixing rules are unable to predict phase behavior of non-ideal mixtures and, in this case, asymmetric mixing rules ($k_{ij} \neq k_{ji}$) can be used to improve the model predictions.

The PR-EoS does not accurately predict liquid densities since it was originally tuned to reproduce vapor pressure data of pure non-polar substances. In order to improve liquid densities estimation Péneloux and Rauzy (1982) introduced a volume- translation parameter (c):

$$P = \frac{RT}{v - b} - \frac{a\alpha(T_r, \omega)}{(v + c)(v + b + 2c) + (b + c)(v - b)} \quad \textbf{(2.8)}$$

CEoS have been extensively applied to describe phase behavior of bitumen/solvent mixtures and, in particular, saturation pressures and gas solubilities (VLE). Mehrotra and Svrcek (1988) used the PR-EoS to model solubility data for mixtures of Cold Lake bitumen with nitrogen, methane,

carbon dioxide and ethane. Kokal and Sayegh (1990) used the PR-EoS with the volume-translation parameter proposed by Péneloux *et al.* to calculate the gas-saturated liquid densities of heavy oils at different pressures and temperatures. Jamaluddin *et al.* (1991) used a modified Martin EoS to predict the solubility data and the saturated liquid density of bitumen/CO_2 mixtures. The predictions were comparable, and sometimes more accurate than those obtained using a PR-EoS.

Castellanos-Díaz *et al.* (2011) proposed a characterization methodology using the Advanced Peng-Robinson (APR) equation of state to model phase behavior of bitumen and solvent mixtures including both VLE and LLE. Agrawal *et al.* (2012) tested this approach using a symmetric temperature dependent interaction parameter and successfully matched saturation pressures and liquid-liquid boundaries for mixtures of bitumen, methane, and CO_2. However, the model underpredicted asphaltene yields at high solvent dilutions. To overcome this failure, Johnston *et al.* (2017b) evaluated the APR-EoS using several asymmetric mixing rules for bitumen/*n*-pentane mixtures. They found that compositional dependant mixing rules improved asphaltene yield predictions but still were not able to capture the whole range of conditions. Similar results were presented by Mancilla-Polanco *et al*. (2018) for bitumen/propane mixtures, and by Perez-Claro *et al.* (2019) for bitumen/*n*-butane mixtures. It is possible that APR-EoS fails to predict phase compositions in the LL region at all conditions because it cannot account for the change in asphaltene properties due to self-association.

Cubic Plus Association (CPA)

The CPA equation of state is a combination of a physical term and an association term. The physical term describes the non-association molecular interactions like short-range repulsion and dispersion attractions and can be represented by a CEoS. The association term describes the polar interactions, such as asphaltene self-association. The version of CPA presented here was proposed by Kontogeorgis *et al.* (1996), where the physical term is given by Soave-Redlich-Kwong (SKR) and the association term was derived by Michelsen and Hendriks (2001), and is given by:

$$P = \frac{RT}{v-b} - \frac{a}{v(v+b)} - \frac{1}{2}\frac{RT}{v}\left(1+\rho\frac{\partial lng}{\partial\rho}\right)\sum_i x_i \sum_{A_i}\left(1-X_{A_i}\right) \qquad \textbf{(2.9)}$$

where a and b are intermolecular interaction parameters, ρ is the molar density, g is a radial distribution function, x_i is the mole fraction of component i, subscript A indicates the type of site

on a given molecule, and X_{A_i} is the fraction of site A in component i that is not bonded to other sites. The radial distribution is given by:

$$g = \frac{1}{1 - 1.9b\frac{1}{4v}} \tag{2.10}$$

The parameters a and b are given by:

$$a = 0.42747\frac{R^2T_c^2}{P_c}(1+c)\left(1-\sqrt{\frac{T}{Tc}}\right)^2 \tag{2.11}$$

$$b = 0.08664\frac{RT_c}{P_c} \tag{2.12}$$

where c is given by:

$$c = 0.48508 + 1.55171\omega - 0.15613\omega^2 \tag{2.13}$$

Parameters a and b for mixtures can be calculated from the pure component parameters using classical van der Waals mixing rules (Equations 2.6 and 2.7). The key element in the CPA EoS is the association strength ($\Delta^{A_iB_j}$), that is directly related with the variable X_{A_i} as follows:

$$X_{A_i} = \left(1 + \frac{1}{v}\sum_j x_j \sum_{B_i} X_{B_j}\Delta^{A_iB_j}\right)^{-1} \tag{2.14}$$

When $i \neq j$, the interaction represents cross-association and, when $i = j$, the interaction represents self-association. The self-association strength can be expressed as follows:

$$\Delta^{A_iB_i} = g\left[exp\left(\frac{\varepsilon^{A_iB_i}}{RT}\right) - 1\right]b_{ii}\beta^{A_iB_i} \tag{2.15}$$

where $\varepsilon^{A_iB_i}$ is the association energy, and $\beta^{A_iB_i}$ the association volume. The cross-association strength can be calculated using the following expression:

$$\Delta^{A_iB_j} = \sqrt{\Delta^{A_iB_i}\Delta^{A_jB_j}} \tag{2.16}$$

To apply the CPA-EoS each component must be classified according to the association type with a specific number of association sites per molecule (up to 4). Hence, the CPA requires the determination of the following parameters for each component: T_c, P_c, ω and k_{ij} for the physical term; and $\varepsilon^{A_iB_i}$ and $\beta^{A_iB_i}$ for the association term.

Li and Firoozabadi (2010) applied the CPA-EoS to model asphaltene precipitation from *n*-alkane diluted bitumens. In their work the physical term was described by PR-EoS, and the association term by the thermodynamic perturbation theory. The model always underpredicted *n*-pentane yields at high dilutions and overpredicted most yields at intermediate dilutions; but successfully captures asphaltene yield trends. The model also fails to match onset points. Later Li and Firoozabadi (2010) used the same approach to model the asphaltene precipitation in live oils from both depressurization and CO_2 mixing. They assumed that the cross-association energy was temperature dependant and successfully captured the bubble point, onset points and yields for different oils. Arya *et al.* (2015) also used a temperature dependant cross-association energy to model asphaltene precipitation from depressurization and from gas injection. The physical term was described by SRK-EoS. They successfully matched asphaltene onsets to the experimental data.

Shirani *et al.* (2012) and Nazemi *et al.* (2020) used a CPA-EoS to model asphaltene precipitation in live oil samples, both from depressurization and solvent injection. They used both the PR and SRK-EoS to describe the physical term and found that both can predict asphaltene precipitation, but the SKR had higher accuracy.

Zhang *et al.* (2019) used a CPA-EoS to model *n*-alkane diluted bitumen phase behavior, including onsets, yields and phase compositions. Two oil characterization approaches were proposed: CPA-C3 accounts for the self-association components based on the propane insoluble content and CPA-C5 based on the *n*-pentane insoluble content. In each case, the CPA parameters were tuned to asphaltene yields from one solvent. The CPA-C3 approach was able to predict yields for propane and higher *n*-alkanes carbon number mixtures. The CPA-C5 approach required less tuning and matched yield data for *n*-pentane and higher *n*-alkanes carbon number mixtures. However, it failed to predict asphaltene yields for propane diluted bitumen. The authors concluded that an asphaltene self-association energy distribution could improve CPA model predictions.

Perturbed Chain Statistical Association Fluid Theory (PC-SAFT)

Chapman *et al.* (1989) developed the SAFT-EoS to model phase equilibria of associating fluids by extending the Wertheim's first order thermodynamic perturbation theory. The SAFT theory

considers the reference fluid as a mixture of independent segments (hard spheres) which bond to form chain-like molecules. The theory predicts the change in the free energy upon bonding in terms of the residual Helmholtz energy (A^{res}), as the sum of tree terms contributions from different intermolecular forces (Figure 2.6). The residual Helmholtz energy is given by:

$$A^{res} = A^{seg} + A^{chain} + A^{assoc} \quad \textbf{(2.17)}$$

where A^{seg} is the contribution from the dispersion forces between segments, A^{chain} is the contribution from covalent bonds formed between chains, and A^{assoc} accounts for the contribution from association between molecules.

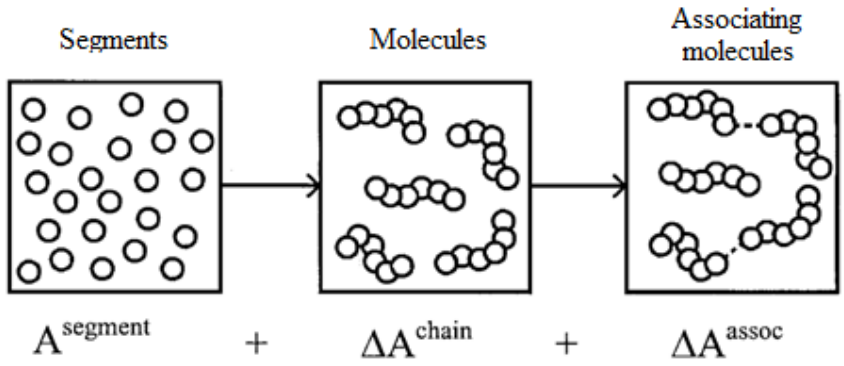

Figure 2.6. Residual Helmholtz energy contribution for SAFT EoS (Ting *et al.* 2003).

The perturbed-chain SAFT equation of state was developed by Gross and Sadowski (2001) who applied the second order Barker and Henderson's perturbation theory to properly account for the effect of the chain molecules length in the dispersion energy. The PC-SAFT equation assumes non-spherical molecules to be chains of jointed spherical segments. The model accounts for size and shape effects and has successfully been applied to large polymeric fluids similar to asphaltene molecules. The residual Helmholtz energy described by the PC-SAFT for mixtures of non-associating fluids is given by (Gonzalez *et al.* 2005):

$$A^{res} = A^{seg} + A^{chain} = m\left(A_0^{hs} + A_0^{disp}\right) + A^{chain} \quad \textbf{(2.18)}$$

where A_0^{hs} and A_0^{disp} are the hard-sphere and dispersion contributions to the Helmholtz energy respectively, and m is the average number of segments per molecule. The specific form for each term can be found elsewhere (Gonzalez *et al.* 2005). In addition to m, two more parameters are

required for each non-association component: the diameter of each molecular segment (σ) and the segment-segment interaction energy (ε/k). Although asphaltenes self-associate, it was assumed that asphaltenes are already associated as nano-aggregates and the self-association was not used; therefore is not discussed here.

PC-SAFT equation of state has been used to predict asphaltene precipitation induced by pressure depletion or gas injection in live oils (Gonzalez *et al.*, 2005; Panuganti *et al.*, 2012; Ting *et al.*, 2003). These studies fitted model parameters to asphaltene precipitation data from *n*-alkane titration and demonstrated that model predictions at other conditions were in good agreement with experimental data. Tavakkoli *et al.* (2016) used the PC-SAFT to model asphaltene precipitation from *n*-alkane diluted crude oils and developed a procedure that considered asphaltene polydispersity and the kinetics of asphaltene aggregation. Usually PC-SAFT parameters are tuned to asphaltene precipitation data at ambient conditions where time variability is not considered. Tavakkoli *et al.* (2016) showed that while asphaltene precipitation varied with time near the onset of precipitation, it was nearly invariant at a 90 wt% precipitant content. They recommended that the PC-SAFT asphaltene parameters be tuned at this condition to have a more accurate prediction of the onset and the amount of asphaltene precipitation. In general, PC-SAFT EoS is an effective tool to model asphaltene precipitation data; however, the model parameters must be tuned for each oil and each solvent limiting the predictive capability of the model.

2.3.2. Regular Solution Theory

The regular solution theory is an activity coefficient model that assumes a liquid-liquid equilibrium between a light phase (solvent-rich phase) and a heavy phase (asphaltene-rich phase). The equilibrium condition is obtained by equating the fugacities of component i in each liquid phase, as follows:

$$x_i^H \gamma_i^H f_i^0 = x_i^L \gamma_i^L f_i^0 \qquad \textbf{(2.19)}$$

where x_i and γ_i are the mole fraction and activity coefficient of component i, respectively, and superscripts H and L represents the heavy and light phase, respectively.

The composition of each liquid phase is calculated from the equilibrium ratios for each component (K_i). For a liquid-liquid equilibrium the standard state fugacity f_i^0 for both phases are equal and cancel out, then the equilibrium ratio is defined as follows:

$$K_i = \frac{x_i^H}{x_i^L} = \frac{\gamma_i^L}{\gamma_i^H}{}^H{}_i \tag{2.20}$$

In the Modified Regular Solution (MRS) theory, the activity coefficient of component i is the sum of an enthalpic and entropic contribution. The enthalpic term is based on the Scatchard-Hildebrand theory of regular solutions to account for the enthalpy of mixing of molecules with different cohesive energies (Hildebrand and Scott, 1962). The entropic term was added to account for the major differences in size of the components in solution. It is based on the Flory-Huggins lattice theory for polymer-like species (Flory, 1941; Huggins, 1941). The activity coefficient is then given by:

$$ln\,\gamma_i^\alpha = ln\,\gamma_{\mathrm{RS},i}^\alpha + ln\,\gamma_{\mathrm{FH},i}^\alpha \tag{2.21}$$

where superscript α denotes the heavy or light phase and subscripts FH and RS refer to the Flory-Huggins entropic contribution and the regular solution enthalpic contribution, respectively. The contributions are given by:

$$ln\,\gamma_{\mathrm{FH},i}^\alpha = ln\left(\frac{v_i}{v_m^\alpha}\right) + 1 + \left(\frac{v_i}{v_m^\alpha}\right) \tag{2.22}$$

$$ln\,\gamma_{\mathrm{RS},i}^\alpha = \frac{v_i^\alpha}{RT}(\delta_i - \delta_m)^2 \tag{2.23}$$

where v is the molar volume and δ is the solubility parameter at the temperature and pressure of the system, the subscript m denotes the mixture, R is the universal gas constant and T is temperature. The activity coefficient for component i can be rewritten as follows:

$$ln\,\gamma_i^\alpha = ln\left(\frac{v_i}{v_m^\alpha}\right) + 1 + \left(\frac{v_i}{v_m^\alpha}\right) + \frac{v_i^\alpha}{RT}(\delta_i - \delta_m)^2 \tag{2.24}$$

When Equation 2.24 is substituted in Equation 2.20 the following expression for the equilibrium ratio of component i is obtained:

$$K_i = exp\left[\frac{v_i^H}{v_m^H} - \frac{v_i^L}{v_m^L} + \frac{v_i^H}{RT}(\delta_i^H - \delta_m^H)^2 + \frac{v_i^L}{RT}(\delta_i^L - \delta_m^L)^2\right] \tag{2.25}$$

The inputs parameters of the MRS model are the molar volumes and solubility parameters of each component in the mixture.

The first attempt to model asphaltene precipitation using the regular solution theory was made by Hirschberg *et al.*, (1984). They treated asphaltenes as a single component and concluded that a more detailed characterization was necessary to obtain better predictions. The MRS model was adapted by Alboudwarej *et al.*, (2003) to predict asphaltene precipitation from *n*-alkane diluted bitumens at atmospheric conditions. The bitumen was divided into pseudo-components based on the SARA fractions, and the asphaltenes were divided into fractions of different molecular weigh. Later, Akbarzadeh *et al.*, (2005) applied the MRS model at various temperatures (0 to 100°C) and pressures (up to 7 MPa) and proposed correlations to estimate the solubility parameters of saturates and aromatics as a function of temperature. The model accurately predicted the asphaltene precipitation data as shown in Figure 2.7. Powers *et al.*, (2016) used the MRS model to fit asphaltene precipitation data and developed a correlation to estimate the asphaltene solubility parameter for native and reacted oils. Yarranton *et al.*, (2018) updated the correlations to calculate the solubility parameters of saturates, aromatics and resins.

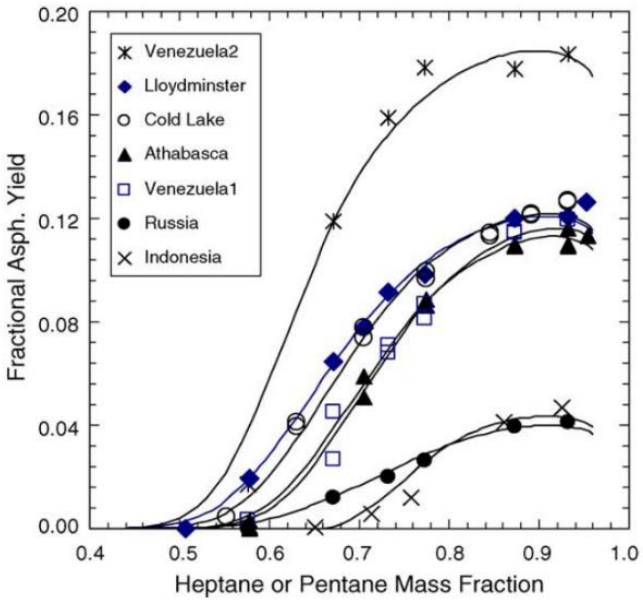

Figure 2.7. Asphaltene precipitation yield from various crude oils diluted with *n*-heptane (or *n*-pentane for the Indonesian oil) at 23°C. Data from Akbarzadeh *et al.*, (2005).

A major disadvantage of the MRS model is its inability to calculate phase compositions due to the assumption that only asphaltenes and resins partition into the heavy phase. Recently, Ramos-Pallares and Yarranton, (2020) extended the MRS model to account for the partitioning of all components into the heavy phase. The updated model can successfully predict the compositions of the liquid phases formed in *n*-alkane diluted bitumens.

Different authors successfully determined the onset of asphaltene precipitation for crude oils diluted with *n*-alkanes using a regular solution approach (Esmaeili and Maaref, 2018; Mofidi and Edalat, 2006; Wang and Buckley, 2001). The MRS model coupled with a kinetic model was applied to predict the asphaltene precipitation during the hydrocracking of a heavy oil (Félix and Ancheyta, 2020). Various modifications to the Flory-Huggins model have been reported in the literature to improve the prediction of asphaltene precipitation from *n*-alkane and crude oil mixtures using a regular solution approach. Shahebrahimi and Zonnouri (2013) modified the entropic contribution of the regular solution theory by combining the Flory-Huggins model with the Non-Random Two Liquid (NRTL) model. They obtained more accurate results for both the onset and the amount of asphaltene precipitation compared to other models. Nourbakhsh *et al.*, (2011); Pazuki and Nikookar, (2006) added an adjustable parameter to the Flory-Huggins theory, defining the interaction parameter between the asphaltenes and the solvent as a function of their molecular weight.

Tharanivasan *et al.*, (2011) adapted the MRS model to predict asphaltene precipitation caused by compositional changes and depressurization from live oils. They characterized the heavier oil components into SARA fractions and assigned properties to these fractions following the methodology of Akbarzadeh *et al.* (2005). The solubility parameters of light *n*-alkanes were calculated using gas solubility data reported in the literature. The densities of light *n*-alkanes when dissolved in the liquid phase were calculated using effective liquid densities correlations. The model predicted the density of the live oil and was tuned to match the onset and amount of asphaltene precipitation. More recently, Ferreira, (2020) used the MRS model to fit the precipitation data from mixtures of bitumen, *n*-pentane and CO_2 in order to estimate the solubility parameter of the dissolved CO_2. However, the application of the MRS model to live oils has been limited because the solubility parameters of other dissolved gases are unknown.

Chapter 3. Experimental Methods

This chapter describes the experimental techniques used to collect the phase behavior data presented in this thesis. The experimental data to be collected are illustrated in Figure 3.1 as solid symbols. The left-hand figure is a pressure-composition phase diagram that shows the phase boundaries encountered in the fluids studied in this thesis; V is vapor, L_1 is the light liquid phase (solvent-rich liquid phase), and L_2 is the heavy liquid phase (asphaltene-rich liquid phase). The vapor-liquid boundary (VL_1) was determined in a blind cell apparatus using the constant composition expansion method. The onset point is the solvent content at which the second liquid phase first appears. The right-hand plot shows the yields which are defined as the mass of certain material in the heavy phase, divided by the mass of bitumen in the feed. "C_5-Asphaltene" indicates the *n*-pentane insoluble asphaltenes and "Pitch*" refers to the solvent-free bitumen content in the heavy phase. The liquid-liquid (L_1L_2) boundary was determined visually with a solvent titration in a High-Pressure Microscope (HPM). The yields and phase compositions (in terms of solvent, maltenes, and C5-asphaltenes) were measured at different solvent concentrations within the liquid-liquid region in a blind cell apparatus. The apparatus and procedures are described in more detail below.

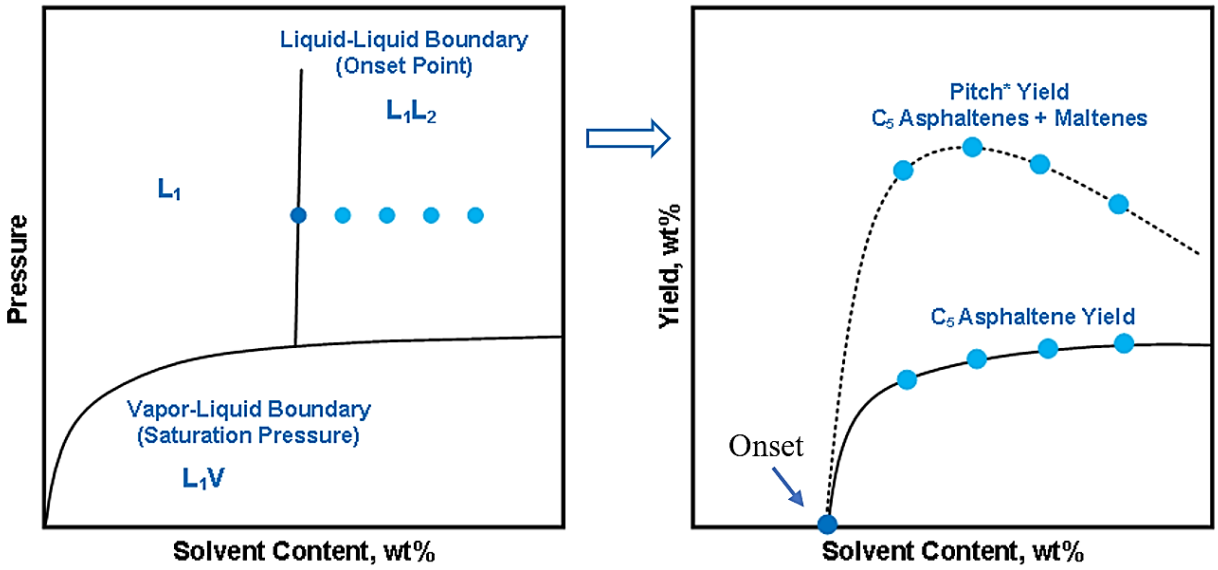

Figure 3.1. Phase behavior data to be collected for methane/n-pentane diluted bitumen.

3.1. Materials

The samples in this study were prepared using WC-B-A3 bitumen where WC = Western Canada, B = bitumen, A3 is a specific reservoir. This sample was the fifth from that reservoir used in our research group and its properties may vary slightly from previously reported results. The bitumen was supplied by CNOOC International Ltd. (JACOS) and was originally obtained from a SAGD process and was previously treated to remove water and solids. The residual water content was less than 1.5 wt%. Selected properties and the SARA assay of the WC-B-A3 bitumen are presented in Table 3.1. The SARA assay includes saturates, aromatics, resins, asphaltenes and toluene insolubles (TI); toluene insolubles include sand, clay, and some adsorbed hydrocarbons. The SARA assay was performed by Elaine Baydak following an experimental procedure described elsewhere (H. Alboudwarej et al., 2002). The density and viscosity of the bitumen were measured in a previous study (Ferreira, 2020). Data from another bitumen (WC-B-B3) were used in part of this study (Johnston *et al.*, 2017a). Selected properties for this bitumen are also provided in Table 3.1. Technical grade *n*-pentane and toluene (purity > 99%) were purchased from Fischer Chemical. Methane (purity > 99%) was purchased from Praxair.

Table 3.1. Selected properties and SARA assay of WC-B-A3 bitumen from this study and the WC-B-B3 bitumen from (Johnston *et al.*, 2017a).

Property	**WC-B-A3**	**WC-B-B3**
Specific Gravity	1.010	1.020
Viscosity at 50°C and 0.1 MPa, mPa·s	6,600	3,100
Saturates, wt%	20.01	17.00
Aromatics, wt%	37.97	47.10
Resins, wt%	21.54	16.70
C_5-Asphaltenes, wt%	20.44	19.20
Toluene Insolubles (TI), wt%	0.04	-

3.2. Vapor-Liquid Boundary: Saturation Pressure

The saturation pressures were measured for mixtures of solvent and WC-B-A3 bitumen at solvent contents up to 30 wt% and temperatures ranging from 50 to 130°C. The solvent was a mixture of methane and *n*-pentane, with methane contents ranging from 5 to 20 wt%. The saturation pressures were measured using a blind cell apparatus, shown in Figure 3.2. The apparatus consists of five

100 cm³ stainless-steel cylinders (blind cells) each equipped with floating pistons but no mixers. The volume of fluid in the blind cells (and hence the pressure) is controlled by a variable volume positive displacement pump (Quizix Q5000 SP-5200 Pump System) used to inject or remove hydraulic oil. The maximum operating pressure for each blind cell is 70 MPa. The blind cells are housed in an air bath which controls temperature within ± 0.1°C and can operate at temperatures ranging from 20 to 300°C.

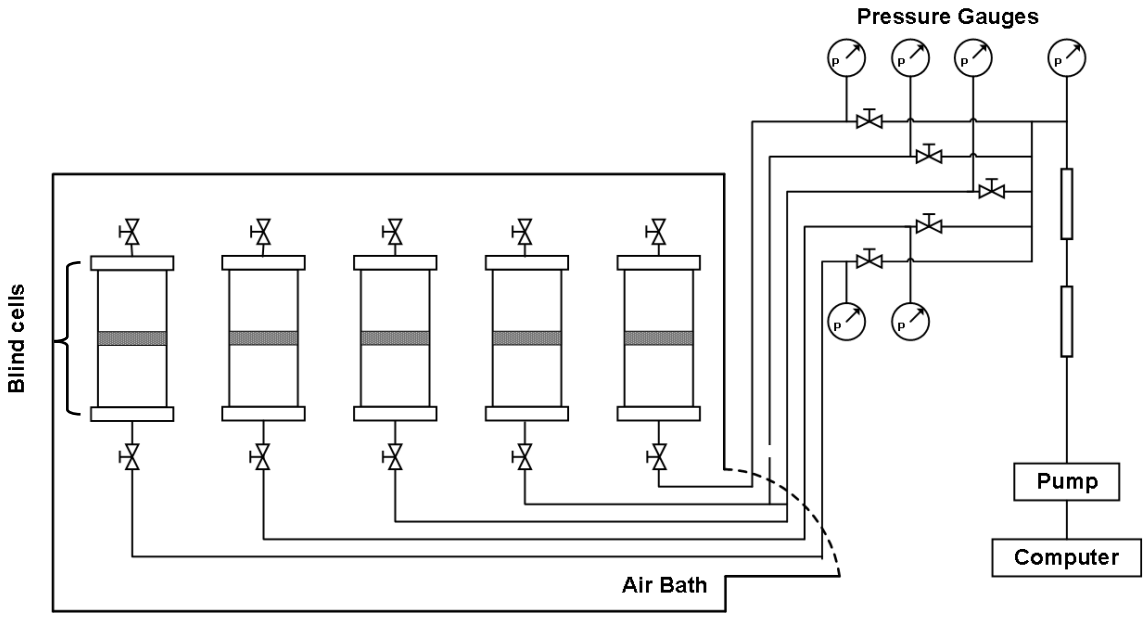

Figure 3.2. Schematic of the blind cell apparatus (Johnston, 2017b)

The mixtures were prepared in 100 cm³ stainless-steel cylinders (blind cells). To prepare the mixtures, the floating piston was temporarily fixed at the bottom of each blind cell and known masses of bitumen and *n*-pentane were added at atmospheric conditions. Both end caps of the blind cell were attached leaving an air-filled space of known volume, termed the available volume. A positive displacement pump was used to displace methane into the cell from a stainless-steel transfer cylinder filled with methane at its saturation pressure. The final pressure in the blind cell was set to obtain a target methane mass based on the ideal gas law as follows:

$$P_f = \frac{m_{C_1}}{V_{avail}} \frac{RT}{MW_{C_1}} \quad \textbf{(3.1)}$$

where P_f is the pressure in the blind cell, m_{C1} is the target mass of methane injection, M_{C1} is the molecular weight of methane, V_{avail} is the available volume in the blind cell, T is temperature, and

R is the universal gas constant. The fraction of the air in the air/methane filled space was 1.5 mol% and was shown to have negligible effect on the measured saturation pressure (Appendix A). The mass of the blind cell was recorded before and after the addition of each fluid. The mass of each fluid was determined from the change in mass with a precision of ± 0.01 g.

The blind cells were then pressurized to well above the saturation pressure of the mixture at the test conditions. The cell was inverted twice a day for 7 days to mix the fluids. After mixing, the sample fluid was compressed to a pressure well above its expected saturation pressure at the experimental temperature. The air bath was set at the experimental temperature and the sample fluid was left to equilibrate for 24 h. The saturation pressure was determined following a stepwise isothermal volume expansion. The volume was measured by the computer-controlled pump with a precision of ±0.001 cm^3. The saturation pressure was then determined in two ways: 1) from the pump response as discussed below; 2) from the change in slope of the pressure-volume isotherm as described elsewhere (Agrawal *et al.*, 2012).

The pump was run in the pressure mode and the pressure set point was decreased stepwise. After each step, sufficient time was given for the pressure to stabilize. When the mixture was in the liquid phase, the hydraulic oil flow rate from the pump was nearly zero within approximately 15 minutes, indicating that the mixture had reach the equilibrium (less than ± 0.010 cm^3 variation in flow rate at constant temperature and pressure). At pressures below the saturation pressure, the setpoint pressure was not stable after 15 minutes and the pump continuously withdrew hydraulic oil to compensate the pressure exerted by the evolving gas in the mixture. The saturation pressure was taken to be the intermediate pressure between the lowest pressure at which the hydraulic oil flow rate stabilized and the highest pressure at which did not stabilized. After the saturation pressure was detected, the pump was run in the volume mode and controlled volumes of hydraulic oil were removed from the system. After each volume step, the system was considered to have reached equilibrium when the pressure and temperature were constant for at least one hour. The equilibrium pressures were plotted against the cumulative hydraulic oil volume and the saturation pressure was determined from the change in slope of the pressure-volume isotherm, as shown in Figure 3.3. The saturation pressures from the pressure-volume isotherm were used for data validation only and were within 190 kPa of the pump method measurements in all cases. The

uncertainty of the pressure-volume based saturate pressures is ±200 kPa based on a 90% confidence interval (Johnston *et al.*, 2017a). Hence, the uncertainty of the saturation pressure from the pump response is no more than ±200 kPa.

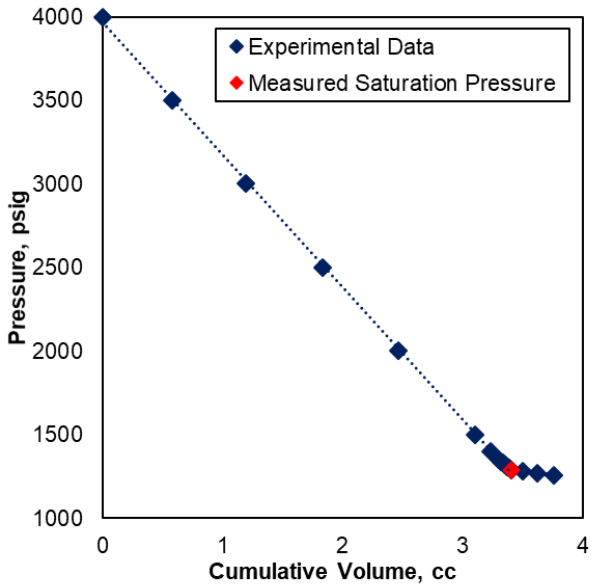

Figure 3.3. Pressure-volume isotherm for a 15 wt% solvent in bitumen at 130°C.

3.3. Density Measurements

The densities of the solvent mixtures of methane and *n*-pentane were measured using an Anton Paar DMA 4500M U-tube density meter at temperatures from 21 to 130°C and pressures from 10 to 60 MPa. The density meter was connected to a stainless-steel transfer cylinder and a PVT cell, each equipped with a floating piston. The transfer cylinder and the PVT cell were connected to a positive displacement pump that maintained a constant pressure in the density meter. The temperature of the system was controlled by an air bath to within ±0.01°C. A schematic of the apparatus is shown in Figure 3.4.

The solvent mixture was prepared at a specified ratio of methane to *n*-pentane in the transfer cylinder. A known mass of liquid *n*-pentane was added to the cylinder at atmospheric conditions. Then, methane was injected to a target pressure and its mass was determined gravimetrically.

Finally, the mixture was pressurized well above its saturation pressure at atmospheric temperature and the transfer cylinder was inverted twice a day for 3 days to mix the fluids.

A volume of 50 cm^3 of the solvent mixture was injected to the apparatus from the transfer cylinder, and then to the PVT cell. The temperature and pressure of the system were set to the experimental conditions and the density was measured once the system have reached the equilibrium. The equilibrium condition was that both density and temperature were constant for 30 min. The precision and repeatability of the measurement were 0.01 and 0.05 kg/m^3, respectively (Ramos-Pallares *et al.*, 2017)

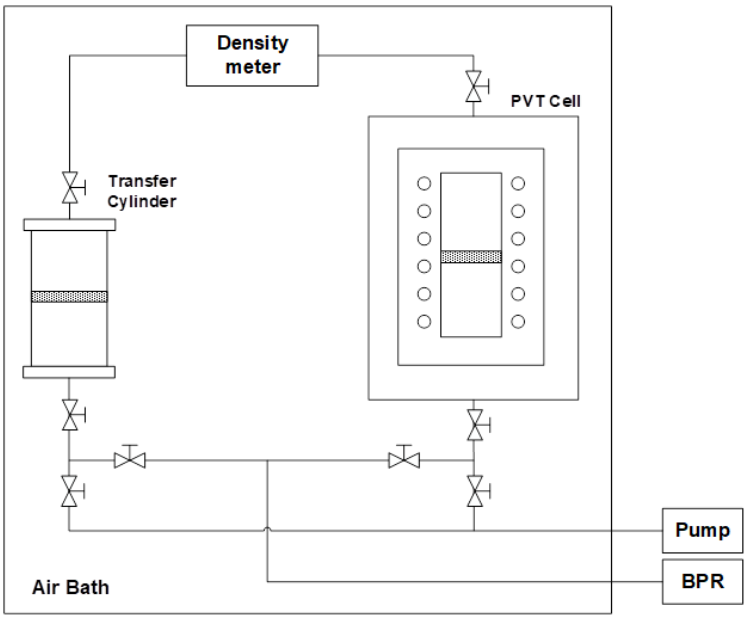

Figure 3.4. Schematic of the density meter apparatus used to measure solvent densities at elevated pressures and temperatures.

3.4. Liquid-Liquid Boundary: Onset of Asphaltene Precipitation

The onsets for mixtures of solvent and WC-B-A3 bitumen were measured at temperatures of 21 and 130°C and pressures of 10 and 60 MPa. The onset was detected visually using a High-Pressure Microscope (HPM) coupled with a PVT cell, Figure 3.5. The HPM system consists of a cell with two sapphire windows, a light source and a high focal length camera connected to a computer to capture digital images and videos. The gap between the windows is adjustable (100-400 µm) and

was set to 100 µm. The HPM system is placed in-line between two high pressure cylinders with floating pistons and magnetic stirrers, both of which are connected to a computer-controlled pump and a back-pressure regulator (BPR). The pump and the BPR are used to push fluid back and forth between the mixing cylinders through the gap between windows in the HPM. The HPM is rated for temperatures up to 200°C and pressures up to 70 MPa. The dead volume of the apparatus is required to accurately determine the injected fluid volumes that enter the mixing cylinders and is 7.7 ±0.2 cm³ (Agrawal *et al.*, 2012).

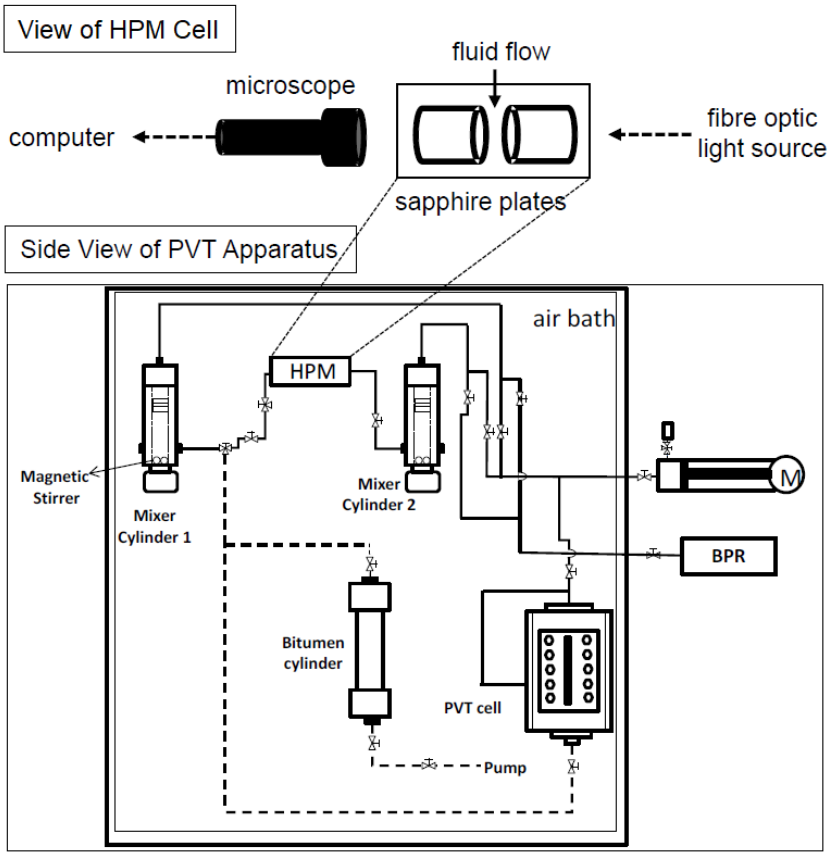

Figure 3.5. Schematic of High-Pressure Microscope (HPM) apparatus (Agrawal *et al*. 2012).

The onset point (L_1L_2 boundary) was measured by titrating the bitumen with the solvent mixture of methane and *n*-pentane. The procedure from Agrawal *et al*. (2012) was followed. Prior to any measurement, the HPM assembly was cleaned with toluene and vacuum-dried at 130°C to remove any toluene traces. The floating pistons of both mixing cylinders were displaced to the bottom of

each cylinder and the experimental pressure was set on the hydraulic oil side of the pistons using the BPR. The initial pump reading, the mass of the hydraulic oil container, the temperature, and the pressure were recorded.

A specified amount of bitumen was injected into Mixing Cylinder 1 of the HPM (sample cylinder) while maintaining a constant pressure. The pump reading, mass of the hydraulic oil container, temperature, and pressure were recorded after the bitumen injection. The volume of injected bitumen was determined in two ways: 1) from the difference between the initial and the final pump readings; 2) from the volume of displaced hydraulic oil after adding the dead volume. The pump reading was taken as the accurate measurement and the hydraulic oil displacement was used only for validation. On average, the hydraulic oil displacement was within 3% of the volume from the pump readings. The mass of the bitumen injected was calculated from the calculated injected volume and its density at experimental conditions.

The solvent was first injected at a pressure above the saturation pressure (liquid state) in a cleaned and vacuumed PVT cell. Then, the methane/*n*-pentane mixture was injected stepwise (at a constant flow rate of 10 cm^3/h for each step) from the PVT cell to the mixing cylinder that contained the bitumen. The volume injected ranged from an amount equivalent to a 5 wt% solvent increment at the first injection to a 2 wt% increment near the onset. The average injection time was approximately 30 min. This relatively low flow rate was used to avoid high local solvent concentrations that would lead to undesired premature asphaltene precipitation. The magnetic stirrers in the mixer cylinders were turned on both during solvent injections and sample mixing. After each injection step, the volume of injected solvent was determined from cathetometer readings of the PVT cell and verified with the pump readings of displaced volume during the injection. The contents of the mixing cylinder were displaced slowly to the other mixing cylinder to displace the solvent remaining in the transfer line. Then, the fluid in the HPM was moved back and forth between the two cylinders, typically 4 to 5 times for a total of 90 minutes, until the mixture was visually uniform for at least one pass. During this process, the sample fluid was observed using the HPM cell to determine if a second phase had formed. The stepwise injection of solvent was repeated until a second phase was observed. The total time from the first injection to the observed onset was typically 2 weeks.

The solvent content at the heavy phase onset point was reported as the intermediate content between the highest content at which no phase was observed and the lowest content at which the second phase appeared, Figure 3.6. Note that a small number of particles are visible below the onset, Figure 3.6a. These are mostly toluene insoluble particles such as sand and clay inherent in the bitumen (Mullins *et. al.*, 2007). These particles are visible in all non-opaque images below the onset of precipitation. There may also be some prematurely precipitated asphaltene particles caused by high local solvent concentrations at the solvent/bitumen interface after an injection step; however, most of these premature asphaltenes tend to redissolve after mixing. The onset is detected by a significant increase in number of visible particles, Figure 3.6b. The uncertainty in the onset measurement is half the increment of the titration (typically 2 to 3 wt%) plus 0.5 wt%, giving a combined uncertainty of ±1.5 to ±2 wt%.

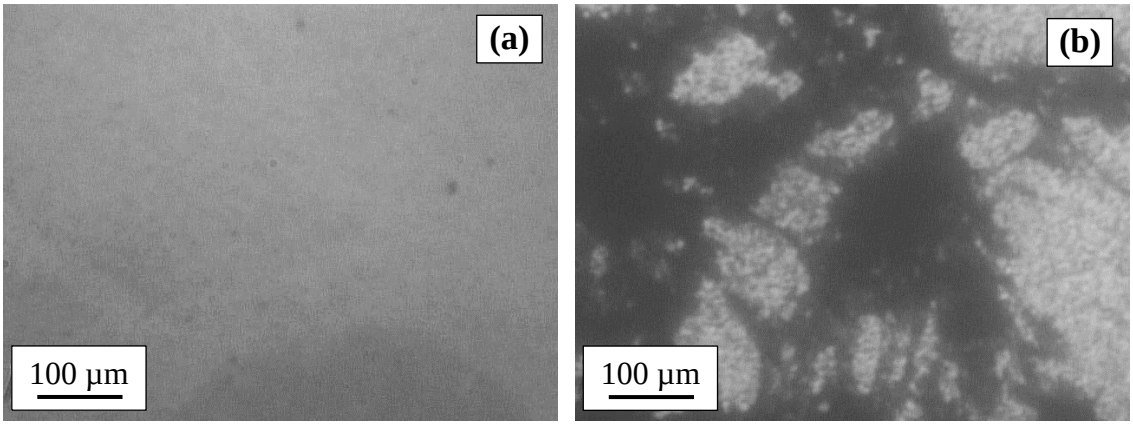

Figure 3.6. HPM micrographs of WC-B-A3 bitumen diluted with a solvent mixture of 13 wt% methane and 87 wt% *n*-pentane at 21°C and 10 MPa: a) 35 wt% solvent (below onset); b) 37 wt% solvent (above onset). The onset was reported as 36 ±1.5 wt% solvent. The particles visible in (a) are toluene insoluble material such as sand and clay.

3.5. Asphaltene Yields Determination

The asphaltene yield is defined as the mass of precipitated asphaltenes divided by the mass of bitumen in the feed. The asphaltene yields at atmospheric conditions for mixtures of WC-B-A3 bitumen and *n*-pentane were determined following a bench top procedure. The yields at elevated temperatures and pressures of WC-B-A3 bitumen, *n*-pentane, and methane mixtures were determined using a blind cell apparatus by simultaneously solving the component material

balances for the heavy and the light phase. In the blind cell apparatus, only the composition of the light phase can be measured because the location of the interface between the two liquid phases is unknown. Therefore, in order to solve the material balances, the solvent content in the heavy phase must be assumed. This assumption adds to the overall uncertainty of the yield determination.

3.5.1. Bench Top Procedure

To determine the yields at atmospheric conditions (21°C and 0.1 MPa) a series of solutions with known masses of WC-B-A3 bitumen and solvent with different solvent contents were prepared in 30 cm^3 centrifuge vials. The solutions were sonicated and agitated for 1 hour and left to settle 24 hours. Each mixture was then centrifuged at 4000 rpm for 5 minutes and the supernatant was pipetted out of the vials. The precipitate was washed with approximately 20 cm^3 of the solvent, sonicated and agitated for 1 hour, and left to settle for 24 hours. The solutions were centrifuged at 4000 rpm for 5 minutes and the supernatant was removed. Finally, the precipitate was dried first in a fume hood for 24 hours and then in a vacuum oven at a temperature of 60°C until the mass was constant.

The precipitate contains mineral solids and organic compounds that co-precipitate with the asphaltenes but are insoluble in toluene (Mullins *et. al.*, 2007). The concentration of toluene insoluble (TI) in the WC-B-A3 bitumen was quantified in the SARA analysis. The asphaltene+TI yields were calculated as the mass of precipitated asphaltenes divided by the initial mass of bitumen. The yields were then adjusted to a TI-free basis. The data are reported as an asphaltene solubility curve where the yield of precipitated TI-free asphaltenes is plotted versus the weight fraction of solvent. The repeatability of the yield is ±0.65 wt% based on a 95% confidence interval and numerous repeats for different oils over many years.

3.5.2. Blind Cell Procedure

The blind cell apparatus described in Section 3.2 was configured to determine asphaltene yields and light phase compositions at elevated pressures and temperatures. The apparatus was modified to collect the light samples as shown in Figure 3.7. The sample cylinders are identical in design to the blind cells.

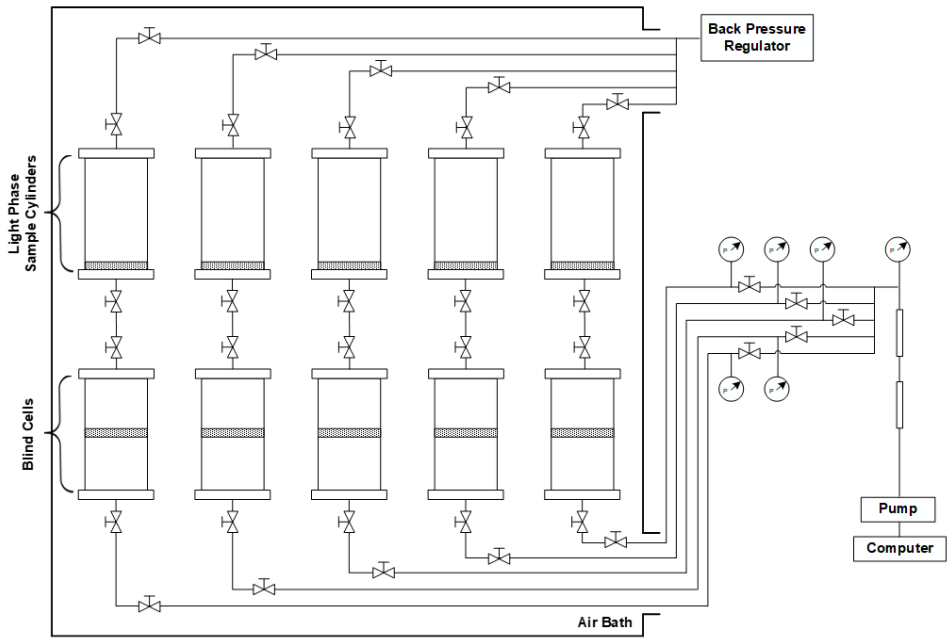

Figure 3.7. Schematic of the blind cell apparatus configured for yield measurements.

The fluid samples used in these experiments were a mixture of WC-B-A3 bitumen, *n*-pentane, and methane. Temperatures of 21 and 130°C and pressures of 10 and 60 MPa were selected to span the range of typical reservoir conditions for crude oils. The experimental maximum methane content was set to avoid the formation of a vapour phase; that is, so that the saturation pressure was below the experimental pressure. The saturation pressure calculation is provided in Section 5.2. The methane content for the fluid samples used in the blind cell apparatus are provided in Table 3.2.

Table 3.2. Methane content of the samples used in the blind cell apparatus.

Apparatus	Pressure MPa	Temperature °C	Methane Content wt%
Blind Cells	10	21	5
	10	130	5
	10	21	8
	10	130	8
	60	21	8
	60	130	8
	60	21	16
	60	130	16

The feed samples were prepared using the same procedure described in Section 3.2. The filled feed sample cylinders were connected to the blind cell apparatus, brought to the experimental pressure and temperature, and mixed by inverting the cylinders twice a day for four days. After mixing, the cylinders were oriented so that the heavy pitch phase settled on the floating piston and left to equilibrate for a minimum of three days. Then at least two light phase samples were collected. The cylinders used to collect the light phase samples were identical to feed sample cylinders except nitrogen was used instead of hydraulic oil. The floating piston of each light phase sample cylinder was placed at the topmost position to minimize the dead volume set at the experimental pressure. To collect a sample, a light phase sample cylinder was connected to the feed cylinder through a 1/8-inch stainless-steel line. The pump was used to displace a target volume from the feed blind cell to the sample cylinder and a back pressure regulator was used to maintain the pressure of the sample cylinder at the experimental pressure. The dead volume from the feed blind cell to the light phase sample cylinder was approximately 1 cm^3. When the light phase sample was collected at high temperatures, the sample cylinder was left to cool at room temperature for one day.

Figure 3.8 summarizes the methodology used to determine the light phase composition. Subsamples of the light phase were collected in order to calculate its composition. To collect a subsample, a target mass of the light phase was slowly removed from the sample cylinder through a 1/8-inch stainless-steel line to a glass vial. The total mass of the subsample was determined from the change in mass of the sample cylinder. The solvent (methane + *n*-pentane) evaporated at the exit of the stainless-steel line. It was assumed that the evaporation losses between the cylinder and the glass vial were only solvent. The remaining fluid in the glass vial (maltenes + asphaltenes) was let to dry in a fume hood at 21°C and atmospheric pressure for 7 days and then it was transferred to dry under vacuum at 60°C until its mass was constant. The evaporated solvent mass was determined gravimetrically as the difference between the total mass of the subsample and the residual mass in the glass vial.

The residue (pitch*) was diluted to a 90 wt% *n*-pentane content to separate the pentane insoluble asphaltenes (C_5-asphaltenes) from the maltenes. The mixture was sonicated and agitated until the residue was completely dispersed and it was left to settle for 24 hours. Then, the samples were centrifuged at 4000 rpm for 5 minutes, and the supernatant was pipetted out. The residue was again

diluted with 90 wt% *n*-pentane and the above steps were repeated. After the final supernatant was removed, the residue (C_5-asphaltenes) was left to dry in a vacuum oven at 60°C until the mass was constant. The C_5-asphaltene content was the mass of the dried final residue divided by the initial mass of the light phase subsample. The maltene mass was the difference between the initial and final mass of the residue. Finally, the light phase composition was determined from the masses of solvent (methane and *n*-pentane combined), maltenes, and C_5-asphaltenes obtained from the subsample.

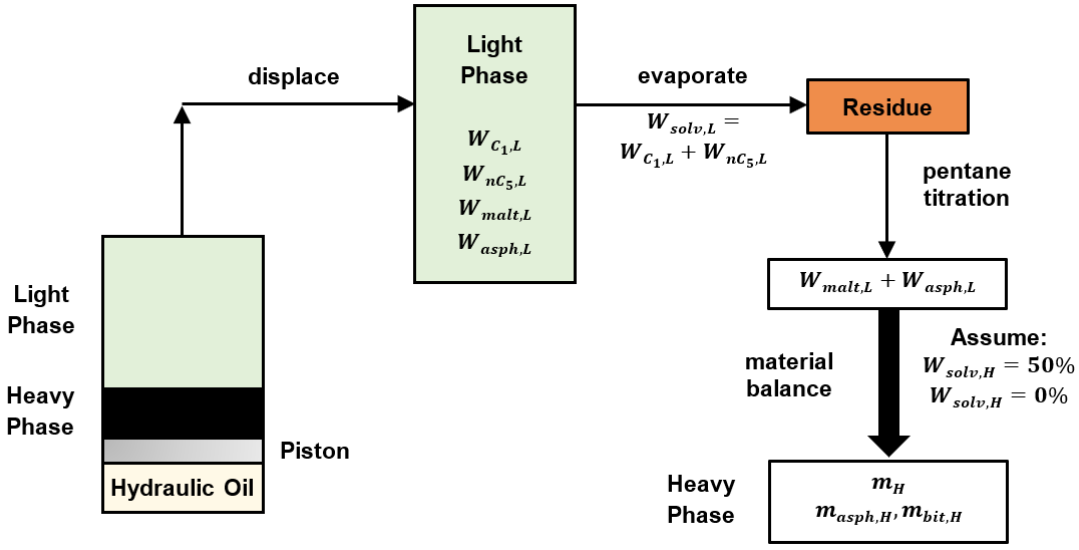

Figure 3.8. Sample collection methodology to measure light phase composition and yields using the blind cell apparatus.

Mass Balances and Yield Calculation:

The C_5-asphaltene and pitch* yields were determined from a material balance. The material balance for a single component is as follows:

$$w_i{}^F - w_i{}^L - \frac{H}{F}(w_i{}^H - w_i{}^L) = 0 \qquad \textbf{(3.2)}$$

where w_i is the mass fraction of component *i*, *H/F* is the mass ratio of the heavy phase to feed, and superscripts *F*, *L*, and *H* denote the feed, light phase and heavy phase respectively. To determine the *H/F* ratio, the material balances of the three components (solvent, maltenes, and C_5-asphaltenes) were solved simultaneously by adjusting *H/F* to minimize the following objective function (OF):

$$OF = \sum_{i-1}^{3} \left| {w_i}^F - {w_i}^L - \frac{H}{F}({w_i}^H - {w_i}^L) \right| \quad \textbf{(3.3)}$$

Once the *H/F* ratio was determined, the mass of each component in the light and heavy phase was calculated from the split ratio and the known feed mass. The C_5-asphaltene and pitch* yields were then calculated as follows:

$$Y_A = \frac{{w_A}^H}{1-{w_S}^F}\frac{H}{F} \quad \textbf{(3.4)}$$

$$Y_{P*} = \frac{1-{w_S}^H}{1-{w_S}^F}\frac{H}{F} \quad \textbf{(3.5)}$$

where *Y* is yield and subscripts *A*, *P**, and *S* denote C_5-asphaltenes, pitch* and solvent respectively.

Without the heavy phase composition, there was one too many degrees of freedom to solve for the *H/F* ratio. Therefore, the following assumptions were made to constrain the material balance; these assumptions were based on precipitation data collected for similar bitumen/solvent systems (Johnston *et al.*, 2017a; Perez-Claro, 2019).

- specify a solvent content in the heavy phase between 0 and 50 wt%
- all component contents must be between 0 and 100 wt%

The C_5-asphaltene and pitch* yields were determined assuming 0, 25, and 50 wt% solvent in the heavy phase. The value at 25 wt% is the reported value and the values at 0 and 50% were used to determine the uncertainty of the yields (see Appendix B for details). The combined uncertainty of the C_5-asphaltene yields ranges from ±1.5 wt% near the onset to ±0.6 wt% at high dilution. The combined uncertainties of the pitch* yields ranged from ±14 wt% closer to the onset to ±8.5 wt% at higher dilutions.

Chapter 4. Asphaltene Precipitation Modeling

This chapter presents the methodology followed in this thesis to predict asphaltene precipitation from bitumen, *n*-pentane and methane mixtures using the Modified Regular Solution (MRS) model (Akbarzadeh *et al.*, 2005; Ramos-Pallares and Yarranton, 2020). The model is briefly reviewed to elucidate the model assumptions. The model inputs are the feed composition, molar volume, and solubility parameter of each component in the mixture. The previously developed fluid characterization methodology, including correlations and values used to calculate the model inputs are presented here. The modifications made to the model for methane diluted bitumen are discussed in Chapter 5.

4.1. Modified Regular Solution (MRS) Model

The regular solution theory is an activity coefficient approach based on the internal energy of mixing for athermal regular solutions. This theory was first applied to model asphaltene precipitation by Hirschberg *et al.* 1984 who treated asphaltenes as a single component. They modified the regular solution theory by adding an entropic contribution term based on the Flory-Huggins polymer solution theory to account for the major difference in sizes between asphaltenes and other molecules in solution. Later, the model was updated to treat asphaltenes as a mixture of pseudo-components and successfully predicted both the onset and the amount of asphaltene precipitation from an *n*-alkane diluted bitumen (Kawanaka *et al.*, 1991; Yarranton and Masliyah, 1996). The modified regular solution model has been extended to model asphaltene precipitation in mixtures of heavy oils and *n*-alkane solvents, live oils, blends and reacted fluids (Akbarzadeh *et al.*, 2004, 2005; Alboudwarej *et al.*, 2001; Powers, 2014; Tharanivasan *et al.*, 2011; Tharanivasan and Yarranton, 2012). In these versions of the model, only asphaltenes and resins are allowed to partition to the heavy phase. Ramos-Pallares and Yarranton, (2020) extended the model to account for the partitioning of all components into the heavy phase.

A liquid-liquid equilibrium is assumed between a light liquid phase (solvent-rich phase) and a heavy liquid phase (asphaltene-rich phase). For any two phases in equilibrium, the fugacities of component i in each phase are equal and given by:

$$f_i = \gamma_i x_i f_i^0 exp\left[\int_0^P \frac{v_i dP}{RT}\right] \quad \textbf{(4.1)}$$

where γ is the activity coefficient, x is the mole fraction, f^0 is the standard fugacity, v is the molar volume, P is pressure, R is the ideal gas constant and T is the absolute temperature. The equilibrium constant, K, is the ratio of the mole fractions of component i in each phase and is calculated as follows:

$$K_i = \frac{x_i^H}{x_i^L} = \left(\frac{\gamma_i^L}{\gamma_i^H}\right)\left(\frac{{f_i^0}^L}{{f_i^0}^H}\right) exp\left[\int_0^P \frac{\Delta v_i dP}{RT}\right] \quad \textbf{(4.2)}$$

where superscripts H and L refers to the heavy and light phase, respectively. For a liquid-liquid equilibrium the last two terms of Equation 4.2 are unity and the expression reduces to:

$$K_i = \frac{x_i^H}{x_i^L} = \frac{\gamma_i^L}{\gamma_i^H} \quad \textbf{(4.3)}$$

In the modified regular solution theory, the activity coefficient of component i is the sum of the Flory-Huggins entropic contribution, and the Scatchard-Hildebrand enthalpic contribution for regular solutions as follows:

$$ln\,\gamma_i^\alpha = ln\,\gamma_{\mathrm{RS},i}^\alpha + ln\,\gamma_{\mathrm{FH},i}^\alpha \quad \textbf{(4.4)}$$

where superscript α denotes the heavy or light phase and subscripts FH and RS refer to the Flory-Huggins entropic contribution and the regular solution enthalpic contribution, respectively. The two contributions are given by:

$$ln\,\gamma_{\mathrm{FH},i}^\alpha = ln\left(\frac{v_i}{v^\alpha}\right) + 1 - \left(\frac{v_i}{v^\alpha}\right) \quad \textbf{(4.5)}$$

$$ln\,\gamma_{\mathrm{RS},i}^\alpha = \frac{v_i}{RT}\sum_j^n \sum_k^n \phi_j\,\phi_k\left(D_{ij} - 0.5D_{jk}\right) \quad \textbf{(4.6)}$$

where v is the molar volume at the temperature and pressure of the system, ϕ is the volume fraction, and n is the total number of components in the mixture. The volume fraction of component i is defined as:

$$\phi_i = \frac{x_i v_i}{\sum x_i v_i} \quad \textbf{(4.7)}$$

and the term D_{jk} is defined as follows:

$$D_{jk} = \left(\delta_j - \delta_k\right)^2 + 2l_{jk}\delta_j\delta_k \quad \textbf{(4.8)}$$

where δ is the solubility parameter at the temperature and pressure of the system and l_{jk} is the interaction parameter between the two components j and k.

For asphaltene precipitation modeling, the mixture is defined as a solution of asphaltene nano-aggregates with the other oil components and any added solvent. Once the nano-aggregates are formed, it is assumed that they are stable and the mixture can be treated as a solution with no specific interactions between components. Therefore, the interaction parameter is zero and Equation 4.6 reduces to:

$$ln\,\gamma_{\mathrm{RS},i}^{\alpha} = \frac{v_i}{RT}(\delta_i - \delta^{\alpha})^2 \qquad \textbf{(4.9)}$$

Equations 4.5 and 4.9 are combined to obtain the following expression for the activity coefficient of component i:

$$ln\,\gamma_i^{\alpha} = ln\left(\frac{v_i}{v^{\alpha}}\right) + 1 - \left(\frac{v_i}{v^{\alpha}}\right) + \frac{v_i}{RT}(\delta_i - \delta^{\alpha})^2 \qquad \textbf{(4.10)}$$

The solubility parameter of the light or heavy phase is calculated as a volumetric average of all components in the phase. Similarly, the molar volume of the light or heavy phase is determined as the molar average of all components in the phase.

The model, as described above, provides accurate predictions of asphaltene precipitation from heavy oils diluted with *n*-alkane solvents. However, it is applied with the assumption that only asphaltenes and resins can partition to the heavy phase and therefore it cannot provide predictions for the total amount and composition of the heavy phase. Ramos-Pallares and Yarranton (2020) adapted the regular solution approach for the partitioning of all components between the two liquid phases. They developed the following expressions for the activity coefficients of each phase:

$$ln\,\gamma_i^{L} = ln\left(\frac{v_i}{v^{L}}\right) + 1 - \left(\frac{v_i}{v^{L}}\right) + \frac{v_i}{RT}(\delta_i - \delta^{L})^2 \qquad \textbf{(4.11)}$$

$$ln\,\gamma_i^{H} = \frac{v_i}{RT}(\delta_i - \delta^{H})^2 \qquad \textbf{(4.12)}$$

In other words, the light phase remains a regular solution with the Flory-Huggins entropic term, but the heavy phase is a true regular solution, as originally defined by Hildebrand. The different formulations for each phase seem to represent different end points in an unknown excess entropy function. The light phase is consistent with the maximum configurational entropy of mixing predicted from the Flory-Huggins theory by considering the dissimilarity in molecular sizes of the

mixture components. For the heavy phase, molecules are considered to have similar sizes resulting in an entropy of mixing lower than the one predicted by the Flory-Huggins theory and closer to the ideal entropy of mixing. Hence, the model is an approximation that may not apply at all conditions. For example, the model may not accurately represent the entropy of a phase at intermediate dilutions where the molecular configuration of the mixture does not approach either of the extremes in the configurational entropy of mixing. The model also does not apply at the mixture critical point where the composition and activity coefficients of both liquid phases must be the same. Nonetheless, the model matches a wide range of asphaltene precipitation data (including the amount of the heavy phase) from heavy oils diluted with *n*-alkanes.

Once the equilibrium constants are calculated, the phase equilibrium compositions for each component can be calculated using standard techniques. The yields are calculated from the heavy phase compositions and the amount of bitumen in the feed. The inputs to the model are the temperature and pressure plus the mass or mole fraction, molecular weight, density, and solubility parameter of each component.

4.2. Fluid Characterization for the MRS Model

To use the model, the fluid must be characterized into pure and/or pseudo-components and the properties of each component determined at the specified temperature and pressure. The solvent is a mixture of pure components (methane and *n*-pentane). The pure component properties are known, except for the methane solubility parameter. The bitumen is divided into pseudo-components representing the SARA fractions (saturates, aromatics, resins and asphaltenes) plus a toluene insoluble fraction. The properties required for the MRS model (density, molecular weight, and solubility parameter) are presented below for each component and pseudo-component.

4.2.1. Solvent Properties

Molecular Weight

The methane and *n*-pentane molecular weights are 16.0425 g/mol and 72.1488 g/mol, respectively (Linstrom and Mallard, 2021).

Density

An effective density correlation is used to calculate the density of methane and *n*-pentane in a liquid phase. The effective density is defined as the density of a component when it is dissolved in a liquid phase. It is recommended for pure components that are gases at a given temperature and pressure because the effective density can be used in a regular solution mixing rule to obtain a more accurate mixture density. The effective densities are calculated from the following expression (Saryazdi *et al*., 2013):

$$\rho = (a_1 + a_2 T) + [(b_1 + b_2 T)P] \tag{4.13}$$

where a_1, a_2, b_1, b_2 are fluid specific parameters, T is the temperature in K, and P is the pressure in MPa. The specific parameters for methane and *n*-pentane are shown in Table 4.1.

Table 4.1. Parameters for the effective liquid density correlation for the solvent, Eq. 4.13. (Saryazdi et al., 2013).

Component	a_1 **kg/m³**	a_2 **kg/(m³ K)**	b_1 **kg/(m³ K MPa)**	b_2 **kg/(m³ K MPa)**
Methane	532.157	-0.69737	0.42606	0.001143
n-Pentane	878.006	-0.82817	-0.09229	0.002648

Solubility Parameter

The solubility parameter of methane is discussed in Chapter 5. The solubility parameter of *n*-pentane is calculated using the following correlation proposed by Barton, (1991):

$$\delta_{TP,i} = \delta_{T_o P_o,i} \sqrt{\frac{\rho_{T_o P,i}}{\rho_{T_o P_o,i}}} - k_i (T - T_o) \tag{4.14}$$

where k is the temperature dependence of the solubility parameter in $MPa^{0.5}/K$, subscript TP indicates the temperature and pressure of the system, and subscript o indicates the standard condition (25°C and 0.1MPa). The solubility parameter of *n*-pentane at standard conditions is reported by Barton as 14.40 $MPa^{0.5}$. The temperature-dependent parameter, k, has a value of 0.0232 $MPa^{0.5}/K$ (Akbarzadeh *et al.*, 2005).

4.2.2. Saturates, Aromatics and Resins Properties

Molecular Weight

The molecular weight for the saturates, aromatics, and resins are presented in Table 4.2 and correspond to average values determined in previous studies (Yarranton *et al.*, 2018).

Table 4.2. Molecular weight for the SAR fractions (Yarranton *et al.*, 2018).

Fraction	Molecular Weight kg/kmol
Saturates	440
Aromatics	500
Resins	1050

Density

The densities for the saturate and aromatic fractions are determined from the following correlation (Tharanivasan *et al.*, 2011):

$$\rho_i = \left(a_{o,i} + b_{o,i}T + c_{o,i}T^2\right)exp\left[\left(a_{1,i} + b_{1,i}T\right)P\right] \quad \textbf{(4.15)}$$

where ρ is the density in kg/m³, a_o, b_o, c_o, a_1, and b_1 are fluid specific parameters, and subscript i indicates either the saturate or aromatic pseudo-component. The fluid specific parameters are presented in Table 4.3.

Table 4.3. Parameters for the saturate and aromatic density correlation, Eq. 4.15. (Tharanivasan *et al.*, 2011).

Fraction	a_o kg/m³	b_o kg/(m³ K)	c_o kg/(m³K²)	a_1 x 10^4 MPa^{-1}	b_1 x 10^4 MPa^{-1} K^{-1}
Saturates	1053.44	-0.5457	-0.000150	-3.113	-3.150
Aromatics	1163.45	-0.5457	-0.000150	-2.681	-2.659

The resins are assumed to be incompressible, therefore only the temperature dependence is considered to calculate their density, as follows:

$$\rho_{resins} = \rho_{resins}^{25℃} - m_{resins}(T - 298.15) \quad \textbf{(4.16)}$$

where ρ is the density in kg/m³, $\rho^{25°C}$ is the density at standard conditions (25°C and 0.1MPa), and m represents a specific constant. The density of the resins at standard conditions is set to the minimum density of asphaltenes at standard conditions, that is, 1047 kg/m³. The specific constant, m, has a value of 0.659 kg/(m³K) (Akbarzadeh *et al.*, 2005).

Solubility Parameter

The solubility parameters of the saturates, aromatics and resins at non-standard conditions are calculated using equation 4.14. The properties needed to calculate the solubility parameter of the SAR fractions are summarized in Table 4.4. The solubility parameters of saturates and aromatics at standard conditions (25°C and 0.1MPa) correspond to average values determined in previous studies (Ramos-Pallares and Yarranton, 2020). The values for the temperature-dependent parameter (k) for saturates and aromatics are taken from Akbarzadeh *et al.*, (2005). The solubility parameter of resins is set to the minimum asphaltene solubility parameter (δ_{min}); and the temperature-dependent parameter (k) for the resins is set to the same value as asphaltenes.

Table 4.4. Solubility parameter at standard conditions, 25°C and 0.1 MPa; (Ramos-Pallares and Yarranton, 2020) and temperature dependence of the solubility parameter (**k**) for SAR fractions, Eq. 4.18; (Akbarzadeh *et al.*, 2005).

Fraction	$\boldsymbol{\delta^{25°C}}$ **MPa$^{0.5}$**	$\boldsymbol{k}$ **MPa$^{0.5}$/K**
Saturates	16.5	0.0222
Aromatics	19.3	0.0204
Resins	δ_{min}	0.0191

4.2.3. Asphaltenes Properties

Asphaltenes are considered as a polydisperse distribution of self-associating molecular aggregates. Therefore, asphaltene properties used in the MRS model (density, molecular weight, and solubility parameter) are also represented as distributions. In this study, the *n*-pentane insoluble asphaltenes (C_5-asphaltenes) are divided into pseudo-components of varying molecular weights, as discussed below.

Molecular Weight

The molecular weight distribution for C_5-asphaltenes is described with the Gamma probability function (Akbarzadeh *et al.*, 2005) given by:

$$f(MW) = \frac{(MW - MW_m)^{\beta-1}}{\Gamma(\beta)}\left[\frac{\beta}{(MW_{avg} - MW_m)}\right]^{\beta} exp\left[\beta\frac{(MW - MW_m)}{(MW_{avg} - MW_m)}\right] \quad \textbf{(4.17)}$$

where MW is the molecular weight in g/mol, β is a factor which determines the shape of the distribution, and subscripts m and avg indicates the monomer molecular weight and the average molecular weight, respectively. In this study, the gamma distribution is divided into 30 pseudo-components, each representing a molecular weight interval of the same width starting from the monomer molecular weight to the maximum molecular weight of the C_5-asphaltenes distribution. The sub-fractionation is required to represent the shape of the yield curve since smaller or less polar asphaltenes partition less to the heavy phase than larger more polar asphaltenes. This difference in their partition coefficients can only be represented with multiple pseudo-components. Using 30 C_5-asphaltene pseudo-components minimized the deviations between the model predictions and the experimental measurements. The number of C_5-asphaltene pseudo-components can be reduced to 10 to improve computation speed without losing much accuracy but such optimization was not needed for this study. The gamma distribution parameters used in this study are MW_m = 800 g/mol, MW_{avg} = 3,000 g/mol, MW_{max} = 15,000 g/mol , and β = 2.1, as recommended by Powers *et al.* (2016).

Density

C_5-asphaltenes are assumed to be incompressible and only the temperature dependence is considered to calculate their density. The densities of each of the C_5-asphaltenes pseudo-components are calculated as follows:

$$\rho_{A,i} = \rho_{A,i}^{25^{\circ}C} - m_i(T - 298.15) \quad \textbf{(4.18)}$$

where ρ is the density in kg/m^3 of the i_{th} pseudo-component, $\rho^{25^{\circ}C}$ is the density at standard conditions (25°C and 0.1MPa) of the i_{th} pseudo-component, m is a component-specific constant, and subscript A indicates any C_5-asphaltene pseudo-component. The component-specific constant, m, is calculated using the following correlation (Ramos-Pallares *et al.*, 2016):

$$m_i = 3.1635 - 0.00239\rho_{A,i}^{25℃} \quad \textbf{(4.19)}$$

The density of each C_5-asphaltene pseudo-component at standard conditions is calculated using the following expression (Powers *et al.*, 2016):

$$\rho_{A,i}^{25℃} = 1047 + 151.4\left[1 - exp\left(-9W_{A,i}\right)\right] \quad \textbf{(4.20)}$$

where $W_{A,i}$ is the cumulative mass fraction of the i_{th} pseudo-component.

Solubility Parameter

The solubility parameter at standard conditions for each C_5-asphaltene pseudo-component is calculated using the following expression (Powers *et al.*, 2016):

$$\delta_{A,i}^{21℃} = \delta_{min} + (\delta_{max} - \delta_{min}){W_{A,i}}^{1.2} \quad \textbf{(4.21)}$$

where the subscripts min and max denote the minimum and maximum solubility parameters in the asphaltene distribution, respectively. The values of δ_{min} and δ_{max} are determined by fitting the asphaltene precipitation data.

Two steps are necessary to apply the model to the mixtures of bitumen, *n*-pentane, and methane examined in this study: 1) the model must be extended to pressures up to 60 MPa because the previous model was only tested to 10 MPa; 2) correlations must be provided for the solubility parameter of methane. The effective densities of the *n*-alkanes are already established up to 60 MPa. The pressure dependence of the saturate and aromatic properties is established up to 10 MPa and the relationship to pressure is assumed to hold up to 60 MPa. The pressure dependence of the resin and asphaltene properties was previously assumed to be negligible and was updated as is discussed in Section 5.1.2. The determination of the methane solubility parameters is discussed in Section 5.2.3.

4.3. MRS Model Implementation

The modified regular solution (MRS) model is implemented using a MATLAB code previously developed by the Heavy Oil Properties and Processing Research Group. The input properties for the model are calculated using the correlations and values presented in Section 4.2 or in Chapter 5. The asphaltene precipitation data at different conditions is calculated using a two-phase flash algorithm that finds the solution to a Rachford-Rice equation. To initialize the flash algorithm,

initial estimates of the equilibrium ratios are set to the activity coefficient of the light liquid phase. Flash calculations are performed until the difference between two consecutive K_i calculations is less than $1 \cdot 10^{-17}$. The outputs of the model include the mass and composition of each phase from which the C_5-asphaltene and pitch* yields are calculated and reported. The C_5-asphaltene yield is the mass of the defined asphaltene components in the heavy phase divided by the mass of bitumen in the feed. The pitch* yield is the mass of the bitumen components in the heavy phase divided by the mass of bitumen in the feed.

Chapter 5. Results and Discussion

This chapter presents the methodology followed to determine the solubility parameter of dissolved methane in a crude oil. First, the existing correlations to determine the maximum and minimum solubility parameter of the asphaltene pseudo-components are extended to 60 MPa by tuning the Modified Regular Solution (MRS) model to asphaltene precipitation data from bitumen and *n*-pentane mixtures. Next, since data for the saturation pressures of mixtures of bitumen, *n*-pentane, and methane were not available, the saturation pressures were measured to ensure that there is no vapor phase at the conditions of the subsequent asphaltene precipitation measurements. Then, the methane solubility parameters are determined by fitting the MRS model to the onsets of precipitation from bitumen, *n*-pentane and methane mixtures. The fitted parameters are compared against literature values and; finally, a temperature and pressure dependent correlation to calculate the methane solubility parameter is proposed.

5.1. Determination of Asphaltenes Solubility Parameters

5.1.1. Onset and Yield Data

The asphaltene yields from WC-B-A3 bitumen diluted with *n*-pentane were measured at atmospheric conditions using the bench top procedure presented in Section 3.5.1. These measurements and those from a previous study (Ferreira, 2020) are presented in Table 5.1. Figure 5.1a shows that the bench top yields from both sources were the same within the experimental error of ±0.65 wt%. In addition, the C_5-asphaltene and pitch* yields from mixtures of WC-B-A3 bitumen and *n*-pentane at temperatures of 21, 90 and 130°C and pressures of 0.1, 10 and 60 MPa were measured in a previous study using the blind cell method (Ferreira, 2020), and are provided in Table 5.2.

The above data were supplemented with asphaltene precipitation data for mixtures of WC-B-B3 bitumen and *n*-pentane previously measured using the blind cell and high pressure microscope methods. The WC-B-B3 dataset also includes three yield measurements made in a PVT cell where the compositions of both the light and heavy phase were measured. Unlike the blind cell method, there was enough information to complete a material balance and the yields have less uncertainty

than those from the blind cell method (±6 wt% versus 6 to 11 wt%). The onset and yields are reported elsewhere (Johnston *et al.*, 2017a) and are provided in Appendix C. Although the SARA assay of the WC-B-B3 bitumen differed somewhat from that of the WC-B-A3 bitumen (Table 3.1), the asphaltene contents and the yields at 21°C and 0.1 MPa from the two bitumens were similar, as shown in Figure 5.1b.

Table 5.1. C_5-Asphaltene yield from mixtures of WC-B-A3 bitumen and *n*-pentane at 21°C and 0.1 MPa. The repeatability of the yield measurements is ±0.65 wt%.

This Thesis		Ferreira (2020)	
Solvent Content	Asphaltene Yield	Solvent Content	Asphaltene Yield
wt%	wt%	wt%	wt%
39.9	0.9	40.1	0.6
48.3	1.5	44.9	0.4
52.0	5.5	50.5	4.6
55.2	9.5	55.1	9.1
58.7	12.6	60.0	12.7
63.2	14.7	65.0	15.0
70.2	17.1	70.0	16.7
79.9	18.7	80.0	19.4
90.0	19.6	90.0	19.3
89.9	19.8	-	-

Table 5.2. C_5-Asphaltene yield from mixtures of WC-B-A3 bitumen and n-pentane at 21°C and 0.1 MPa (Ferreira, 2020). The repeatability of the yield measurements is ±0.65 wt%.

Temperature °C	Pressure MPa	*n*-Pentane Content wt%	C_5-Asphaltene Yield wt%	Pitch* Yield wt%
21	0.1	50.0	3.4	11.1
21	0.1	59.8	11.9	23.0
21	0.1	70.0	16.1	23.0
21	0.1	80.0	18.5	25.6
21	0.1	90.3	19.2	22.6
21	10	53.8	4.2	7.0
21	10	60.6	9.9	15.0
21	10	70.8	15.7	23.7
21	10	80.7	18.3	25.8
21	10	90.3	19.2	23.1
21	60	59.6	5.1	10.3
21	60	65.3	8.6	17.8
21	60	70.0	11.8	20.6
21	60	80.3	14.8	20.6
21	60	90.0	17.2	18.6
90	10	55.2	5.2	8.6
90	10	60.2	6.6	10.1
90	10	70.4	13.6	15.9
90	10	80.2	17.4	25.4
90	10	90.3	18.3	20.3
90	60	58.1	4.5	8.0
90	60	59.0	5.7	11.2
90	60	70.0	12.5	19.7
90	60	91.1	14.9	30.1
130	10	59.1	5.6	24.1
130	10	64.1	8.9	26.7
130	10	70.2	12.6	31.6
130	10	79.8	15.8	30.2

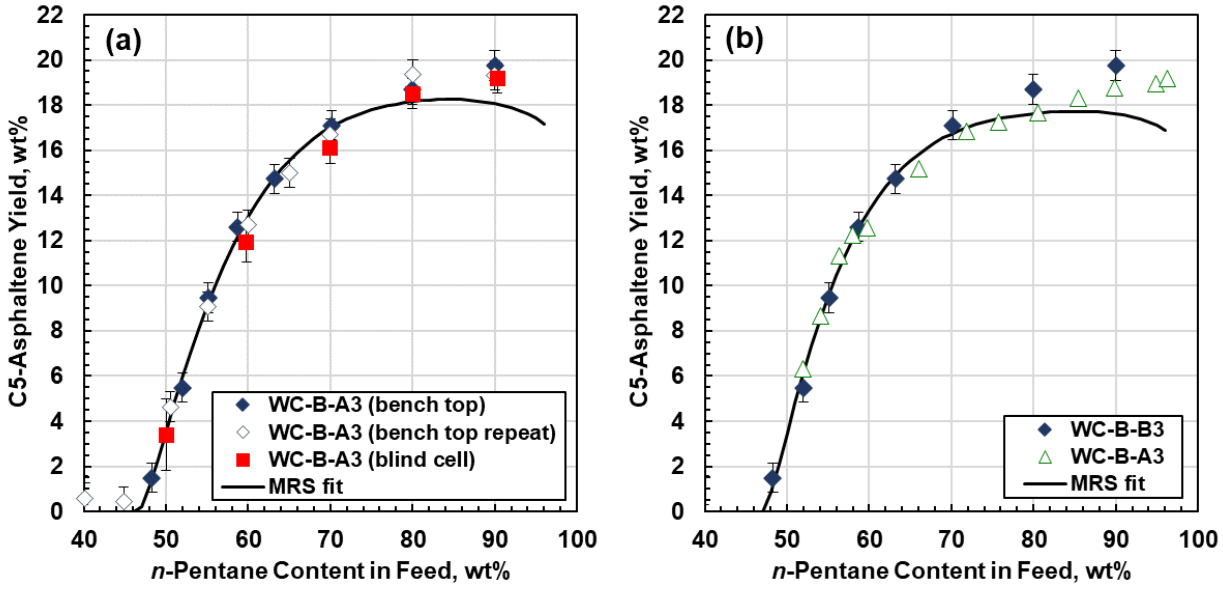

Figure 5.1. MRS modeled and measured C_5-asphaltene yield from mixtures of bitumen and *n*-pentane at 21°C and 0.1 MPa: a) comparison of bench top and blind cell results for WC-B-A3 bitumen; b) comparison of bench top results for WC-B-B3 and WC-B-A3 bitumens.

Figure 5.2 shows that, above the onset, the pitch* yield increased with increasing *n*-pentane content to a maximum of 25 wt% at 80 wt% *n*-pentane, and then decreased towards the C_5-asphaltene yield. Figure 5.3 shows that the C_5-asphaltene yields decreased as the pressure increased, indicating that asphaltene solubility increased with pressure. Figure 5.4 shows that the asphaltene solubility increased slightly as the temperature increased up to 140°C with a possible maximum at approximately 140°C.

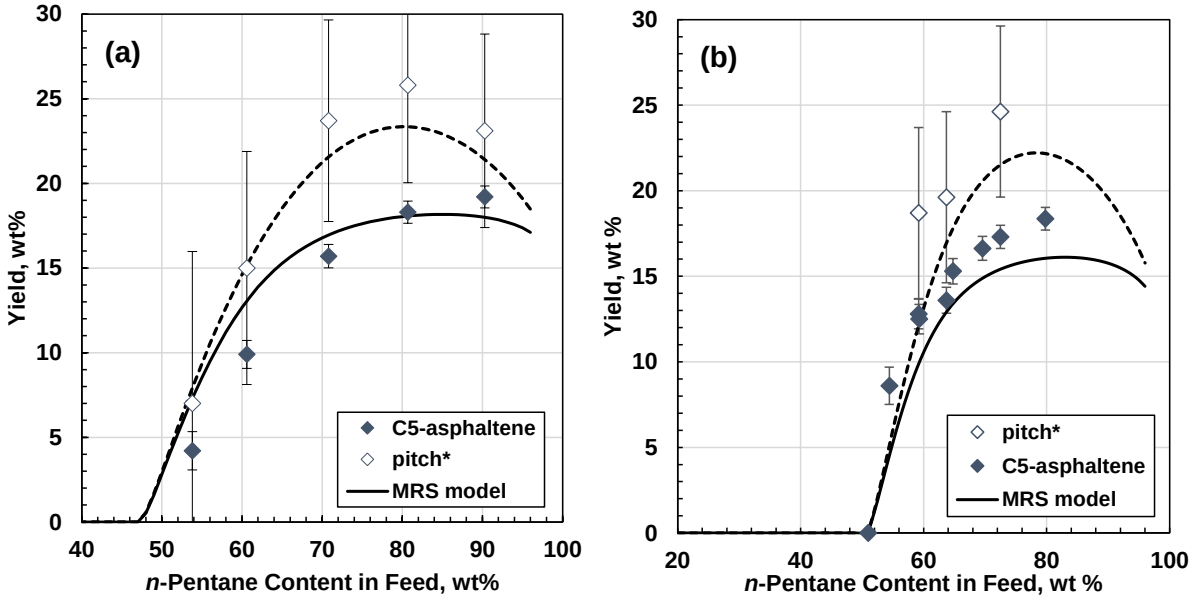

Figure 5.2. Measured and modeled C_5-asphaltene and pitch* yields from *n*-pentane diluted bitumen: a) WC-B-A3 bitumen at 21°C and 10 MPa with yields from blind cell method; b) WC-B-B3 bitumen at 180°C and 4.8 MPa with yields from blind cell and PVT cell method and the onset condition from an HPM measurement. The asphaltene solubility parameters were determined from Eq. 5.3.

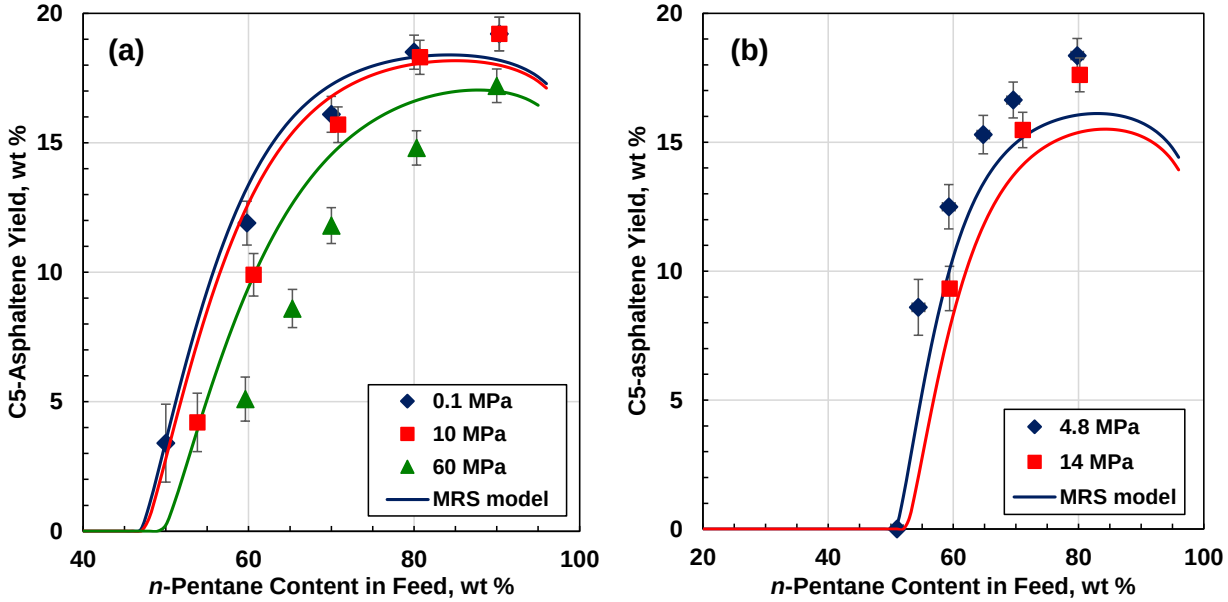

Figure 5.3. Effect of pressure on C_5-asphaltene yields from *n*-pentane diluted bitumen: a) WC-B-A3 bitumen at 21°C; b) WC-B-B3 bitumen at 180°C. The yields were obtained with the blind cell method and the onset condition for the WC-B-B3 bitumen was from an HPM measurement. The asphaltene solubility parameters were determined from Eq. 5.3.

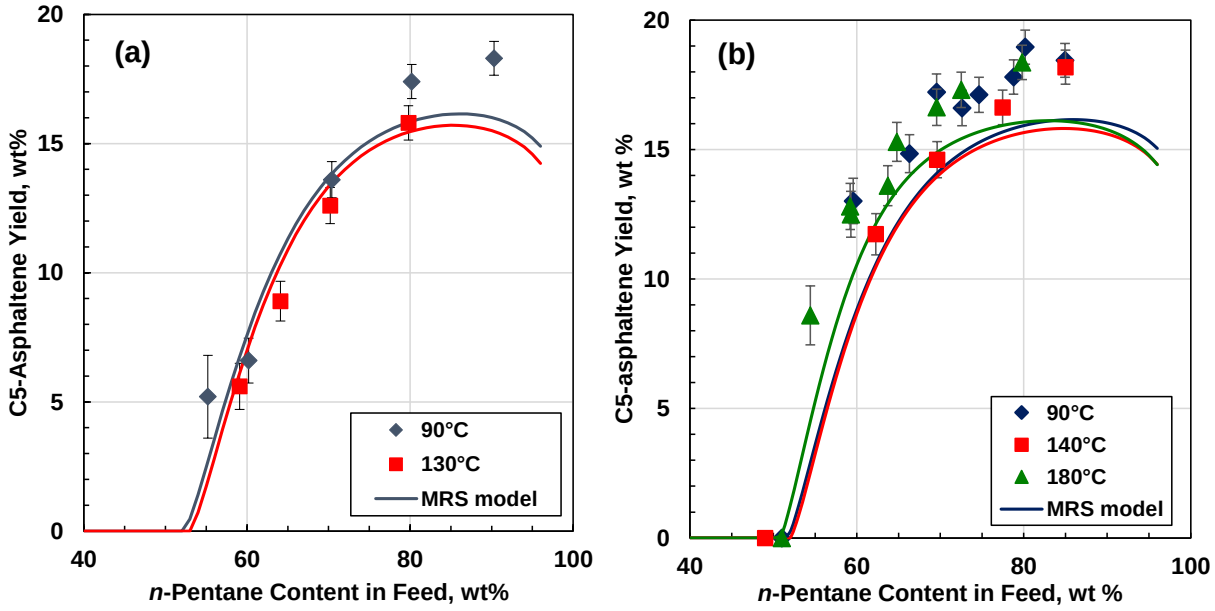

Figure 5.4. Effect of temperature on C_5-asphaltene yields from *n*-pentane diluted bitumen: a) WC-B-A3 bitumen at 10 MPa; b) WC-B-B3 bitumen at 4.8 MPa. The yields were obtained with the blind cell method and the onset condition for the WC-B-B3 bitumen was from an HPM measurement. The asphaltene solubility parameters were determined from Eq. 5.3.

5.1.2. MRS Modeling for Asphaltene Solubility Parameter

In previous applications of the MRS model, the asphaltene solubility parameters were tuned at ambient conditions only and the solubility parameters at other conditions were determined from a correlation that assumed asphaltenes as incompressible. However, this approach was only tested up to 10 MPa while the data in this study extend to 60 MPa. Therefore, the previous approach was tested on the high-pressure data and updated as described below.

Previous Asphaltene Solubility Parameter Correlation

The MRS model was fitted to the ambient condition data from Table 5.2 to determine the asphaltene minimum and maximum solubility parameters, as shown in Figure 5.1a (blue diamonds). The minimum and maximum asphaltene solubility parameters at 25°C and 0.1 MPa for the WC-B-A3 asphaltenes were 19.71 and 20.17 $MPa^{0.5}$, respectively. The temperature dependence of the asphaltene solubility parameters was initially calculated using the previously developed correlation from (Ramos-Pallares and Yarranton, 2020):

$$\delta_{A,i} = \delta_{A,i}{}^{o} - 0.0191(T - 298.15) \qquad \textbf{(5.1)}$$

where $\delta_{A,i}$ is the asphaltene solubility parameter (in $MPa^{0.5}$) at the system temperature T (in K), and the superscript o indicates the standard condition (25°C and 0.1 MPa). Figure 5.5 shows the asphaltene yields predicted at 90°C and two different pressures using the MRS model with Eq. 5.1 (dashed and dotted lines). The model captured the effect of pressure up to 10 MPa but significantly under-predicted the yields at higher pressures.

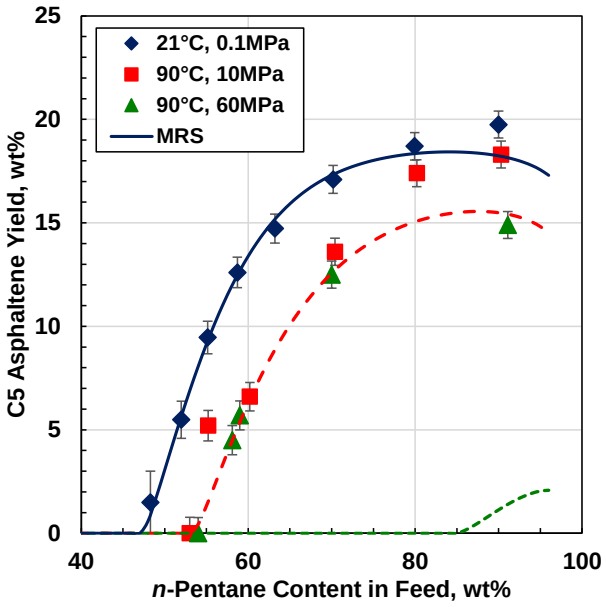

Figure 5.5. MRS measured and modeled C_5-asphaltene yield for mixtures of WC-B-A3 bitumen and *n*-pentane. The asphaltene solubility parameters were determined from Eq. 5.1. The solid and dashed lines are from the model with the previous and updated asphaltene solubility parameter correlation, respectively.

Updated Asphaltene Solubility Parameter Correlation

A possible explanation for the model error at high pressure is that Eq. 5.1 does not account for pressure. The solubility parameter is a function of the internal energy of vaporization and molar volume as follows:

$$\delta = \left(\frac{\Delta U^{vap}}{v}\right)^{1/2} = \left(\frac{\Delta U^{vap}\rho}{MW}\right)^{1/2} \qquad (5.2)$$

where ΔU^{vap} is the internal energy of vaporization (J/mol), v is the molar volume (cm^3/mol), MW is molecular weight (kg/mol), and ρ is density (kg/m^3). The solubility parameter is proportional to the square root of density and; therefore, for a compressible fluid, it depends indirectly on pressure. Eq. 5.2 is based the assumption that asphaltenes are incompressible and this

approximation has been shown to be valid up to 10 MPa (Ramos-Pallares and Yarranton, 2020). Above 10 MPa, it appears that the asphaltene compressibility must be accounted for. Since the compressibility of the asphaltenes is unknown, a linear dependence was assumed for the sake of simplicity. The expression for the solubility parameter of the asphaltenes is then given by:

$$\delta_{TP,A} = \delta_{T_o P_o,A}\sqrt{1 + B_A P} - k_A(T - T_o) \qquad (5.3)$$

where B_A is a constant (1/MPa), P is the pressure (MPa), k_A is the temperature dependence of the solubility parameter ($MPa^{0.5}$/K).

The pressure dependence of the asphaltene solubility parameter was determined by fitting Eq. 5.3 to the asphaltene solubility parameters that had been tuned to match the yields measured at each temperature and pressure. Two datasets were used: 1) C_5-asphaltene yields from *n*-pentane diluted WC-B-B3 bitumen at temperatures from 21 to 250°C and pressures from 0.1 to 13.8 MPa (Johnston *et al.*, 2017a); 2) C_5-asphaltene yields from *n*-pentane diluted WC-B-A3 at temperatures from 21 to 130°C and pressures from 0.1 to 60 MPa (Tables 5.1 and 5.2). The tuned values for the minimum and maximum solubility parameters of the asphaltenes are listed in Table 5.3 and shown in Figure 5.6. The minimum and maximum asphaltene solubility parameters at standard conditions were tuned separately for each bitumen and were 19.78 and 20.24 $MPa^{0.5}$, respectively, for WC-B-A3 bitumen and 19.87 and 20.29 $MPa^{0.5}$, respectively, for WC-B-B3 bitumen. The values for the WC-B-A3 bitumen are slightly different from the previously tuned values due to the pressure dependence in Eq. 5.3. The parameters B_{asph} and k_{Asph} were adjusted to fit the data and the fitted values are provided in Table 5.4. The correlated solubility parameters are compared with the fitted values in Figure 5.6. The solubility parameters increased with pressure as anticipated. In addition, the temperature dependence factor, represented as the slope of the plotted solubility parameters, was found to be steeper for the maximum asphaltene solubility parameters than for the minimum parameters. The absolute average deviation (AAD) of the correlation (Eq. 5.3) was ±0.26 $MPa^{0.5}$ with an R^2 of 0.94.

Table 5.3. Fitted minimum and maximum asphaltene solubility parameters for *n*-pentane diluted WC-B-B3 and WC-B-A3 bitumen.

Bitumen	Pressure	Temperature	δ_{min}	δ_{max}
	MPa	°C	$Mpa^{0.5}$	$Mpa^{0.5}$
WC-B-B3	0.1	21	19.87	20.29
WC-B-B3	4.8	90	18.67	18.98
WC-B-B3	4.8	140	17.59	17.95
WC-B-B3	4.8	180	16.89	17.13
WC-B-B3	10.3	250	15.51	15.76
WC-B-B3	13.8	180	16.95	17.19
WC-B-A3	0.1	21	19.79	20.24
WC-B-A3	10	20	19.82	20.27
WC-B-A3	10	90	18.52	18.92
WC-B-A3	10	130	17.70	18.12
WC-B-A3	60	21	20.20	20.69
WC-B-A3	60	90	19.02	19.48

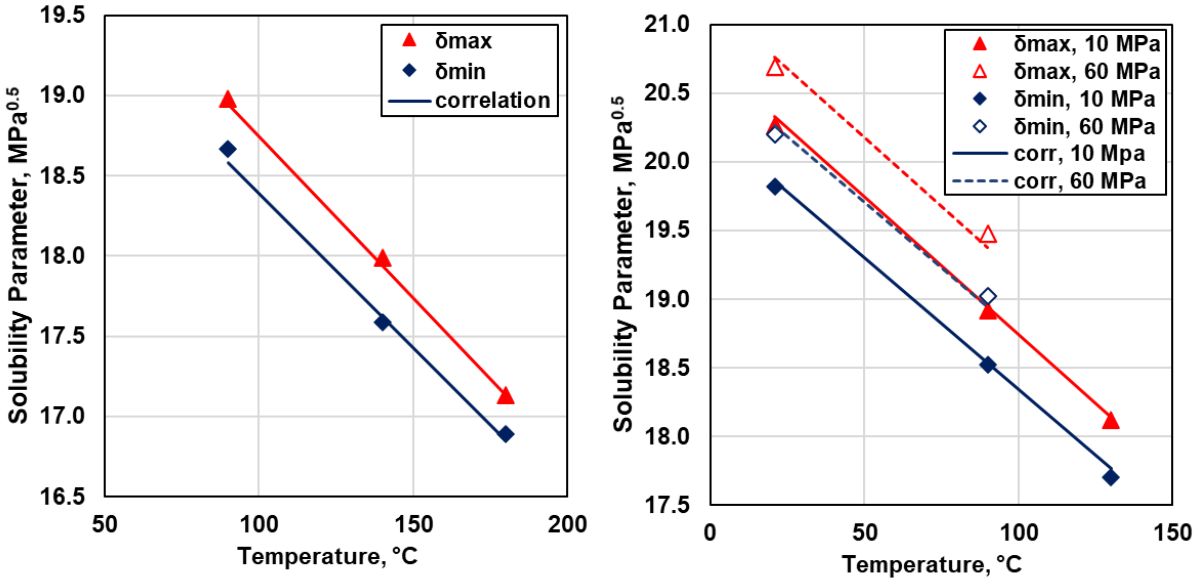

Figure 5.6. Fitted and correlated minimum and maximum solubility parameters of the asphaltene fraction for: a) WC-B-B3 at 4.8 MPa; b) WC-B-A3 at 10 and 60 MPa.

Table 5.4. Fitted parameters for solubility parameter correlation (Eq. 5.3).

δ_A	B_A 1/MPa	k_A $MPa^{0.5}/K$
Minimum	0.000831	0.0187
Maximum	0.000873	0.0201

The C_5-asphaltene and pitch* yields for *n*-pentane diluted WC-B-A3 and WC-B-B3 bitumens were then modeled using the MRS model with Eq. 5.3. Figure 5.2a shows that at near standard conditions the model matches both the asphaltene and pitch* yields to almost within the experimental error. Figure 5.2b provides an example illustrating how the model matches the onset but tends to under-predict the yields at higher temperatures. The effects of pressure and temperature are further illustrated using the C_5-asphaltene yields as shown in Figures 5.3 and 5.4, respectively. The results at other conditions are provided in Appendix D. The model also matched the onset of precipitation to within the error of the measurement at most conditions but, as noted above, tended to underestimate the yields at high dilution at higher temperatures.

There are two reasons for the model deviations. First, the model predicts that yields will decrease at very high dilutions while the measured yields remain high, as shown in Figure 5.1. The model is based on partition coefficients and, like any partition coefficient model, will predict that at high dilution there are not enough heavy phase components to saturate the large volume of light phase and therefore the heavy phase disappears. It is not clear why the measured yields do not decrease at very high *n*-alkane contents. A possibility is that asphaltenes self-associate more at high *n*-alkane contents and become less soluble. The second source of deviation is that the yields vary with temperature and pressure slightly differently for each oil. The model correlations are based on average trends and therefore will overpredict the yields for some oils and underpredict the yields for others, as shown in Figures 5.2 to 5.4.

The overall average absolute deviations were 1.6 wt% *n*-pentane for the onsets, 1.6 wt% for the asphaltene yields, and 5.3 wt% for the pitch* yields. Overall, the use of Eq. 5.3 significantly improved the performance of the MRS model at high pressure. Therefore, the MRS model with Eq. 5.3 was selected to model the onsets and asphaltene yields from mixtures of bitumen, *n*-

pentane, and methane. Since the measured and modeled pitch* yields are relatively uncertain, the emphasis will be placed on the onset and C_5-asphaltene yields.

5.2. Saturation Pressure of Methane, *n*-Pentane, and Bitumen Mixtures

Before determining the methane solubility parameters, it was necessary to measure the saturation pressures of the relevant mixtures in order to ensure that there was no vapor phase present in the liquid-liquid phase equilibrium experiments. The maximum methane content in the precipitation experiments was then set to avoid the formation of a vapor phase; that is, the experimental pressure was always above the saturation pressure.

The measured saturation pressures for several mixtures of WC-B-A3 bitumen, *n*-pentane, and methane are reported in Table 5.5. As expected, the saturation pressure of the mixtures increased monotonically with increasing solvent content and temperature. The saturation pressures were modeled as described below and the fitted equation was used to set the minimum pressure for the onset, yield, and phase composition experiments.

Table 5.5. Measured saturation pressures of mixtures of WC-B-A3 bitumen, *n*-pentane, and methane. The repeatability of the measurements is ±0.2 MPa (Perez-Claro *et. al.*, 2019).

Methane Content wt%	*n*-Pentane Content wt%	Temperature °C	Saturation Pressure MPa
6.0	24.0	50	20.2
3.0	27.0	50	9.3
1.5	28.5	50	5.0
3.0	12.0	50	14.4
1.5	13.5	50	6.7
6.0	24.0	130	27.3
1.5	28.5	130	7.0
3.0	12.0	130	19.1
1.5	13.5	130	8.9

The saturation pressures were modeled with a three component (bitumen, *n*-pentane, methane) bubble point flash calculation using the following partition coefficients:

$$K_{C1} = \frac{x_m^V}{x_m^L} = \frac{H_m}{P} \quad \textbf{(5.4)}$$

$$K_p = \frac{x_p^V}{x_p^L} = \frac{\gamma_p P_{v,p}}{P} \quad \textbf{(5.5)}$$

$$K_b = \frac{x_b^V}{x_b^L} = 0 \quad \textbf{(5.6)}$$

where K is the partition coefficient, x is mole fraction, P is pressure (MPa), H_m is a fitting parameter akin to the Henry constant for methane in bitumen (MPa), γ_p is a fitting parameter akin to the activity coefficient of *n*-pentane in bitumen, and $P_{v,p}$ is the vapor pressure of pentane (MPa). The subscripts *b*, *m*, and *p* denote bitumen, methane, and propane, respectively, and the superscripts *L* and *V* denote the liquid and vapor phase respectively. It was assumed (by setting $K_b = 0$) that the bitumen contribution to the saturation pressure was negligible. It was further assumed that there was no interaction between the methane and the *n*-pentane. Gas phase fugacities were neglected for the sake of simplicity and because this method is not intended as a thermodynamic model but rather as a semi-empirical short cut.

The following empirical expression for H_m was found to fit saturation pressure data for mixtures of bitumen and methane taken from (Svrcek and Mehrotra, 1982):

$$H_m = 95160\exp\left\{\frac{-451.6}{T}\right\} + 1070\mathrm{P} \quad \textbf{(5.7)}$$

where H_m and P are in MPa and T is the temperature in K.

The vapor pressure of *n*-pentane was calculated from Poling *et al*. (2001) correlation. Figure 5.8 shows saturation pressures of mixtures of *n*-pentane and bitumen from Johnston *et al.* (2017a). To model this data, it was assumed that the mole fraction of bitumen in the vapor phase was negligible. The saturation pressure is then given by:

$$P = x_p \gamma_p P_{v,p} \quad \textbf{(5.8)}$$

where subscript *p* indicates *n*-pentane, γ is the activity coefficient and P_v is the vapor pressure of *n*-pentane given by (Poling *et al.*, 2001):

$$P_{v,p} = 0.3375\exp\left\{\left(\frac{469.8}{1-T}\right)X(T_r)\right\} \quad \textbf{(5.9)}$$

$$X(T_r) = -7.30698T_r + 1.75845T_r^{1.5} - 2.1629T_r^{2.5} - 2.913T_r^5 \quad \textbf{(5.10)}$$

where $P_{v,p}$ is in kPa and T is in K. An activity coefficient of 1.25 was found to fit the data. The average deviation in the fitted solubilities was 210 kPa. The procedure involved converting mass fraction to mole fractions. A molecular weight of 520 g/mol was used for this bitumen.

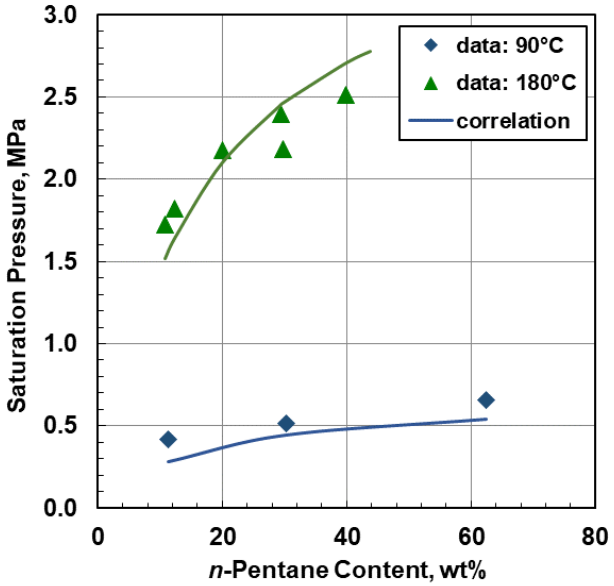

Figure 5.7. Measured and correlation saturation pressure of mixtures of *n*-pentane and bitumen. Data from Johnston *et al*. (2017). The repeatability of the measured saturation pressures is ±0.2 MPa.

All of the terms in the partition coefficient equations are now fixed except for the pressure and temperature. The temperature is an input and the bubble point flash calculation was used to predict the saturation pressures for mixtures of bitumen, *n*-pentane, and methane. The measured and predicted saturation pressures are compared in Figure 5.9. The average absolute deviation of the predicted pressures was 0.26 MPa (3.3%), slightly higher than the experimental uncertainty of ±0.2 MPa.

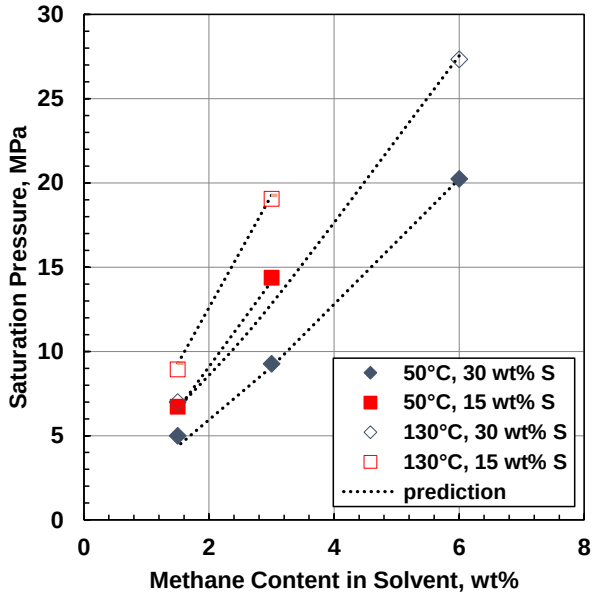

Figure 5.8. Measured and predicted saturation pressure of mixtures of WC-B-A3 bitumen, *n*-pentane, and methane. The uncertainty of the measured saturation pressure is ±0.2 MPa.

5.3. Determination of Methane Solubility Parameter

5.3.1. Onset and Yield Data

The onsets of asphaltene precipitation measured in the HMP apparatus for mixtures of WC-B-A3 bitumen, *n*-pentane, and methane are provided in Table 5.6. The average uncertainty of the measurement is ±1.5 wt% solvent. Figure 5.10 shows the measured onsets in terms of total solvent content (methane + *n*-pentane). The onsets decreased with increasing methane content in the solvent; that is, less solvent was required to trigger precipitation. This trend confirms that asphaltenes are less soluble in the presence of dissolved methane. The onsets increased with increasing temperature, suggesting that asphaltene solubility increases at high temperatures. Pressure had no effect on the onsets beyond the error of the measurements.

Table 5.6. Measured asphaltene onsets for mixtures of WC-B-A3 bitumen, methane, and *n*-pentane. The uncertainty of the onsets is ±1.5 wt%.

Temperature °C	Pressure MPa	Methane Content wt%	*n*-Pentane Content wt%	Onset (C_1 + *n*-C_5) wt%
21	10	4.9	31.7	36.6
21	10	3.2	34.6	37.8
21	13	7.0	26.2	33.2
21	60	5.0	32.0	37.0
21	60	6.7	24.3	31.0
130	21	5.3	32.7	38.0
130	60	5.5	35.2	40.7

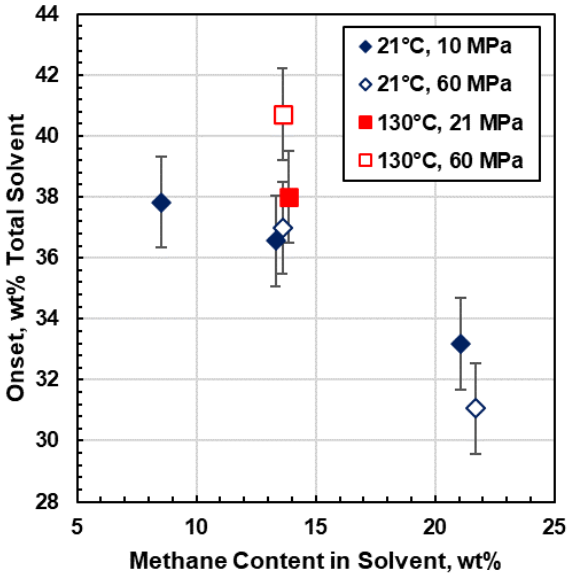

Figure 5.9. Effect of methane content on measured onsets of asphaltenes precipitation from mixtures of WC-B-A3 bitumen, *n*-pentane, and methane.

The yields for WC-B-A3 bitumen, *n*-pentane, and methane mixtures measured in the blind cell apparatus are provided in Table 5.7. Figure 5.11 shows that measured C_5-asphaltene yields were the same at all conditions, indicating that all of the C_5-asphaltenes partitioned into the heavy phase at all the experimental conditions. Figure 5.12 shows that the pitch* yield decreased with increasing solvent content at the measured conditions (solvent contents from 70 to 90 wt%). The

decrease in yield is consistent with greater component partitioning to the solvent-rich phase as its mass relative to the heavy phase increases. Figure 5.12a shows that increasing the methane content in the feed solvent increased the pitch* yield, which is consistent with poorer component solubility in methane. Figure 5.12b shows that the pitch* yield appeared to decrease with increasing pressure; that is, oil components become more soluble at higher pressures. Figure 5.12c shows that increasing temperature from 21 to 130°C had no consistent measurable effect on the pitch* yield.

Table 5.7. Measured C_5-asphaltene and pitch* yields from WC-B-A3 bitumen, *n*-pentane, and methane mixtures. The uncertainty of the C_5-asphaltene yields is ±0.6 wt%. The uncertainty of the pitch* yield increases towards the onset and ranges from ±8.5 to 14 wt%.

Temperature °C	Pressure MPa	Methane Content wt%	*n*-Pentane Content wt%	C_5-Asphaltene Yield wt%	Pitch* Yield wt%
21	10	5.0	65.2	20.2	33.2
21	10	5.2	74.8	19.2	32.3
21	10	4.9	85.0	19.5	27.7
21	10	7.9	72.2	19.9	38.5
21	10	7.8	82.2	20.3	34.8
130	10	5.2	64.8	20.3	39.4
130	10	5.2	74.8	20.3	30.2
130	10	7.5	82.7	20.3	27.3
130	10	7.9	72.1	20.4	42.9
130	10	9.0	81.1	20.2	32.9
21	60	8.2	61.9	20.3	31.9
21	60	7.8	72.1	20.3	28.9
21	60	7.8	82.1	20.3	26.6
21	60	15.9	74.1	20.3	46.5
130	60	7.8	62.3	20.4	37.2
130	60	8.2	81.8	20.3	35.2
130	60	15.8	64.4	20.4	35.2

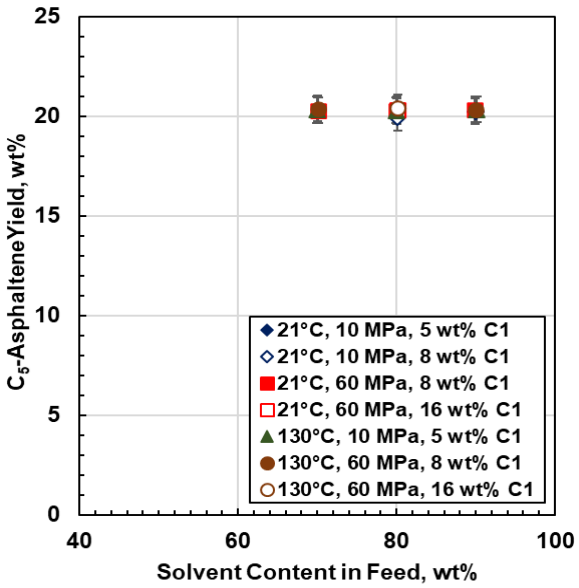

Figure 5.10. Measured C_5-asphaltene yields from WC-B-A3 bitumen, *n*-pentane, and methane mixtures at all conditions.

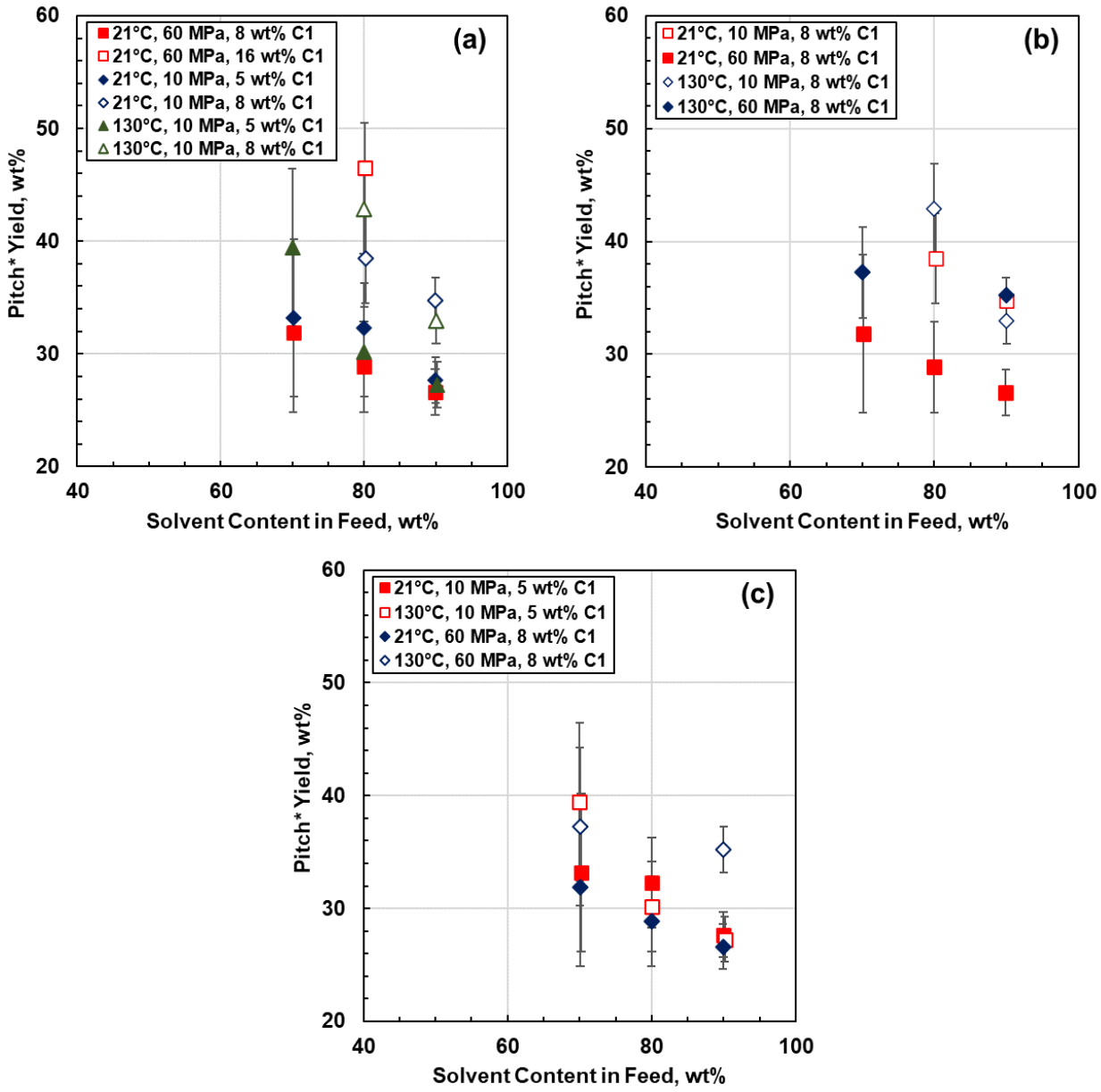

Figure 5.11. Measured pitch* yields from WC-B-A3 bitumen, *n*-pentane, and methane mixtures: a) effect of methane content; b) effect of pressure; c) effect of temperature.

The yield data for the mixtures of WC-B-A3 bitumen, *n*-pentane, and methane at a 5 wt% methane content were similar to data previously collected for mixtures of bitumen and *n*-butane (Perez-Claro *et al.*, 2019), as shown in Figure 5.12a. The comparison of the methane/*n*-pentane blend to *n*-butane is not exact because the methane content was fixed at 5 wt% and therefore the ratio of methane/*n*-pentane changed as the solvent content changed. Nonetheless, the onsets and yields

from both solvents were of similar magnitude. The methane/*n*-pentane blend was a slightly poorer solvent than *n*-butane (lower onset and higher yields). In both cases, the yields were generally insensitive to temperature and pressure (up to 10 MPa). Figure 5.12b shows that the yields from mixtures of bitumen, *n*-pentane, and methane at an 8 wt% methane content approached the yields from mixtures of bitumen and propane (Mancilla-Polanco *et al.*, 2018). The similarity between the three systems gives confidence that the regular solution approach previously applied to mixtures of bitumen and other *n*-alkanes including *n*-butane (Ramos Pallares and Yarranton, 2020) can also be applied to bitumen/solvent mixtures containing methane.

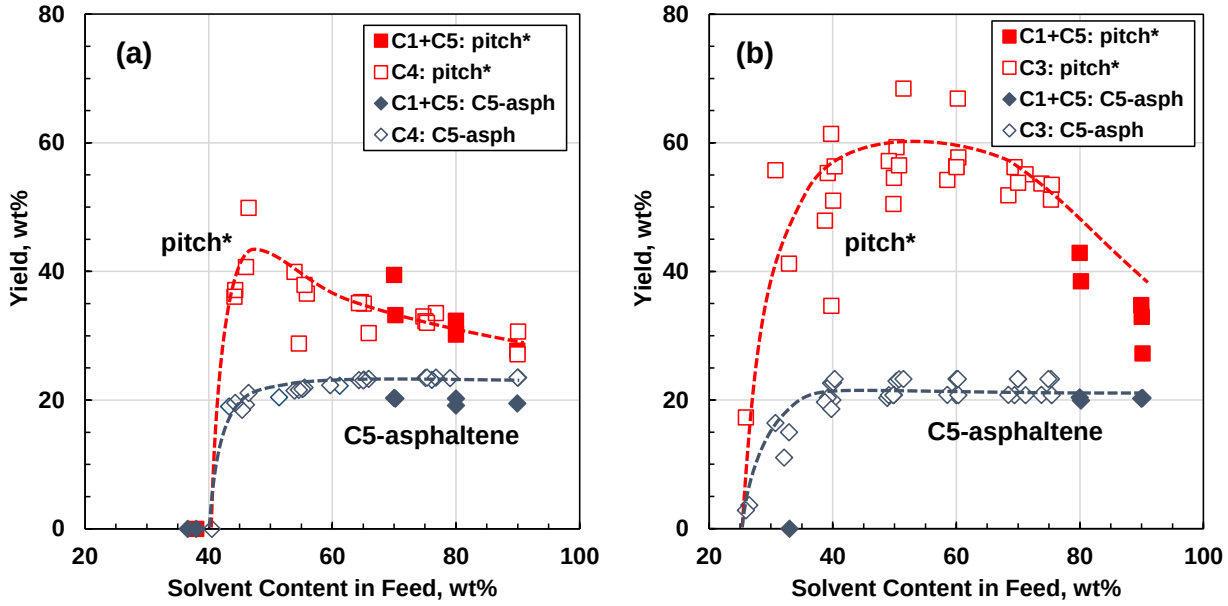

Figure 5.12. Comparison of C_5-asphaltene and pitch* yields from mixtures of bitumen with different solvents: a) WC-B-A3 bitumen, *n*-pentane and methane (C_1+C_5) at 5 wt% methane content, 21 and 130°C, and 10 MPa versus WC-B-A3 bitumen and *n*-butane (C_4) at 5 to 10 MPa and 21 to 180°C from Perez-Claro *et al*. (2019); b) WC-B-A3 bitumen, *n*-pentane and methane (C_1+C_5) at 8 wt% methane content, 21 and 130°C, and 10 MPa versus WC-B-B3/B4 bitumen and propane (C_3) at 2 to 10 MPa and 21 to 130°C from (Mancilla-Polanco *et al.*, 2018). The bitumens used in each study were different samples from the same reservoir and had slightly different C_5-asphaltene contents. The dashed lines are visual aids only.

5.3.2. Morphology of the Heavy Phase

The heavy liquid phase formed in the WC-B-A3 bitumen, *n*-pentane and methane mixtures was observed using a High-Pressure Microscope (HPM). The morphology of the heavy phase was not

required to achieve the objective of this thesis but does provide another point of comparison with other mixtures of bitumen and solvent. At a temperature of 21°C, the heavy phase appeared as irregular liquid-like merged particles that stuck to the HPM glass (Figure 5.13a and 5.13c). These particles slowly formed a smoother liquid-like structure over time, as shown in Figure 5.13b. At a temperature of 130°C the heavy phase appeared as smaller and more regular liquid-like particles that rapidly coalesced into a continuous liquid phase (Figure 5.14). Increasing pressure up to 60 MPa did not appear to change the morphology of the heavy phase, both at 21 or 130°C. Similar results were observed for bitumen/*n*-butane and bitumen/propane mixtures (Mancilla, 2017; Perez, 2019), confirming the similarity between these mixtures and the mixtures with *n*-pentane and methane.

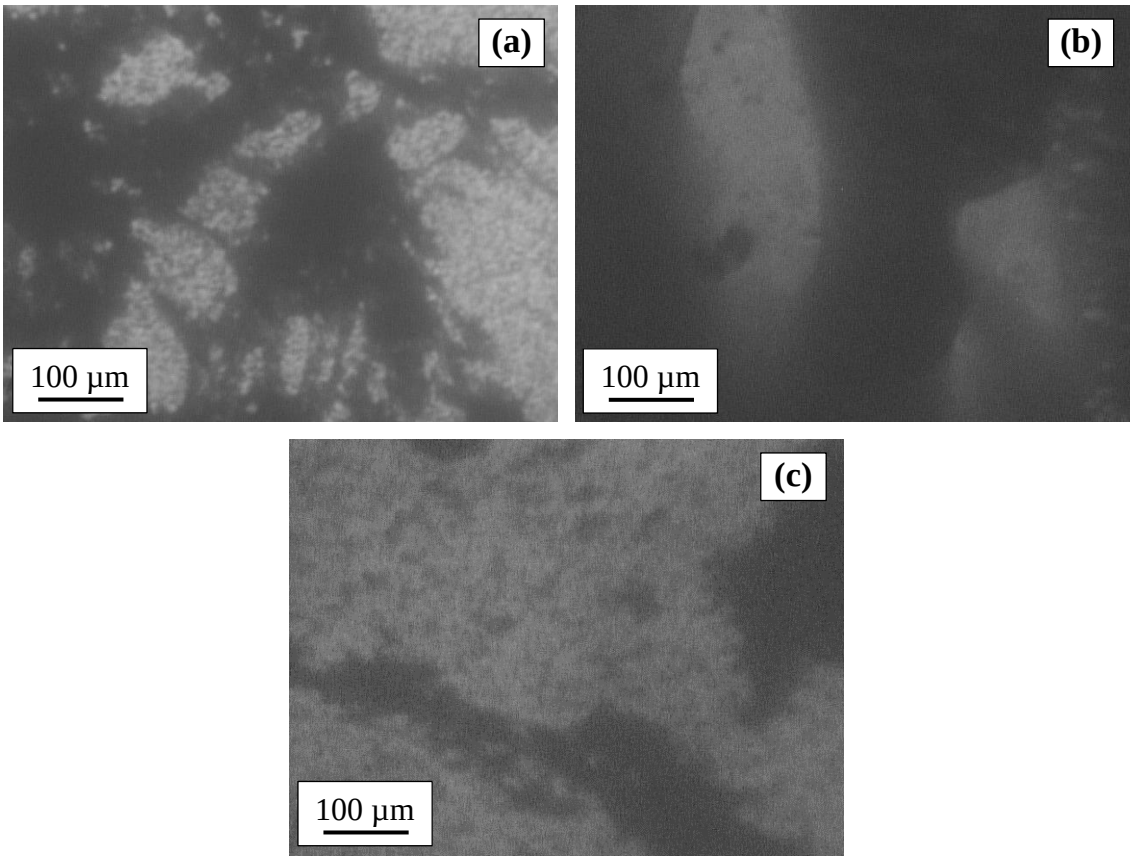

Figure 5.13. HPM micrographs of the heavy phase for WC-B-A3 bitumen, *n*-pentane, and methane mixtures: a) 21°C and 10 MPa, taken immediately after reaching the onset condition; b) 21°C and 10 MPa taken 24 hours after reaching onset condition; c) 21°C and 60 MPa taken immediately after reaching the onset condition.

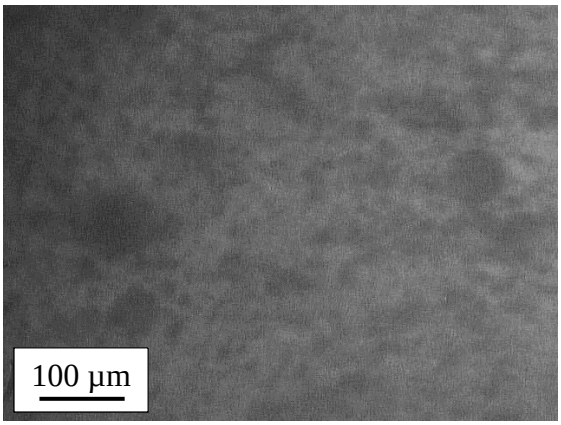

Figure 5.14. HPM micrographs of the heavy phase for WC-B-A3 bitumen, *n*-pentane, and methane mixtures at 130°C and 21 MPa taken immediately after reaching the onset.

5.3.3. MRS Modeling for Methane Solubility Parameter

The asphaltene precipitation data presented in the previous section were fitted using the MRS model. Since the C_5-asphaltene yields from the mixtures of WC-B-A3 bitumen, *n*-pentane and methane were insensitive to the solvent content above the onset and the pitch* yields had high uncertainty, only the onset data were used in this study. The solubility parameter of methane (δ_{C_1}) was tuned to fit the onsets of precipitation at each experimental condition. The fitted values are presented in Table 5.8 and range from 6.12 to 9.46 $MPa^{0.5}$. Based on the uncertainty of ±1.5 wt% in the onset measurement, the uncertainty of the methane solubility parameters is ±0.7 $MPa^{0.5}$. This uncertainty does not include any contributions from flaws in the model assumptions.

Table 5.8. Fitted methane solubility parameters for mixtures of WC-B-A3 bitumen, *n*-pentane and methane. The uncertainty of the methane solubility parameters is ±0.7 $MPa^{0.5}$.

Temperature °C	Pressure MPa	Methane Content wt%	Solubility Parameter $MPa^{0.5}$
21	10	4.9	9.13
21	10	3.2	8.60
21	13	7.0	9.46
21	60	5.0	8.98
21	60	6.7	8.78
130	21	5.3	6.76
130	60	5.5	6.12

The fitted values are compared with methane solubility parameters found in the literature in Figure 5.15a. The highest value of 13.9 $MPa^{0.5}$ was determined from the heat of vaporization and molar volume of methane at its normal boiling point (Marcus, 2016). Values at standard conditions have been determined from solubility data: 9.6 $MPa^{0.5}$ (Barton, 1991), and 11.8 $MPa^{0.5}$ (Prausnitz and Shair, 1961). Effective liquid molar volumes for the methane were used in the determination of the solubility parameter. The values from (Romero-Yanes *et al.*, 2021) were calculated from the solubility parameter equation derived from an equation of state solved with molar volumes from a property database. The range in reported solubility parameters indicates that the magnitude of the methane solubility parameter depends on the method used to estimate it and the method to determine the molar volumes used in the calculation.

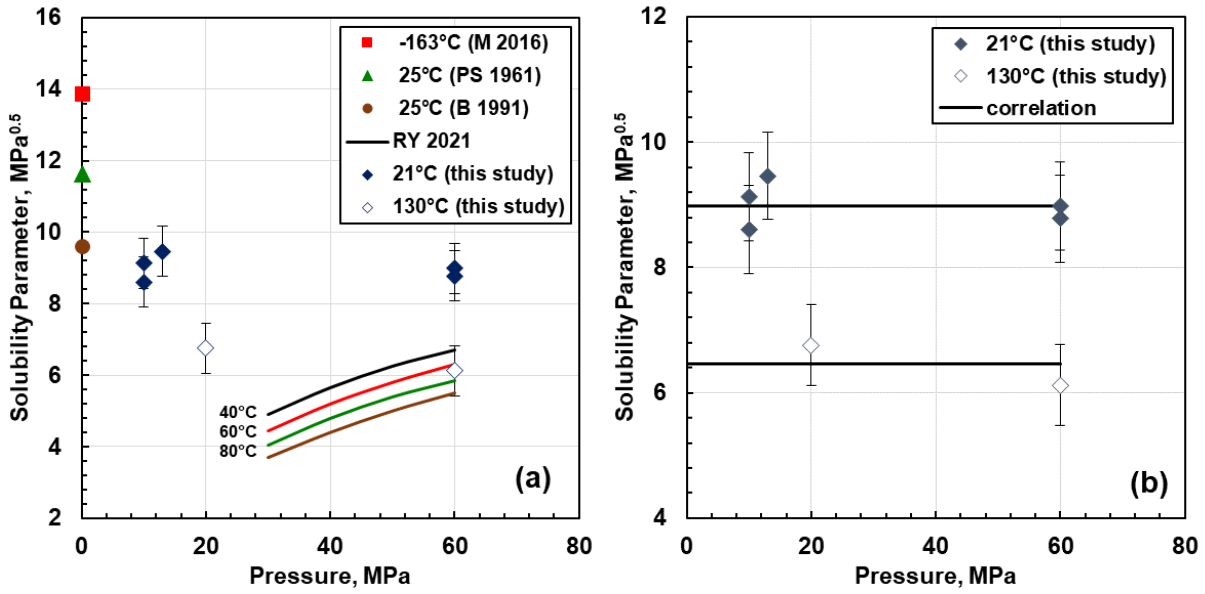

Figure 5.15. Methane solubility parameters: a) comparison between fitted values in this study and values from literature; b) correlation based on the values from this study. The legend references are as follows: M 2016 = (Marcus, 2016), PS 1961 = (Prausnitz and Shair, 1961), B 1991 = (Barton, 1991), RY 2021 = (Romero-Yanes *et al.*, 2021).

The methane solubility parameters from this study fall between the literature values. The change in solubility parameter with temperature is similar to that observed for other *n*-alkanes (Akbarzadeh *et al.*, 2005) and that predicted by (Romero-Yanes *et al.*, 2021); that is, the solubility parameter decreases when temperature increases. However, contrary to expectation, the solubility

parameters from this study are independent of pressure. The component solubility parameter correlations in the MRS model have the following functional form:

$$\delta_{TP,i} = \delta_{T_oP_o,i}\sqrt{\frac{\rho_{T_oP,i}}{\rho_{T_oP_o,i}}} - k_i(T - T_o) \qquad \textbf{(4.14)}$$

where k is the temperature dependence of the solubility parameter in $MPa^{0.5}/K$, subscript TP indicates the temperature and pressure of the system, and subscript o indicates the standard condition (25°C and 0.1MPa). The solubility parameter is proportional to the square root of pressure and since density increases with pressure, the solubility parameter is expected to increase with pressure. Romero-Yanes also predicted that the methane solubility parameter increases with increasing pressure (Figure 5.15a). Eq. 4.14 was derived with the assumption that the heat of vaporization was independent of pressure. If the assumption is incorrect, then the pressure dependencies in the model correlations for the other components may be incorrect and may have skewed the fitted methane solubility parameters. In this case, the fitted values at the lowest pressures are expected to be less affected and more accurate than the values at higher pressures.

Since the determination of the methane solubility parameters appears to be model dependent, the following correlation was developed exclusively for use in the MRS model based on the fitted methane solubility parameters from this study:

$$\delta_{methane} = 8.891 - 0.0232(T - 298.15) \qquad \textbf{(5.11)}$$

where T is in K. The correlation is shown in Figure 5.15b. The MRS modeled onsets using the proposed correlation are compared with the measured onsets in Figure 5.16. The AAD and MAD for the modeled onsets were 1.1 and 2.7 wt% solvent, respectively, compared with an experimental error of ±1.5 wt%.

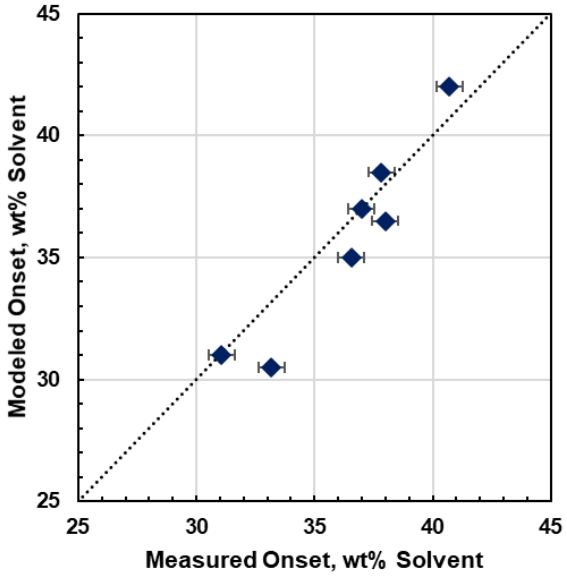

Figure 5.16. Cross-plot of MRS modeled onsets vs measured onsets for WC-B-A3 bitumen, *n*-pentane, and methane mixtures.

The MRS modeled yields using the proposed correlation and the measured yields are compared in Figures 5.17. The model was run at a fixed methane content to provide a consistent yield curve. However, the methane content in the measurements varied slightly and consequently the comparisons in the figures are not exact. The model was rerun at the exact experimental conditions to determine the model deviations. The AAD and MAD for the C_5-asphaltene yields (above the experimental onset) were 0.2 and 1.1 wt%, respectively. The model matched the C_5-asphaltene yields to within the error of the measurements because all of the asphaltenes precipitated at all conditions above the onset. The model yield deviations can be significantly higher near the onset if the onset is not matched. The AAD and MAD for the pitch* yields (above the experimental onset) were 8.1 and 14 wt%, respectively. The model tended to over-predict the pitch* yields. Similar errors were reported when applying the model to mixtures of bitumen and propane and bitumen and *n*-butane (Ramos-Pallares and Yarranton, 2020). The error is attributed to the relatively coarse characterization of the maltene fraction of the oil which is represented as three pseudo-components (saturates, aromatics, and resins). At this stage, there is too little data on the property distributions within these fractions to justify changing the characterization. In addition, the error is not caused by the methane solubility parameters which are the focus of this study.

Based on results for other *n*-alkanes and bitumens (Ramos-Pallares and Yarranton, 2020), the MRS model with the proposed methane property correlations is expected to apply to mixtures of other bitumens and methane with similar accuracy.

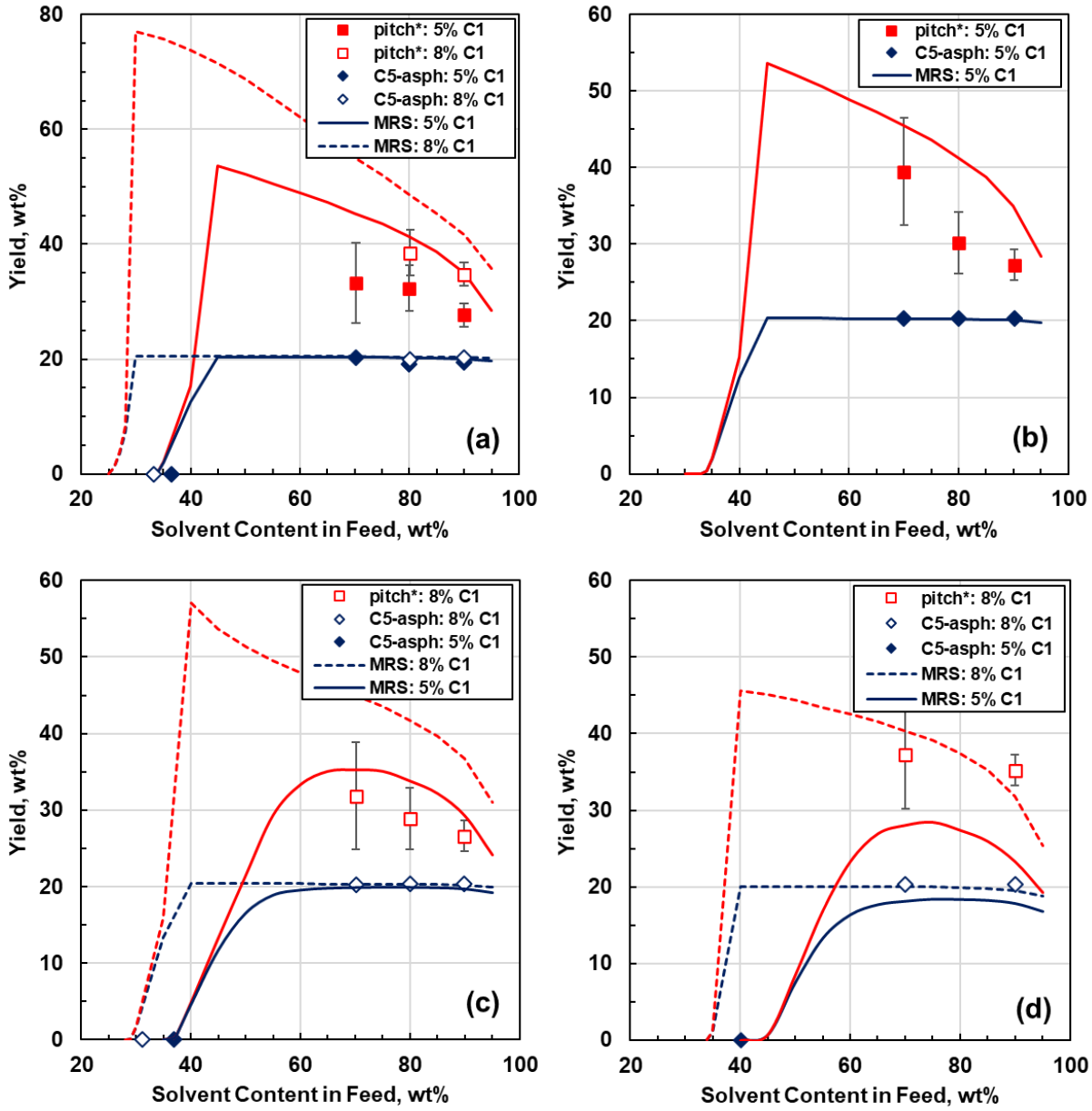

Figure 5.17. MRS modeled yields and measured yields for WC-B-A3 bitumen, *n*-pentane, and methane mixtures: a) 21°C and 10MPa; b) 21°C and 60 MPa; c) 130°C and 10 MPa; d) 130°C and 60 MPa.

Although the correlation is limited for use in the MRS model, it provides plausible values of the methane solubility parameter. The predicted solubility parameter at the normal boiling point of -116°C is 13.3 $MPa^{0.5}$, approaching the value of 13.9 $MPa^{0.5}$ from Marcus (2016). The predicted solubility parameter at standard conditions (25°C and 0.1MPa) is 8.9 $MPa^{0.5}$, approaching the value of 9.6 $MPa^{0.5}$ from Barton (1991). Figure 5.18 shows that the predicted methane solubility parameter at standard conditions is consistent with the solubility parameters of *n*-alkanes that are liquids at or near standard conditions. The temperature dependence of the correlation (the constant of 0.232 $MPa^{0.5}/K$) is the same value used for other *n*-alkanes and recommended by Barton (1991). Only the lack of pressure dependence is inconsistent with the behavior of other *n*-alkanes.

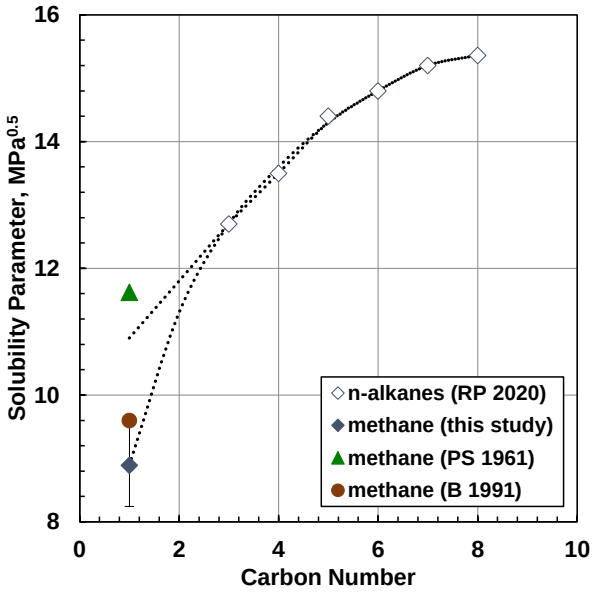

Figure 5.18. Alkane solubility parameters at standard conditions as a function of carbon number. The legend references are as follows: RP 2020 = (Ramos-Pallares and Yarranton, 2020), PS 1961 = Prausnitz and Shair (1961) , B 1991 = Barton (1991). The dotted lines are visual aids only.

Chapter 6. Conclusions and Recommendations

The main contributions of this thesis are: 1) the determination of the methane solubility parameter at different temperatures and pressures; 2) the improvement of the performance of the Modified Regular Solution (MRS) model in predicting asphaltene precipitation from oils with dissolved gases. The updated model can be used to predict asphaltene solubility in field applications such as solvent assisted recovery processes where methane is a constituent of the heavy oil or natural gas is used as a cosolvent. Determining the methane solubility parameter is also a first step to predict the asphaltene precipitation from depressurized conventional oils with high contents of dissolved gases. The major conclusions and recommendations for future studies are presented below.

6.1. Conclusions

6.1.1. Experimental Methods

Previously developed experimental procedures for measuring asphaltene precipitation data were successfully applied to mixtures of WC-B-A3 bitumen, *n*-pentane, and methane. The onsets were measured in a High-Pressure Microscope apparatus with an average uncertainty of ±1.5 wt% solvent. The C_5-asphaltene and pitch* yields were determined using the blind cell methodology developed by Johnston (2017). The material balance was solved assuming a solvent content in the heavy phase of 25 wt%, based on precipitation data collected for similar bitumen/solvent systems (Johnston, 2017; Perez-Claro, 2019). The C_5-asphaltene yields were not sensitive to this assumption and were determined with an average uncertainty of ±0.65 wt%. On the other hand, pitch* yields were sensitive to the assumption, with uncertainties ranging from ±6 to 11 wt% based on solvent contents from 0 to 50 wt%. The uncertainty for the pitch* yields increased towards the onset.

A new procedure was developed to determine the saturation pressures based on the pump response operating at pressure mode. The procedure was validated using the previous procedure described by (Agrawal *et al.*, 2012) from the change in slope of the pressure-volume isotherm. The new approach significantly reduced the equilibration times between the isothermal volume expansions.

The saturation pressures were measured in a blind cell apparatus with an uncertainty of ±0.2 MPa.

6.1.2. Experimental Results

The yields for WC-B-A3 bitumen, *n*-pentane, and methane mixtures were measured at temperatures of 21 and 130°C, and pressures of 10 and 60 MPa. The C_5-asphaltene yields were insensitive to temperature and pressure. For the studied experimental conditions all of the C_5-asphaltenes were rejected from the solvent-rich phase and partitioned into the heavy phase, which, is consistent with methane being a poor solvent for asphaltenes. Increasing methane content on the feed solvent increased pitch* yields, which is also consistent with poorer asphaltene and resin solubility in methane. The pitch* yields were not sensitive to temperature but decreased with increasing pressure; that is, the solubility of asphaltenes and resins in the mixture increased with pressure.

The onsets of precipitation were measured at temperatures from 21 and 130°C and pressures from 10 up to 60 MPa. The onsets decreased with increasing methane content in the solvent; that is, less solvent was required to trigger precipitation. The onsets increased with increasing temperature, but pressure had no effect on the onsets beyond the error of the measurements. The micrographs taken above the onset condition indicated that the heavy phase was liquid regardless of the pressure and temperature. The phase behavior of mixtures of bitumen, *n*-pentane, and methane were similar to the phase behavior observed for mixtures of bitumen and propane (Mancilla-Polanco *et al.*, 2018) and bitumen and *n*-butane (Perez-Claro *et al.*, 2019).

6.1.3. Modeling

The MRS model, in particular the correlation to determine the resins and asphaltene solubility parameter, was updated to apply to pressures up to 60 MPa. The previous correlation assumed incompressibility of these fractions, which lead to significant deviations in the MRS model predictions at pressures above 10 MPa. To introduce this pressure dependency, fitted values of the minimum and maximum asphaltene solubility parameter were obtained using the MRS model applied to a dataset of asphaltene onsets and yields from mixtures of bitumen and *n*-pentane. The MRS model with the updated correlation matched the onsets, C_5-asphaltene yields, and pitch*

yields with average absolute deviations of 1.6 wt% *n*-pentane, 1.6 wt%, and 5.3 wt%, respectively. The model tended to under-predict yields at high solvent contents and high temperatures.

Fitted values of the methane solubility parameter were obtained using the MRS model applied to a dataset of asphaltene onsets from mixtures of WC-B-A3 bitumen, methane, and *n*-pentane. A correlation to determine the methane solubility parameter at different pressures and temperatures was developed for use in the MRS model. The MRS model with the correlation matched the onsets, C_5-asphaltene yields, and pitch* yields with average absolute deviations of 1.1 wt% *n*-pentane, 0.8 wt%, and 8.1 wt%, respectively. The model tended to overestimate the pitch* yields. The correlated value of the methane solubility parameter at standard conditions of 9.1 $MPa^{0.5}$ was slightly lower than value of 9.6 $MPa^{0.5}$ reported in the literature.

Solubility parameters determined from solubility data are sensitive to the method used to calculate them and to the effective liquid molar volumes used in this calculation. Therefore, caution is advised in using the correlation with other models. Instead, the dataset presented in this contribution can be used to obtain methane solubility parameters appropriate for any model of interest.

6.2. Recommendations

The MRS model tended to over-predict pitch* yields at all studied conditions. This error is attributed to the relatively coarse characterization of the maltene fraction of the oil which is represented as three pseudo-components (saturates, aromatics, and resins). It is recommended to develop a more detailed characterization of this fraction representing the pseudo-components as a distribution rather than as single pseudo-components. The pitch* yields measured in this study and previous studies with other *n*-alkanes (Johnston *et al.*, 2017a; Mancilla-Polanco *et al*., 2018; Perez-Claro *et al.*, 2019) could provide a starting point for developing the characterization.

The methane solubility parameter determined with the MRS model in this study is independent of pressure; however, the solubility parameter is expected to increase with increasing pressure. The correlations to determine the solubility parameters in the model assumed that the heat of vaporization is independent of pressure. This assumption may have skewed the fitted methane

solubility parameters. In this study, the model was updated to include the pressure dependencies of asphaltenes and resins up to 60 MPa; however, it is recommended to reevaluate the pressure dependencies of the other components to avoid deviations in the model predictions at high pressures. To do so, it would be necessary to collect asphaltene precipitation data at elevated pressures from mixtures of *n*-heptane or toluene with each of these components. These data could be fitted with MRS model to fit the component solubility parameters at these conditions and fitted parameters could be used to develop a pressure and temperature dependent correlation for the solubility parameters of these components.

It is recommended to collect phase composition data for WC-B-A3 bitumen, *n*-pentane, and methane mixtures at temperature and pressure conditions relevant to field applications. This information will help to reduce the uncertainties in the pitch* yields caused by the assumption made on the solvent content in the heavy phase.

References

Acevedo, S., Gutierrez, L. B., Negrin, G., Pereira, J. C., Mendez, B., Delolme, F., Dessalces, G., Broseta, D. (2005). Molecular weight of petroleum asphaltenes: A comparison between mass spectrometry and vapor pressure osmometry. *Energy and Fuels*, *19*(4), 1548–1560. https://doi.org/10.1021/ef040071

Agrawal, P., Schoeggl, F. F., Satyro, M. A., Taylor, S. D., Yarranton, H. W. (2012). Measurement and modeling of the phase behavior of solvent diluted bitumens. *Fluid Phase Equilibria*, *334*, 51–64. https://doi.org/10.1016/j.fluid.2012.07.025

Agrawala, M., Yarranton, H. W. (2001). An asphaltene association model analogous to linear polymerization. *Industrial and Engineering Chemistry Research*, *40*(21), 4664–4672. https://doi.org/10.1021/ie0103963

Akbarzadeh, K., Alboudwarej, H., Svrcek, W. Y., Yarranton, H. W. (2005). A generalized regular solution model for asphaltene precipitation from n-alkane diluted heavy oils and bitumens. *Fluid Phase Equilibria*, *232*(1–2), 159–170. https://doi.org/10.1016/j.fluid.2005.03.029

Akbarzadeh, K., Dhillon, A., Svrcek, W. Y., Yarranton, H. W. (2004). Methodology for the characterization and modeling of asphaltene precipitation from heavy oils diluted with n-alkanes. *Energy and Fuels*, *18*(5), 1434–1441. https://doi.org/10.1021/ef049956b

Alboudwarej, H., Beck, J., Svrcek, W. Y., Yarranton, H. W., Akbarzadeh, K. (2002). Sensitivity of asphaltene properties to separation techniques. *Energy and Fuels*, *16*(2), 462–469. https://doi.org/10.1021/ef010213p

Alboudwarej, H., Svrcek, W., Yarranton, H., Akbarzadeh, K. (2001). Asphaltene characterization: Sensitivity of asphaltene properties to extraction techniques. *Canadian International Petroleum Conference 2001, CIPC 2001*, 1–11. https://doi.org/10.2118/2001-063

Alboudwarej, Hussein, Akbarzadeh, K., Beck, J., Svrcek, W. Y., Yarranton, H. W. (2003). Regular Solution Model for Asphaltene Precipitation from Bitumens and Solvents. *AIChE Journal*, *49*(11), 2948–2956. https://doi.org/10.1002/aic.690491124

Alshareef, A. H. (2020). Asphaltenes: Definition, Properties, and Reactions of Model Compounds. *Energy and Fuels*, *34*(1), 16–30. https://doi.org/10.1021/acs.energyfuels.9b03291

Arya, A., von Solms, N., Kontogeorgis, G. M. (2015). Determination of asphaltene onset conditions using the cubic plus association equation of state. *Fluid Phase Equilibria*, *400*, 8–19. https://doi.org/10.1016/j.fluid.2015.04.032

Badamchi-Zadeh, A., Yarranton, H. W., Svrcek, W. Y., Maini, B. B. (2009). Phase behaviour and physical property measurements for VAPEX solvents: Part I. Propane and athabasca bitumen. *Journal of Canadian Petroleum Technology*, *48*(1), 54–61. https://doi.org/10.2118/09-01-54

Barton, A. F. M. (1991). *CRC Handbook of Solubility Parameters and Other Cohesion Parameters* (CRC Press).

BP. (2019). BP Statistical Review of World Energy 2019|68th Edition. In *BP World Energy*. https://doi.org/10.2307/3324639

Castellanos-Díaz, O., Modaresghazani, J., Satyro, M. A., Yarranton, H. W. (2011). Modeling the phase behavior of heavy oil and solvent mixtures. *Fluid Phase Equilibria*, *304*(1–2), 74–85. https://doi.org/10.1016/j.fluid.2011.02.011

Castellanos Díaz, O., Sánchez-Lemus, M. C., Schoeggl, F. F., Satyro, M. A., Taylor, S. D., Yarranton, H. W. (2014). Deep-vacuum fractionation of heavy oil and bitumen, part I: Apparatus and standardized procedure. *Energy and Fuels*, *28*(5), 2857–2865. https://doi.org/10.1021/ef500489y

Chacón-Patiño, M. L., Rowland, S. M., Rodgers, R. P. (2017). Advances in Asphaltene Petroleomics. Part 1: Asphaltenes Are Composed of Abundant Island and Archipelago Structural Motifs. *Energy and Fuels*, *31*(12), 13509–13518. https://doi.org/10.1021/acs.energyfuels.7b02873

Chapman, W. G., Gubbins, K. E., Jackson, G., Radosz, M. (1989). SAFT: Equation-of-state solution model for associating fluids. *Fluid Phase Equilibria*, *52*(C), 31–38. https://doi.org/10.1016/0378-3812(89)80308-5

de Boer, R. B., Leerlooyer, K., Eigner, M. R. P., van Bergen, A. R. D. (1995). Screening of crude oils for asphalt precipitation: theory, practice, and the selection of inhibitors. *SPE Production and Facilities*, *10*(1), 55–61. https://doi.org/10.2118/24987-PA

Dehghani, S. A. M., Sefti, M. V., Mansoori, G. A. (2007). Simulation of natural depletion and miscible gas injection effects on asphaltene stability in petroleum reservoir fluids. *Petroleum Science and Technology*, *25*(11), 1435–1446. https://doi.org/10.1080/10916460600695264

Dickie, J. P., Yen, T. F. (1967). Macrostructures of the Asphaltic Fractions by Various Instrumental Methods. *Analytical Chemistry*, *39*(14), 1847–1852. https://doi.org/10.1021/ac50157a057

Dini, Y., Becerra, M., Shaw, J. M. (2016). Phase behavior and thermophysical properties of peace river bitumen + propane mixtures from 303 K to 393 K. *Journal of Chemical and Engineering Data*, *61*(8), 2659–2668. https://doi.org/10.1021/acs.jced.6b00034

Energy Fact Book of Natural Resources of Canada. (2018).

Esmaeili, S., Maaref, S. (2018). Applying the Patel-Teja EoS with regular solution theory to predict the onset of asphaltene precipitation. *Fluid Phase Equilibria*, *473*, 112–126. https://doi.org/10.1016/j.fluid.2018.06.002

Fahim, M. A., Alsahhaf, T. A., Elkilani, A. (2010). Refinery Feedstocks and Products. In *Fundamentals of Petroleum Refining* (pp. 11–31). Elsevier. https://doi.org/10.1016/B978-0-444-52785-1.00002-4

Félix, G., Ancheyta, J. (2020). Regular solution model to predict the asphaltenes flocculation and sediments formation during hydrocracking of heavy oil. *Fuel*, *260*(July 2019), 1–7. https://doi.org/10.1016/j.fuel.2019.116160

Ferreira, N. (2020). *Determination of Solubility Parameter of Carbon Dioxide in Heavy Oil* [Master's thesis, University of Calgary].

Flory, P. (1941). Thermodynamics of high polymer solutions. *Journal of Chemical Physics*, *10*, 51–61. https://doi.org/10.1007/s12045-017-0481-2

Fu, C. T., Puttagunta, V. R., Vilcsak, G. (1988). Gas solubility of methane and ethane in Cold Lake bitumen at in situ conditions. *J. Can. Pet. Technol.*, *27*(4, Jul.-Aug. 1988), 79–85. https://doi.org/10.2118/88-04-06

Gonzalez, D. L., Ting, P. D., Hirasaki, G. J., Chapman, W. G. (2005). Prediction of asphaltene instability under gas injection with the PC-SAFT equation of state. *Energy and Fuels*, *19*(4), 1230–1234. https://doi.org/10.1021/ef049782y

Gray, M. R. (2015). *Upgrading oilsands bitumen and heavy oil* (First). The University of Alberta Press.

Gray, M. R., Tykwinski, R. R., Stryker, J. M., Tan, X. (2011). Supramolecular assembly model for aggregation of petroleum asphaltenes. *Energy and Fuels*, *25*(7), 3125–3134. https://doi.org/10.1021/ef200654p

Groenzin, H., Mullins, O. C. (1999). Asphaltene molecular size and structure. *Journal of Physical Chemistry A*, *103*(50), 11237–11245. https://doi.org/10.1021/jp992609w

Gross, J., Sadowski, G. (2001). Perturbed-chain SAFT: An equation of state based on a perturbation theory for chain molecules. *Industrial and Engineering Chemistry Research*, *40*(4), 1244–1260. https://doi.org/10.1021/ie0003887

Haddadnia, A., Sadeghi Yamchi, H., Zirrahi, M., Hassanzadeh, H., Abedi, J. (2018). New Solubility and Viscosity Measurements for Methane-, Ethane-, Propane-, and Butane-Athabasca Bitumen Systems at High Temperatures up to 260 °c. *Journal of Chemical and Engineering Data*, *63*(9), 3566–3571. https://doi.org/10.1021/acs.jced.8b00443

Hildebrand, J. H., Prausnitz, J. M., and Scott, R. L. (1970). *Regular and Related Solutions*. Van Nostrand Reinhold Co.

Hirschberg, A., deJong, L. N. J., Schipper, B. A., Meijer, J. G. (1984). Influence of Temperature and Pressure on Asphaltene Flocculation. *Society of Petroleum Engineers Journal*, *24*(3), 283–293. https://doi.org/10.2118/11202-PA

Hu, Y. F., Guo, T. M. (2001). Effect of temperature and molecular weight of n-alkane precipitants on asphaltene precipitation. *Fluid Phase Equilibria*, *192*(1–2), 13–25.

https://doi.org/10.1016/S0378-3812(01)00619-7

Huggins, M. L. (1941). Solutions of long chain compounds. *The Journal of Chemical Physics*, *9*(5), 440. https://doi.org/10.1063/1.1750930

Jafari Behbahani, T., Naderi, F. (2014). Modeling asphaltene precipitation under gas injection and pressure depletion conditions. *Petroleum Science and Technology*, *32*(23), 2878–2888. https://doi.org/10.1080/10916466.2014.900082

Jamaluddin, A. K. M., Kalogerakis, N. E., Chakma, A. (1991). Predictions of Co2 solubility and CO2 saturated liquid density of heavy oils and bitumens using a cubic equation of state. *Fluid Phase Equilibria*, *64*(C), 33–48. https://doi.org/10.1016/0378-3812(91)90004-Q

Johnston, K. A., Satyro, M. A., Taylor, S. D., Yarranton, H. W. (2017b). Can a Cubic Equation of State Model Bitumen-Solvent Phase Behavior? *Energy and Fuels*, *31*(8), 7967–7981. https://doi.org/10.1021/acs.energyfuels.7b01104

Johnston, K. A., Schoeggl, F. F., Satyro, M. A., Taylor, S. D., Yarranton, H. W. (2017a). Phase behavior of bitumen and n-pentane. *Fluid Phase Equilibria*, *442*, 1–19. https://doi.org/10.1016/j.fluid.2017.03.001

Johnston, K. A. (2017). *Measurement and Modeling of Pentane-Diluted Bitumen Phase Behavior*. [Doctoral dissertation, University of Calgary].

Joshi, N. B., Mullins, O. C., Jamaluddin, A., Creek, J., McFadden, J. (2001). Asphaltene precipitation from live crude oil. *Energy and Fuels*, *15*(4), 979–986. https://doi.org/10.1021/ef010047l

Kawanaka, S., Park, S. J., Mansoorl, G. A. (1991). Organic deposition from reservoir fluids: a thermodynamic predictive technique. *SPE Reservoir Engineering (Society of Petroleum Engineers)*, *6*(2), 185–192. https://doi.org/10.2118/17376-PA

Kokal, S. L., Sayegh, S. G. (1990). Gas-Saturated Bitumen Density Predictions Using The Volume-Translated Peng-Robinson Equation Of State. *Journal of Canadian Petroleum Technology*, *29*(05). https://doi.org/10.2118/90-05-07

Kontogeorgis, G. M., Voutsas, E. C., Yakoumis, I. V., Tassios, D. P. (1996). An equation of state for associating fluids. *Industrial and Engineering Chemistry Research*, *35*(11), 4310–4318. https://doi.org/10.1021/ie9600203

Kord, S., Ayatollahi, S. (2012). Asphaltene precipitation in live crude oil during natural depletion: Experimental investigation and modeling. *Fluid Phase Equilibria*, *336*, 63–70. https://doi.org/10.1016/j.fluid.2012.05.028

Li, Z., Firoozabadi, A. (2010). Cubic-plus-association equation of state for asphaltene precipitation in live oils. *Energy and Fuels*, *24*(5), 2956–2963. https://doi.org/10.1021/ef9014263

Linstrom, P., Mallard, W. (2021). NIST Standard Reference Database. In *NIST Chemistry WebBook*. https://doi.org/10.18434/T4D303,

Mancilla-Polanco, A., Johnston, K., Richardson, W. D. L., Schoeggl, F. F., Zhang, Y., Yarranton, H. W., Taylor, S. D. (2019). Phase behavior of heavy-oil/propane mixtures. *SPE Journal*, *24*(2), 596–617. https://doi.org/10.2118/184988-PA

Mancilla-Polanco, A. A. (2017). *The Phase Behavior of Heavy Oil and Propane Mixtures* [Master's thesis, University of Calgary].

Marcus, Y. (2016). Solubility parameters of permanent gases. *Journal of Chemistry*, *2016*. https://doi.org/10.1155/2016/4701919

McKenna, A. M., Donald, L. J., Fitzsimmons, J. E., Juyal, P., Spicer, V., Standing, K. G., Marshall, A. G., Rodgers, R. P. (2013). Heavy petroleum composition. 3. Asphaltene aggregation. *Energy and Fuels*, *27*(3), 1246–1256. https://doi.org/10.1021/ef3018578

Mehrotra, A. K., Svrcek, W. Y. (1988). Properties of Cold Lake Bitumen Saturated with Pure Gases and Gas Mixtures. *The Canadian Journal of Chemical Engineering*, *66*(4), 656–665. https://doi.org/10.1002/cjce.5450660419

Merino-Garcia, D., Andersen, S. I. (2003). Isothermal titration calorimetry and fluorescence spectroscopy study of asphaltene self-association in toluene and interaction with a model resin. *Petroleum Science and Technology*, *21*(3–4), 507–525. https://doi.org/10.1081/LFT-120018535

Michelsen, M. L., Hendriks, E. M. (2001). Physical properties from association models. *Fluid Phase Equilibria*, *180*(1–2), 165–174. https://doi.org/10.1016/S0378-3812(01)00344-2

Mofidi, A. M., Edalat, M. (2006). A simplified thermodynamic modeling procedure for predicting asphaltene precipitation. *Fuel*, *85*(17–18), 2616–2621. https://doi.org/10.1016/j.fuel.2006.05.019

Mullins, O.C., Sheu, E.Y., Hammami, A., Marshal, A.G. (2007). *Asphaltenes, Heavy Oils and Petroleomics.* Springer.

Nazemi, R., Daryasafar, A., Bazyari, A., Shafiee Najafi, S. A., Ashoori, S. (2020). Modeling asphaltene precipitation in live crude oil using cubic plus association (CPA) equation of state. *Petroleum Science and Technology*, *38*(3), 257–265. https://doi.org/10.1080/10916466.2019.1692866

Nourbakhsh, H., Yazdizadeh, M., Esmaeilzadeh, F. (2011). Prediction of asphaltene precipitation by the extended Flory-Huggins model using the modified Esmaeilzadeh-Roshanfekr equation of state. *Journal of Petroleum Science and Engineering*, *80*(1), 61–68. https://doi.org/10.1016/j.petrol.2011.10.007

Nourozieh, H., Kariznovi, M., Abedi, J. (2016). Measurement and modeling of solubility and saturated-liquid density and viscosity for methane/athabasca-bitumen mixtures. *SPE Journal*, *21*(1), 180–189. https://doi.org/10.2118/174558-PA

Panuganti, S. R., Vargas, F. M., Gonzalez, D. L., Kurup, A. S., Chapman, W. G. (2012). PC-SAFT characterization of crude oils and modeling of asphaltene phase behavior. *Fuel*, *93*, 658–669. https://doi.org/10.1016/j.fuel.2011.09.028

Pazuki, G. R., Nikookar, M. (2006). A modified Flory-Huggins model for prediction of asphaltenes precipitation in crude oil. *Fuel*, *85*(7–8), 1083–1086. https://doi.org/10.1016/j.fuel.2005.10.005

Péneloux, A., Rauzy, E. (1982). A consistent correction for Redlich-Kwong-Soave Volumes. *Fluid Phase Equilibria*, *8*, 7–23. file:///E:/mendeleybe/z/JelKep_2011_1szemiotika.pdf

Peng, D. Y., Robinson, D. B. (1976). A New Two-Constant Equation of State. *Industrial and Engineering Chemistry Fundamentals*, *15*(1), 59–64. https://doi.org/10.1021/i160057a011

Perez-Claro, Y. A., Schoeggl, F. F., Taylor, S. D., Yarranton, H. W. (2019). Phase Behavior of Mixtures of Bitumen and n-Butane. *Energy and Fuels*, *33*(9), 8530–8543. https://doi.org/10.1021/acs.energyfuels.9b02113

Perez-Claro, Y. A. (2019). *Phase Behavior of Mixtures of Heavy Oil and n-Butane*. [Master's thesis, University of Calgary].

Powers, D. P., Sadeghi, H., Yarranton, H. W., Van Den Berg, F. G. A. (2016). Regular solution based approach to modeling asphaltene precipitation from native and reacted oils: Part 1, molecular weight, density, and solubility parameter distributions of asphaltenes. *Fuel*, *178*, 218–233. https://doi.org/10.1016/j.fuel.2016.03.027

Powers, D. P. (2014). *Characterization and Asphaltene Precipitation Modeling of Native and Reacted Crude Oils* [Doctoral dissertation, University of Calgary].

Prausnitz, J. M., Shair, F. H. (1961). A Thermodynamic Correlation of Gas Solubilities. *AIChE Journal*, *7*(4), 682–687.

Punnapala, S., Vargas, F. M. (2013). Revisiting the PC-SAFT characterization procedure for an improved asphaltene precipitation prediction. *Fuel*, *108*, 417–429. https://doi.org/10.1016/j.fuel.2012.12.058

Ramos-Pallares, F., Lin, H., Yarranton, H. W., Taylor, S. D. (2017). Prediction of the liquid viscosity of characterized crude oils by use of the generalized Walther model. *SPE Journal*, *22*(5), 1487–1505. https://doi.org/10.2118/186093-ER

Ramos-Pallares, F., Taylor, S. D., Satyro, M. A., Marriott, R. A., Yarranton, H. W. (2016). Prediction of viscosity for characterized oils and their fractions using the expanded fluid model. *Energy and Fuels*, *30*(9), 7134–7157. https://doi.org/10.1021/acs.energyfuels.6b01419

Ramos-Pallares, F., Yarranton, H. W. (2020). Extending the modified regular solution model to predict component partitioning to the asphaltene-rich phase. *Energy and Fuels*. https://doi.org/10.1021/acs.energyfuels.9b03489

Rogel, E., León, O., Torres, G., Espidel, J. (2000). Aggregation of asphaltenes in organic solvents using surface tension measurements. *Fuel*, *79*(11), 1389–1394. https://doi.org/10.1016/S0016-2361(99)00273-2

Romero-Yanes, J. F., da Costa, M. F. L., Sampaio, J. P. G., Chacón-Valero, A. M., Feitosa, F. X., de Sant'Ana, H. B. (2021). Experimental phase behavior and solubility parameter for crude oil + methane [T = 311.15–373.15 K] and crude oil + methane + CO2 mixtures [T = 343.15–383.15 K]. *Fuel*, *288*(November 2020). https://doi.org/10.1016/j.fuel.2020.119675

Romero-Yanes, J. F., Feitosa, F. X., Fleming, F. P., de Sant'Ana, H. B. (202 C.E.). Phase Behavior for Crude oil and Methane Mixtures: Crude Oil Property Comparison. *Fuel*, *34*, 5188–5195.

Saryazdi, F., Motahhari, H., Schoeggl, F. F., Taylor, S. D., Yarranton, H. W. (2013). Density of hydrocarbon mixtures and bitumen diluted with solvents and dissolved gases. *Energy and Fuels*, *27*(7), 3666–3678. https://doi.org/10.1021/ef400330j

Shahebrahimi, Y., Zonnouri, A. (2013). A new combinatorial thermodynamics model for asphaltene precipitation. *Journal of Petroleum Science and Engineering*, *109*, 63–69. https://doi.org/10.1016/j.petrol.2013.07.013

Shirani, B., Nikazar, M., Mousavi-Dehghani, S. A. (2012). Prediction of asphaltene phase behavior in live oil with CPA equation of state. *Fuel*, *97*, 89–96. https://doi.org/10.1016/j.fuel.2012.02.016

Speight, J. G. (2014). The Chemistry and Technology of Petroleum. In *The Chemistry and Technology of Petroleum*.

Svrcek, W. Y., Mehrotra, A. K. (1982). Gas Solubility, Viscosity and Density Measurements for Athabasca Bitumen. *Journal of Canadian Petroleum Technology*, *21*(4), 31–38. https://doi.org/10.2118/82-04-02

Tanaka, R., Sato, E., Hunt, J. E., Winans, R. E., Sato, S., Takanohashi, T. (2004). Characterization of asphaltene aggregates using X-ray diffraction and small-angle X-ray scattering. *Energy and Fuels*, *18*(4), 1118–1125. https://doi.org/10.1021/ef034082z

Tavakkoli, M., Chen, A., Vargas, F. M. (2016). Rethinking the modeling approach for asphaltene precipitation using the PC-SAFT Equation of State. *Fluid Phase Equilibria*, *416*, 120–129. https://doi.org/10.1016/j.fluid.2015.11.003

Tharanivasan, A. K., Yarranton, D. H. W. (2012). Asphaltene Precipitation from Crude Oil Blends, Conventional Oils, and Oils with Emulsified Water. *Chemical and Petroleum Engineering*, *DOCTOR OF*, 211. https://doi.org/10.1021/ef301200v

Tharanivasan, A. K., Yarranton, H. W., Taylor, S. D. (2011). Application of a regular solution-based model to asphaltene precipitation from live oils. *Energy and Fuels*, *25*(2), 528–538. https://doi.org/10.1021/ef101076z

Ting, P. D., Hirasaki, G. J., Chapman, W. G. (2003). Modeling of asphaltene phase behavior with the SAFT equation of state. *Petroleum Science and Technology*, *21*(3–4), 647–661. https://doi.org/10.1081/lft-120018544

Usui, K., Kidena, K., Murata, S., Nomura, M., Trisunaryanti, W. (2004). Catalytic hydrocracking of petroleum-derived asphaltenes by transition metal-loaded zeolite catalysts. *Fuel*, *83*(14-15 SPEC. ISS.), 1899–1906. https://doi.org/10.1016/j.fuel.2003.08.023

Wang, J. X., Buckley, J. S. (2001). A two-component solubility model of the onset of asphaltene flocculation in crude oils. *Energy and Fuels*, *15*(5), 1004–1012. https://doi.org/10.1021/ef010012l

Wargadalam, V. J., Norinaga, K., Iino, M. (2002). Size and shape of a coal asphaltene studied by viscosity and diffusion coefficient measurements. *Fuel*, *81*(11–12), 1403–1407. https://doi.org/10.1016/S0016-2361(02)00055-8

Yarranton, H. W., Powers, D. P., Okafor, J. C., van den Berg, F. G. A. (2018). Regular solution based approach to modeling asphaltene precipitation from native and reacted oils: Part 2, molecular weight, density, and solubility parameter of saturates, aromatics, and resins. In *Fuel* (Vol. 215, pp. 766–777). https://doi.org/10.1016/j.fuel.2017.11.071

Yarranton, H. W. (2005). Asphaltene self-association. *Journal of Dispersion Science and Technology*, *26*(1), 5–8. https://doi.org/10.1081/DIS-200040234

Yarranton, H. W., Alboudwarej, H., Jakher, R. (2000). Investigation of asphaltene association with vapor pressure osmometry and interfacial tension measurements. *Industrial and Engineering Chemistry Research*, *39*(8), 2916–2924. https://doi.org/10.1021/ie000073r

Yarranton, H. W., Masliyah, J. H. (1996). Molar Mass Distribution and Solubility Modeling of Asphaltenes. *AIChE Journal*, *42*(12), 3533–3543. https://doi.org/10.1002/aic.690421222

Yen, T. F., Gordon Erdman, J., Pollack, S. S. (1961). Investigation of the structure of petroleum asphaltenes by X-ray diffraction. *Preprints*, *6*(1), 21–36.

Zanganeh, P., Dashti, H., Ayatollahi, S. (2018). Comparing the effects of CH4, CO2, and N2 injection on asphaltene precipitation and deposition at reservoir condition: A visual and modeling study. *Fuel*, *217*(January), 633–641. https://doi.org/10.1016/j.fuel.2018.01.005

Zhang, Y., Arya, A., Kontogeorgis, G., Yarranton, H. (2019). Modeling the phase behaviour of bitumen/n-alkane systems with the cubic plus association (CPA) equation of state. *Fluid Phase Equilibria*, *486*, 119–138. https://doi.org/10.1016/j.fluid.2019.01.004

Appendix A: Effect of Air on the Saturation Pressure

The mixtures of WC-B-A3 bitumen, *n*-pentane and methane were prepared in a blind cell apparatus as described in Section 3.2. There is a small fraction of air filling a portion of the blind cell volume, however, it has a negligible effect on the saturation pressure, as shown in Table A.1, and it was not considered as part of the mixture.

Table A.1. Effect of air on the saturation pressures for WC-B-A3 bitumen, *n*-pentane, and methane mixtures.

Methane content wt%	*n*-Pentane Content wt%	Air content wt%	Temperature °C	Saturation Pressure MPa		AD
				Air	No Air	
3.00	26.98	0.06	50	9.08	9.08	0.004
6.00	23.98	0.07	50	20.25	20.23	0.012
1.50	28.48	0.05	50	4.38	4.38	0.002
3.00	11.99	0.08	50	14.16	14.15	0.013
1.50	13.49	0.07	50	6.57	6.57	0.005

Appendix B: Error Analysis for Blind Cell Yields

The uncertainty in the yields is a sum of two components: 1) the uncertainty of a yield measurement; 2) the uncertainty in the yield calculation arising from the assumed solvent content in the heavy phase. The uncertainty of the yield measurement was determined as the 90% confidence interval of the deviations of the yield around a best fit yield curve. First, the data were fit with an empirical best fit linear correlation given by:

$$Y = -0.1982 w_s + 49.152 \quad \textbf{(B.1)}$$

where Y is the yield and w_s is the solvent content in the feed.

Then, the standard deviation of the measurements from the best fit line was determined as follows:

$$s = \sqrt{\frac{\sum_{i=1}^{n} (x_i - \bar{x}_i)^2}{v}} \quad \textbf{(B.2)}$$

where s is the standard deviation, x is the one of the measurements, $\bar{x}$ is the best fit value, and v is the degree of freedom (one less than the number of measurements). For a single new measurement, the error distribution was assumed to be normal and the confidence interval was calculated as follows:

$$CI = \pm z_{(\alpha/2,v)} s \quad \textbf{(B.3)}$$

where CI is the confidence interval and $1 - \alpha$ is the confidence level. The uncertainty of the measurement was determined to be 0.6 wt% for the C_5-asphaltene yield and 7 wt% for the pitch* yield.

The uncertainty of the yield from the assumed solvent content was set as half the difference in the yields calculated at solvent contents of 0 and 50 wt%. The half-differences were determined at each solvent composition and averaged. The standard deviation and confidence interval were then calculated. An example of the difference between the yields is shown in Figure B.1. The uncertainty from this source was negligible for the C_5-asphaltene yields and ranged from 7 wt% at 70 wt% solvent to 1.5 wt% at 90 wt% solvent for the pitch* yields. Hence, the total uncertainty of

the C_5-asphaltene yields was 0.6 wt% and the total uncertainty of the pitch* yields ranged from 8.5 to 14 wt%.

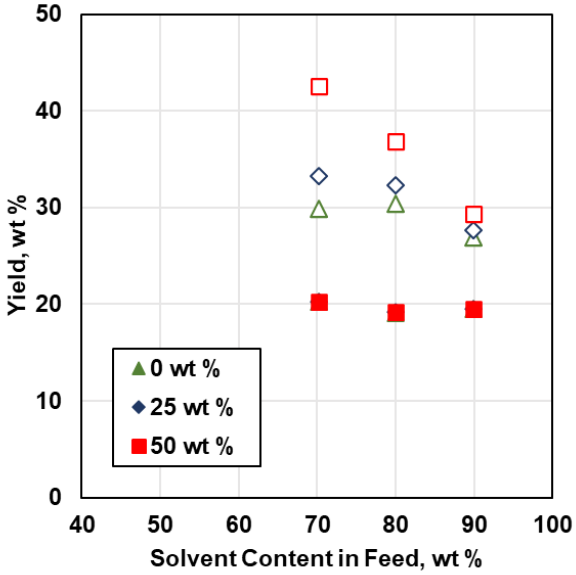

Figure B.1. Difference on C_5-asphaltene yields (closed symbols) and pitch* yields (open symbols) from WC-B-A3 bitumen, *n*-pentane, and methane mixtures assuming different solvent contents in the heavy phase.

Appendix C: Additional Data

This appendix presents the asphaltene precipitation data collected in a previous study (Johnston *et al.*, 2017a) from WC-B-B3 bitumen and *n*-pentane mixtures not included in the body of the thesis. The onsets are presented in Table C.1, the yields at atmospheric conditions and at elevated temperatures and pressures are presented in Table C.2 and Table C.3, respectively.

Table C.1. Onsets for mixtures of WC-B-B3 bitumen and *n*-pentane (C_5) measured in HPM apparatus or extrapolated from yield data.

Temperature °C	Pressure MPa	HPM Onset wt% C_5	Extrapolated Onset wt% C_5
23	0.1	47	47
90	4.8	51	51
140	4.8	49	49
180	4.8	51	49.5
180	13.8	-	52
250	10.3	-	47

Table C.2. Asphaltene yield from mixtures of WC-B-B3 bitumen and *n*-pentane at 21°C and 0.1 MPa. The repeatability of the yield measurements is ±0.65 wt%.

n-Pentane Content wt%	Asphaltene Yield wt%
51.9	6.3
54.0	8.6
56.4	11.3
58.0	12.3
59.8	12.6
66.0	15.2
71.9	16.8
75.8	17.3
80.6	17.7
85.4	18.3
89.9	18.8
94.9	19.0
96.3	19.2

Table C.3. C_5-asphaltene and pitch* yields for mixtures of WC-B-B3 bitumen and *n*-pentane (C_5) measured in the blind cell or PVT cell apparatus. The uncertainties of the C5-asphaltene yields ranged from ±1.5 wt% near the onset to ±0.65 wt% at high dilution. The uncertainties of the pitch* yields are ±5 wt%.

Temperature °C	Pressure MPa	Feed C_5 Content wt%	C_5-Asphaltene Yield wt%	Pitch* Yield wt%
90	4.8	59.6	13.0	-
90	4.8	66.3	14.8	-
90	4.8	72.6	16.6	-
90	4.8	78.8	17.8	-
90	4.8	84.9	18.4	-
90	4.8	64.8	11.5	-
90	4.8	69.5	17.2	-
90	4.8	74.6	17.1	-
90	4.8	80.2	19.0	-
140	4.8	62.3	11.7	-
140	4.8	69.6	14.6	-
140	4.8	77.5	16.6	-
140	4.8	85.0	18.2	-
180	4.8	54.4	8.6	-
180	4.8	59.3	12.5	-
180	4.8	64.8	15.3	-
180	4.8	69.6	16.6	-
180	4.8	79.8	18.4	-
180	4.8	59.2	12.8	18.7
180	4.8	63.7	13.6	19.6
180	4.8	72.5	17.3	24.6
180	13.8	59.4	9.3	-
180	13.8	71.1	15.5	-
180	13.8	80.2	17.6	-
250	10.3	54.7	11.2	-
250	10.3	59.8	15.0	-
250	10.3	66.1	18.0	-
250	10.3	69.8	17.3	-

Appendix D: MRS Model Results from Mixtures of Bitumen and *n*-Pentane

Figures D1 and D2 presents the complete set of MRS modeling results for the mixtures of WC-B-A3 bitumen and *n*-pentane (this study) and WC-B-B3 bitumen and *n*-pentane (Johnston *et al.*, 2017a), respectively. The asphaltene solubility parameters in the model were calculated using Eq 5.3. Pitch* yields were only reported at 180°C for the WC-B-B3 bitumen. Note that while the model significantly over-predicts the pitch* yields from the WC-B-A3 bitumen at 130°C (blind cell method), it only slightly under-predicts the more accurate pitch*yields from the WC-B-B3 bitumen at 180°C (PVT cell method). PVT cell method is described elsewhere (Johnston *et al.*, 2017a).

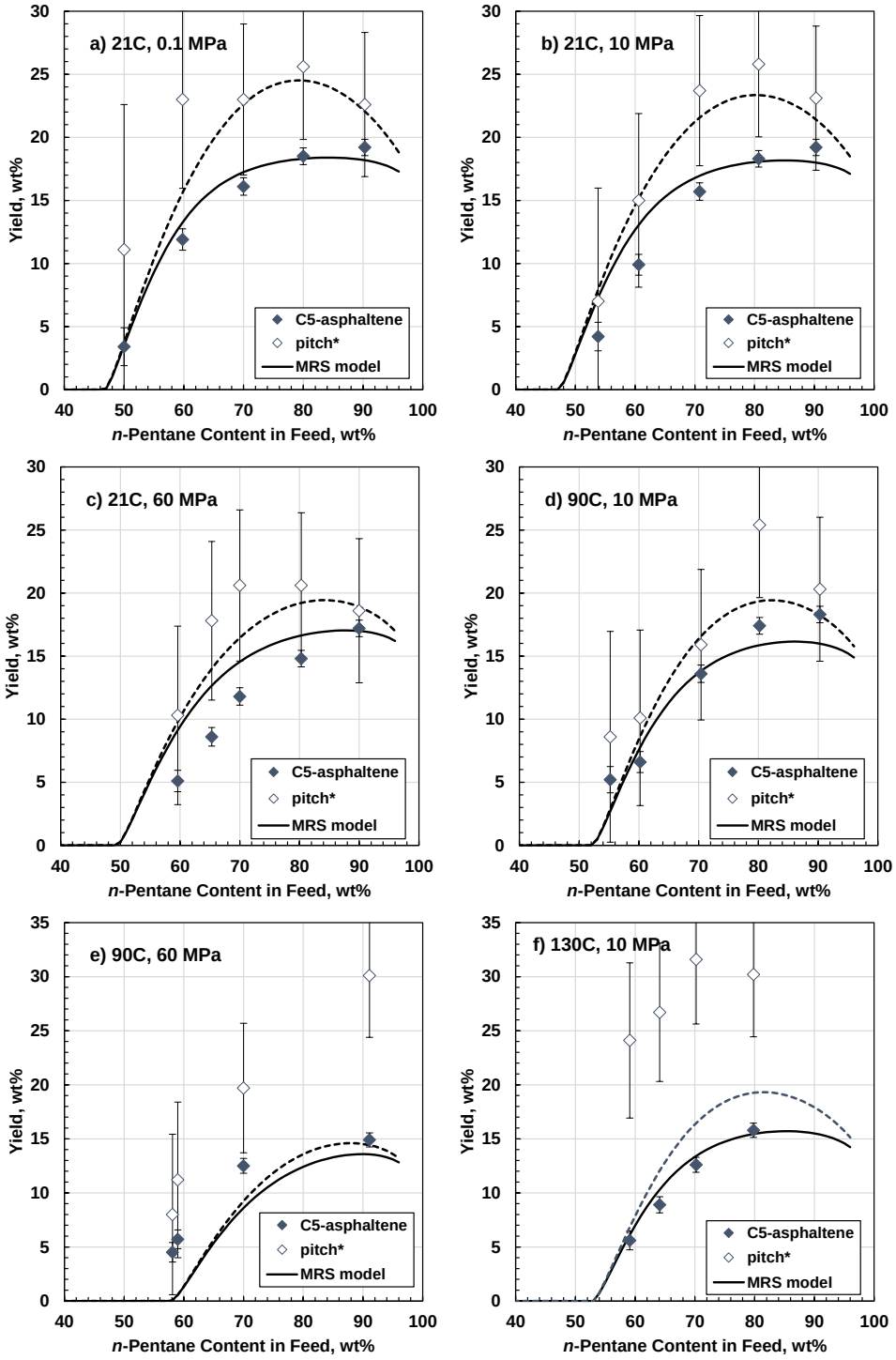

Figure D.1. Measured and modeled C_5-asphaltene yields from mixtures of WC-B-A3 bitumen and *n*-pentane. The yields were obtained with the blind cell method. The solid and dashed lines are the modeled C5-asphaltene and pitch* yields, respectively.

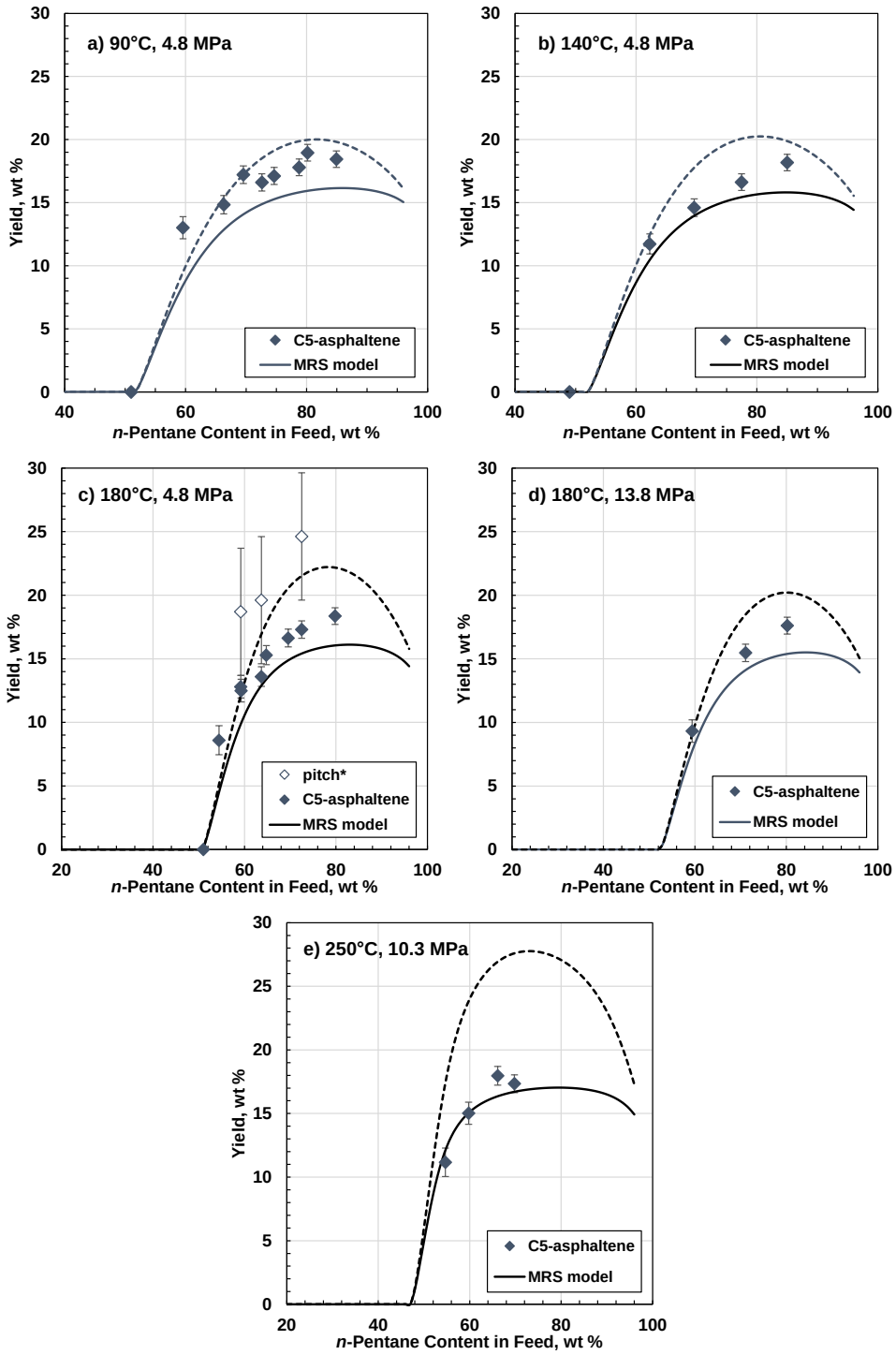

Figure D.2. Measured and modeled C5-asphaltene yields from mixtures of WC-B-B3 bitumen and *n*-pentane. The yields were obtained with the blind cell method and with the PVT cell method (180°C only). The onsets were obtained with the HPM method. The solid and dashed lines are the modeled C5-asphaltene and pitch* yields, respectively.